Journal of Alloys and Compounds 916 (2022) 165219

Contents lists available at ScienceDirect

Journal of Alloys and Compounds

journal homepage: www.elsevier.com/locate/jalcom

Laves type intermetallic compounds as hydrogen storage materials: A review

Volodymyr A. Yartys[a,*], Mykhaylo V. Lototskyy[b]

[a] Institute for Energy Technology, Kjeller 2027, Norway
[b] University of the Western Cape, HySA Systems Centre of Competence, Belville, South Africa

ARTICLE INFO

Article history:
Received 8 March 2022
Received in revised form 6 April 2022
Accepted 19 April 2022
Available online 29 April 2022

Keywords:
Laves phase intermetallics
Intermetallic hydrides
Hydrogen storage and compression
Metal hydride batteries

ABSTRACT

Laves type AB_2 intermetallics belong to the most abundant group of intermetallic compounds containing over 1000 compounds. A large variety of the chemical nature of A (Mg, Ca, Ti, Zr, Rare Earth Metals) and B (V, Cr, Mn, Fe, Co, Ni, Al) metals together with the existence of the extended solid solutions formed by mixing various selected components on both A and B sites dramatically extends the list the known binary and ternary individual compounds. A vast majority of the Laves type intermetallics crystallises with C15 / FCC $MgCu_2$ and C14 / hexagonal $MgZn_2$ types of structures, both formed for a large range of ratios between the atomic radii of the A and B components outside the ideal ratio r_A/r_B= 1.225. Their hydrogenation performance is defined by the chemical composition and structure of the alloys and proceeds according to the following alternative / parallel mechanisms: (a) Formation of the insertion type interstitial hydrides containing up to 6–7 at. H/f.u.AB_2; (b) Amorphisation of the alloys on hydrogenation; (c) Disproportionation with the formation of a binary hydride of the A metal and depleted by A metal B-components based alloys/hydrides. Equilibrium pressures of hydrogen desorption from the AB_2-type hydrides span a huge range of ten orders of magnitude and thus Laves type-based intermetallics satisfy the requirements for various applications including getters of hydrogen gas, volume- and mass-efficient hydrogen storage materials operating at ambient conditions, materials for the efficient thermally driven compression of hydrogen gas with an output pressure of several hundred bar and high capacity and high rate anode materials for the metal hydride batteries operating in a challenging temperature range - at subzero temperatures and also above 60 °C. The paper contains references to 245 publications and will guide the future work in the areas of fundamental research and also in advancing the applications of the hydrides of the Laves type intermetallics.

1. Introduction

Metal hydrides (MH) contribute to the hydrogen-based energy storage enabling operation of various hydrogen energy systems.

Applications of MH utilise a reversible chemical interaction of hydride-forming alloys / intermetallic compounds, M, with hydrogen to form a metal hydride, MH_x, via a direct interaction with hydrogen gas (1a) or electrochemically when atomic hydrogen is formed at the surface of the metal hydride used as an electrode in alkaline electrolyte (1b):

$$M(s) + x/2H_2(g) \underset{desorption}{\overset{absorption}{\rightleftarrows}} MH_x(s) + Q \quad (1a)$$

$$M(s) + xH_2O(l) + xe^- \underset{oxidation}{\overset{reduction}{\rightleftarrows}} MH_x(s) + xOH^-(l) \quad (1b)$$

where (*s*), (*g*) and (*l*) define solid, gas or liquid phases, while molecular or atomic hydrogen is, respectively, supplied from hydrogen gas or via electrochemical reduction of an aqueous electrolyte.

The hydrogenation process is exothermic and often a significant amount of heat is released. The value of the heat effect of reactions (1a and 1b) *Q* is approximately equal to the negated enthalpy, $-\Delta H$, of hydrogen absorption by the metal M.

Several properties of the MH are quite unique. Indeed, (a) metal hydrides form and decompose with extremely quick rates – just in seconds; (b) the volumetric content of the accommodated in the metal lattice hydrogen is very high – reaching a double value as compared to the liquid hydrogen; (c) interaction with hydrogen decrepitates a bulk metal to form fine metal hydride powders

* Corresponding author.
E-mail address: volodymyr.yartys@ife.no (V.A. Yartys).

https://doi.org/10.1016/j.jallcom.2022.165219
0925-8388/

creating clean nonoxidized surfaces; (d) hydrides are able to selectively absorb hydrogen from the gas mixtures thus purifying it; (e) MH are able to significantly change the pressure of hydrogen absorption and desorption as related to the applied temperature thus making it possible to compress hydrogen gas by utilising thermal energy.

Due to the beneficial combination of these properties, MH found numerous applications including [1–14]:

- Compact hydrogen storage, thermally driven hydrogen compression, heat management, hydrogen separation and purification (hydrogen gas is utilised).
- Electrochemical hydrogen storage and conversion (Ni-MH batteries, air – MH batteries and PEM fuel cells utilising hydrogen as a fuel).
- Applications in various technologies utilising intrinsic properties of the MH – in nuclear technologies, in switchable mirrors, as H_2 sensors, in powder metallurgy, in vacuum-plasma technologies, and as catalysts.

MH technology is an application-driven area of R&D where convenient processing conditions and efficient energy conversion can be achieved and these can be adopted to suit a particular application, by tuning operational parameters of the metal-hydrogen systems, including metal hydride component selection, structure and phase composition of the hydride-forming materials, operational conditions – temperature and hydrogen pressure, and hydrogen energy system layout. In each particular case, the success performance needs efficiency of the use of the materials and corresponding systems, including choice of the target composition of the MH material, its manufacturing in the upscaled amounts, development of the MH-containing system components and, importantly, integration of the system as a whole [11–17].

Among a great variety of the MH materials, intermetallic hydrogen storage alloys are of a special importance [18–20]. These materials are used in many electrochemical and gas phase applications related to energy storage (Ni-MH batteries), hydrogen and fuel cell technologies (hydrogen storage, compression, separation and purification), as well as energy conversion (heat management systems, permanent magnet materials). Changing the structure type and component composition of the MH alloys allows to tune their hydrogenation-dehydrogenation properties in a broad range. Subsequently, MH systems utilising metal hydrides are characterised by tuneable performance conditions which can be adopted to suit specific applications by appropriate selection of the type of the Metal-Hydrogen system.

AB_2 (A = Ti, Zr, Rare Earth Metals, Mg; B = Fe, Co, Ni, Mn, other transition metals and nontransition elements) Laves-type intermetallics are known as active hydride-forming compounds absorbing hydrogen up to a limiting composition of 7 at.H/f.u. AB_2. These hydrides reversibly form and decompose in impressively broad range of operating temperatures and equilibrium H_2 pressures, from a few millibar at T~300°C to several kilobar at near-ambient temperatures [4]. These hydrides with a typical hydrogen storage capacity of AB_2H_{3-4} are characterised by a high volumetric hydrogen storage density (~100–150 g_H/L, that is 1.4–2 times higher than the density of H in liquid H_2) and relatively high gravimetric storage capacity (up to 2–2.5 wt% H) [21]. As these features are accompanied by a fast hydrogenation / dehydrogenation kinetics and the alloys are cost-efficient, AB_2 Laves type hydrogen storage alloys attracted a high research interest of the international community. Since start of their thorough studies from the beginning of 1980 s (see, e.g., [22,23]), the number of publications in the field exponentially grew reaching about 10% in the overall number of publications on hydrogen storage materials for the period 2000–2015 (> 16800 papers in total [24]).

A broad review on the Laves phases hydrides and their various applications containing more than 1000 references has been recently published [25]. Though the review contains a separate section dealing with the Laves-type hydrogen storage materials, it mostly presents general features describing their behaviours and their applications and leaves without a consideration various important properties of these materials, first of all, related to the interrelation between the composition and the hydrogenation/dehydrogenation behaviours.

The present review is focused on the analysis of the structural, thermodynamic and kinetic properties of the Laves-phase type hydrides (Sections 2–4), and analyses and presents a vast amount of the literature data published since the 1960 s (Section 5). Special attention is paid to the multi-component AB_2-type Laves phase hydrides (where A is Ti and Zr), which are particularly promising in the development of the hydrogen storage systems [26–29], hydrogen compressors [29–32], low-temperature heat management [33–35] and as advanced negative electrodes of the Ni-MH batteries [36,37]. These applications, along with the analysis of the "composition – properties" relationships, together with the issues related to the large-scale manufacturing of the AB_2-type hydrogen storage alloys, and their technological features, are considered in Section 6.

2. General overview of Laves-type intermetallics

Laves type intermetallics are the most abundant group of intermetallic compounds containing over 360 binary and more than 540 ternary compounds [38].

The reason for the exceptional number of the existing Laves type intermetallics is because the metallic compounds preferably crystallise with the close packing of atoms, with high atomic symmetry of their structures and metallic bonding, and Laves phases satisfy these more comprehensively than other types of the structures observed for these compounds.

Three types of Laves type structures form the most representatives, including hexagonal C14, cubic C15 and hexagonal C36 types. The ordered hexagonal C14 structure has at least 131 binary representatives and 263 ternary compounds, the ordered cubic C15 structure forms at least 219 binary and 272 ternary compounds, and the ordered hexagonal C36 structure - 17 binary and 14 ternary compounds [39]. Therefore, over 900 binary and ternary Laves compounds have been identified, with over 360 Laves phases being binary compounds. Even though Laves type intermetallics further to the conventional 2-layers C14, 3-layers C15 and 4-layers C36 intermetallics also include multilayers stackings, with continuously expanding list of representatives (one recent example is $MgNi_{2-x}Co_x$ – 7-layers Laves type compound [R.V. Denys and V.A. Yartys, 2022]), their practical importance is limited and they will not be considered further in the present review.

For the Laves-type AB_2 intermetallic compounds, rare earth metals, zirconium, titanium and calcium and magnesium are the main elements on the A sites. A variety of elements used on the B sites includes such elements as aluminium, vanadium, chromium, manganese, iron, cobalt, nickel and copper.

Most frequently Laves type structures are formed by the rare earth metals, which exist for the entire range of the rare earths, from La to Lu, forming the whole series of the Laves type intermetallics $REFe_2$, $RECo_2$ and $RENi_2$, with hydrogenation behaviours and properties of the metal hydrides $RE(Fe,Co,Ni)_2$ systematically changing depending on a transition metal – Fe, Co or Ni.

Atomic size factor and electron concentration are the two main factors affecting not only the formation of the Laves type intermetallics with a particular type of the structure – C14 or C15 – but also their hydrogenation properties and electrochemical performance as anode electrodes of the metal hydride batteries.

Table 1
Ratios of atomic radii, R_A/R_B in the binary systems. The Laves type phases are preferably formed in the range of R_A/R_B between 1.19 and 1.32 (listed in bold font in the Table 1), while an ideal value R_A/R_B is 1.225 [25]. The shaded cells indicate a formation of the Laves phases (C14, C15 or C36) in the particular binary systems [39].

B (R [Å])	***A (R [Å])***							
	Sc *(1.641)*	***Y*** *(1.801)*	***La*** *(1.877)*	***Ce*** *(1.825/1.715)*	***Lu*** *(1.734)*	***Ti*** *(1.462)*	***Zr*** *(1.602)*	***Hf*** *(1.580)*
Al *(1.432)*	1.146	**1.258**	**1.311**	**1.274/1.198**	**1.211**	1.021	1.119	1.103
V *(1.346)*	**1.219**	1.338	1.395	1.356/**1.274**	**1.288**	1.086	**1.190**	1.174
Cr *(1.282)*	**1.280**	1.405	1.464	1.424/1.338	1.353	1.140	**1.250**	**1.232**
Mn *(1.264)*	**1.298**	1.425	1.485	1.444/1.357	1.372	1.157	**1.267**	**1.225**
Fe *(1.274)*	**1.288**	1.414	1.473	1.432/1.346	1.361	1.148	**1.257**	**1.240**
Co *(1.252)*	**1.311**	1.438	1.499	1.458/1.370	1.385	1.168	**1.280**	**1.240**
Ni *(1.246)*	**1.317**	1.445	1.506	1.465/1.370	1.392	1.173	**1.286**	**1.268**
Mo *(1.400)*	1.172	**1.286**	1.341	**1.304/1.225**	**1.239**	1.044	1.144	1.129
W *(1.408)*	1.165	**1.279**	1.333	**1.296/1.218**	**1.232**	1.038	1.138	1.122

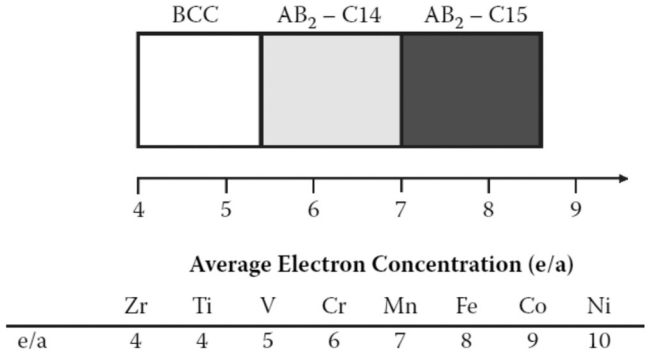

Fig. 1. Formation of the particular types of the crystal structures of the alloys as related to the average electron concentration.
Adopted from [40].

The ideal ratio between the radii of the components $R_A/R_B \approx 1.225$ [25]. Analysis of the experimental data (Table 1) shows that in fact Laves type compounds are formed for R_A/R_B being much different from this value, spanning a range from $R_A/R_B \approx 1.1$ for $HfAl_2$ to $R_A/R_B \approx 1.5$ for $LaNi_2$.

Further to the size factor, electron concentration also affects the formation of the particular Laves type structures. The electron concentration factor *e/a* accounts the average number of the outer electrons per atom for the component atoms [40]. The average electron concentration factor *e/a* of the alloy can be obtained using the following equation

$$(\boldsymbol{e/a})_{\boldsymbol{alloy}} = \sum_{\boldsymbol{i}} (\boldsymbol{e/a})_{\boldsymbol{i}} \boldsymbol{X} (\boldsymbol{at}\%)_{\boldsymbol{i}} \quad (2)$$

Average electron concentrations for the AB_2 alloys are presented in Fig. 1.

Analysis shows that for this group of alloys hexagonal C14 type structures are formed at lower e/a, between 5.3 and 7.0, while cubic C15 type structures appear at higher e/a exceeding 7.0. When e/a is below 5.3, a BCC type of structure replaces Laves type intermetallics (see Fig. 1). Furthermore, Fig. 1 also lists e/a ratios for some commonly used elements contributing to the composition of the alloys which span a range from 4 to 10.

In the non-stoichiometric Laves phases, $AB_{2\pm x}$, mutual substitutions of A↔B may occur (e.g., A-atoms partially occupying B-positions for AB_{2+x} compositions and vice versa for the AB_{2-x} alloys), while, less frequently, A- and B-vacancies for AB_{2+x} and AB_{2-x}, can appear [25]. The substitutional site occupation for the alloy of A- and B-components with atomic fractions *XA* and *XB*, respectively (*XA* + *XB* = 1), can be calculated as:

$$\mathbf{A}_{\boldsymbol{XA}}\mathbf{B}_{\boldsymbol{XB}} = (\mathbf{A}_{\mathbf{1}-\boldsymbol{yB}}\mathbf{B}_{\boldsymbol{yB}})(\mathbf{B}_{\mathbf{1}-\boldsymbol{yA}}\mathbf{A}_{\boldsymbol{yA}})_{\mathbf{2}}, \quad (3)$$

where:

$$\boldsymbol{yA} = \begin{Bmatrix} \mathbf{1} - \mathbf{3}/\mathbf{2}\boldsymbol{XB}, \text{ for } \boldsymbol{XB} < \mathbf{2}/\mathbf{3} \\ \mathbf{0}, \text{ for } \boldsymbol{XB} > \mathbf{2}/\mathbf{3} \end{Bmatrix}; \quad (4)$$

and:

$$\boldsymbol{yB} = \begin{Bmatrix} \mathbf{0}, \text{ for } \boldsymbol{XB} < \mathbf{2}/\mathbf{3} \\ \mathbf{3}\boldsymbol{XB} - \mathbf{2}, \text{ for } \boldsymbol{XB} > \mathbf{2}/\mathbf{3} \end{Bmatrix}; \quad (5)$$

As an example, A- and B-site occupation for the intermetallics $ZrMn_{1.8}$ and $ZrMn_{3.4}$ (see Section 2.1 below) can be written as Zr $(Mn_{0.964}Zr_{0.036})_2$ and $(Zr_{0.682}Mn_{0.318})Mn_2$, respectively.

3. Hydrides of Laves phase intermetallic compounds

3.1. Zirconium and titanium based Laves phases

First characterised AB_2 Laves type hydrides were hydrides of Zr-containing intermetallics ZrV_2, $ZrCr_2$ and $ZrMo_2$ [41]. These studies showed formation of stable at ambient conditions hydrides ZrV_2H_5 and $ZrCr_2H_4$ which partially released hydrogen on their heating (see Fig. 2, *a* and *b*), with residual H content of ZrV_2-based hydride

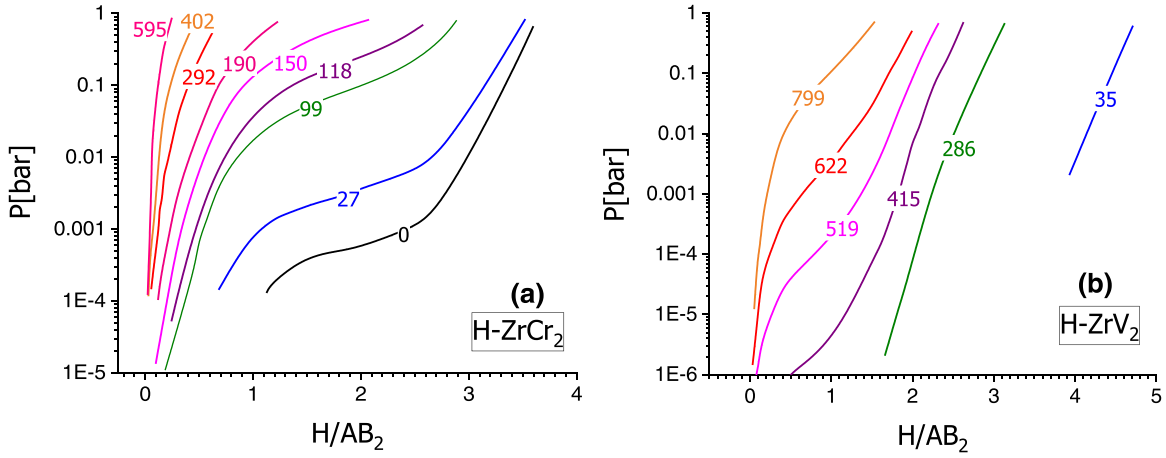

Fig. 2. Temperature- and pressure-dependent equilibria in the $ZrCr_2$-H_2 (a) and ZrV_2-H_2 (b) systems. Curve labels show temperatures (in °C) for the hydrogen desorption isotherms.
Adopted from [41].

remaining rather high, around 1.5 at.H/ZrV_2 even at a very high temperature of 799 °C (1 bar H_2).

$ZrTM_2$ (TM=transition metals) Laves type intermetallics are also formed by Mn, Fe, Co and Ni. They all absorb hydrogen, and the properties of their hydrides are determined by the nature of the TM. The most suitable for the reversible hydrogen storage at convenient conditions is $ZrMn_2$ which absorbs around 3 at.H/f.u. and forms a hydride with desorption pressure slightly below 1 bar H_2 at ambient temperature. For TM=Fe, Co and Ni the hydrogenation of their Laves type intermetallics with Zr requires application of very harsh conditions – pressures of several kbar H_2 and use of elevated temperatures. This results in the formation of an insertion type tetrahydride $ZrFe_2H_4$ for TM=Fe [42] or a disproportionation process resulting in Zr_2CoH_5 and Co for $ZrCo_2$ [43].

A significant number of the works published in 1970–80 s was focused on the studies of the effects of:

- Substitution of the B- and A-components in the ternary and quaternary Laves phases $[Zr,Ti](B1,B2)_2$ where B1,B2 =V,Fe,Cr,Mn,Co,Mo [44–52] and
- Modulations of the stoichiometry of the Laves type alloys $AB_{2\pm x}$ between hypostoichiometric and hyperstoichiomertic compositions for Zr-based [22], [53–60] and Ti-based compounds [61–66].

Indeed, it is well known that compounds of Zr with Mn, Fe, and Co and of Ti with Cr, Mn, Co, Fe can be prepared having compositions substantially deviating from the ideal 1:2 AB_2 stoichiometry (see Fig. 3). For some intermetallics Laves type structures span the area between understoichiomertic (B/A < 2.00) and overstoichiometric (B/A > 2.00) compositions, with systematic, frequently very drastic changes in the properties of the hydride phases (H storage capacity, thermodynamics and kinetics of the metal-H interactions). One typical example is $ZrMn_{2\pm x}$ ($ZrMn_{1.8-3.4}$) hexagonal C14 type hydrides, where H capacities gradually decrease while equilibrium pressures of H_2 absorption increase following an increase of the Mn content in the $ZrMn_{2+x}$ alloys (see Fig. 4). These changes are caused by a contraction of the unit cells of the $ZrMn_{2\pm x}$ following an increase in the content of Mn thus decreasing sizes of the intersices in the metal sublattice.

Similar dependencies were observed during the hydrogenation of the C14 alloys in the Ti-Mn system, where the homogeneity area spans an interval between $TiMn_{1.5}$ and $TiMn_{2.1}$ [61]. These alloys showed high hydrogen-storage capacities, suitable plateau hydrogen dissociation equilibrium pressures and tailored properties as related to the Ti/Mn ratio [61–66]. The best H storage performance (1.86 wt. % H; 118 g_H/L; plateau pressure 0.7 MPa H_2 at 20 °C) was demonstrated by the $TiMn_{1.5}$ alloy [61,66].

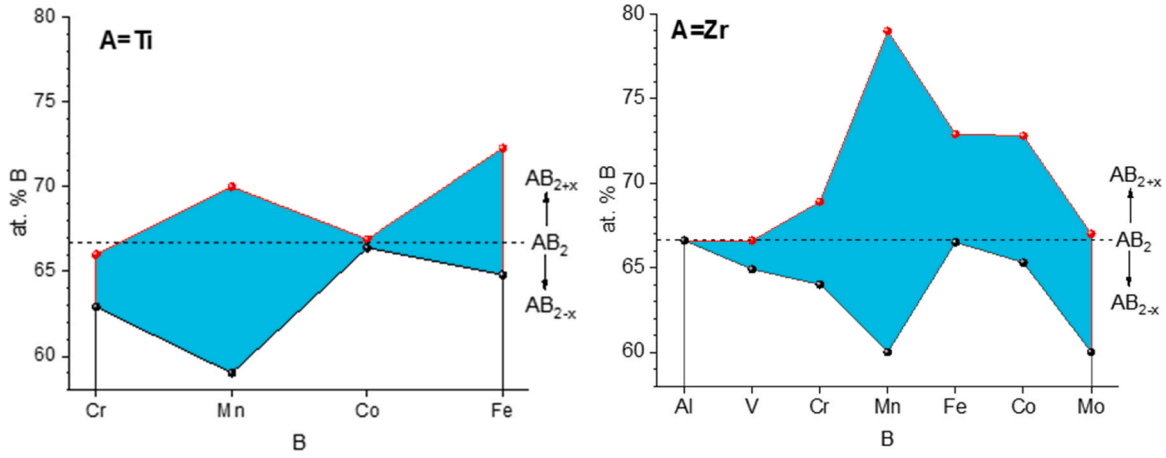

Fig. 3. Homogeneity regions (coloured) for some binary $TiTM_{2\pm x}$ and $ZrTM_{2\pm x}$ Laves phases [39]. Top/red and bottom/black lines correspond to the maximum and minimum concentrations of the B-component).

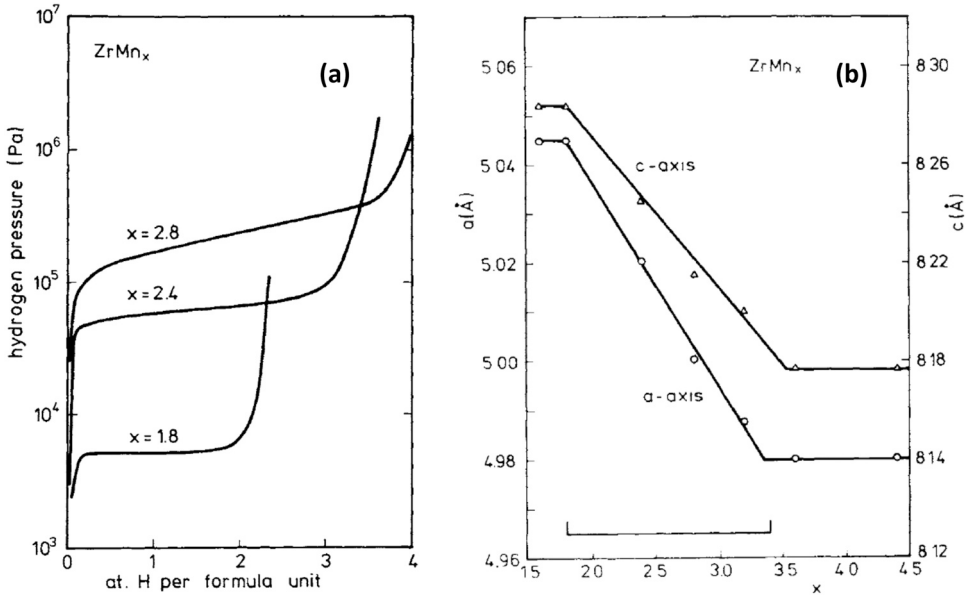

Fig. 4. Gradual increase of the hydrogen absorption pressures for the annealed $ZrMn_{1.8-2.8}$ intermetallics at 50 °C (a) and continuous contraction of the hexagonal C14 type unit cells following an increase of the Mn content in the $ZrMn_{2\pm x}$ intermetallics from 1.8 to 3.4 Mn/Zr (b).
Adopted from [69].

Quasi-binary Laves type intermetallics can be formed by replacing Zr for Ti or having a solid solution of two components B═Al, V, Cr, Mn, Fe, Co and Ni on the B-site. In both cases a formation of unlimited homogeneous solid solutions frequently happens allowing to achieve gradual composition-dependent changes of the properties of the hydrides, their stabilities and H storage capacities. Examples of such composition-dependent changes in H storage behaviours are shown in Fig. 5 below.

The hypostoichiometric C14–$TiMn_{2-x}$ Laves phases were shown to be promising for both gas phase and electrochemical applications due to their high reversible hydrogen storage capacity, fast hydrogenation/dehydrogenation kinetics and tuneability of the hydrogen sorption performances at near-ambient conditions by using the variation of the type and amount of the extra to Mn metal component (M=V, Cr, Fe, Co, Ni, Cu, Mo) and (Mn+M)/Ti stoichiometric ratio in the Ti–Mn–M Laves phase alloys. The corresponding hydrogen storage materials were patented by Japanese companies already in the 1970 s (Matsushita Electric Industrial) [67]. Subsequent detailed studies of the multicomponent alloys based on the C14–$TiMn_{2-x}$ with substitutions on both A(Ti)- and B(Mn)-sides appeared in

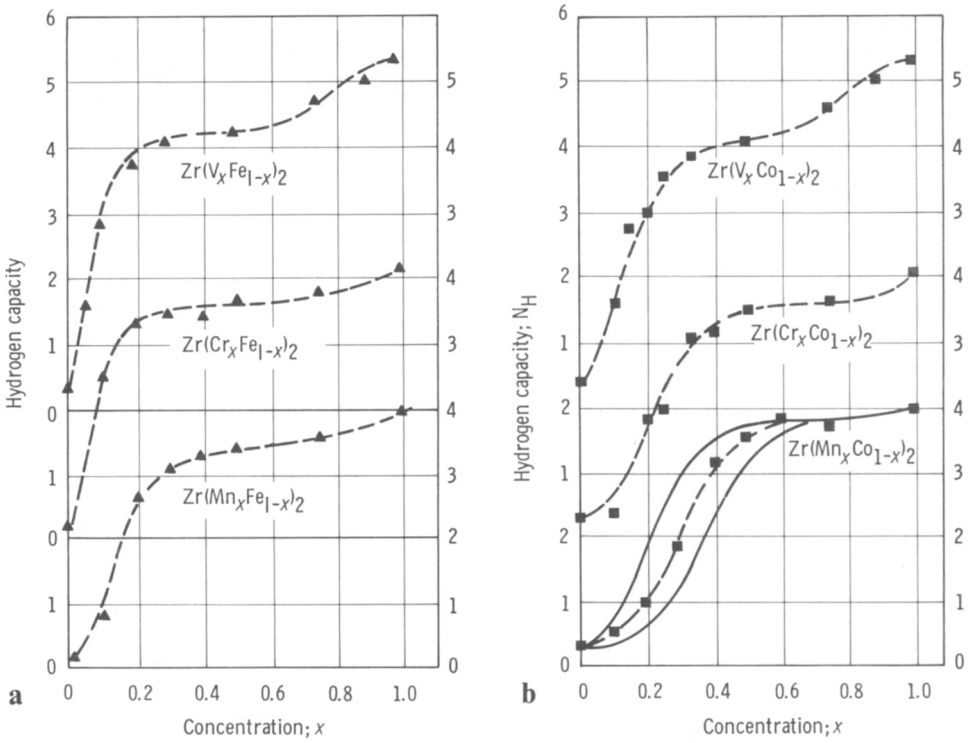

Fig. 5. Hydrogen absorption capacities of $Zr(M1_xM2_{1-x})_2$ pseudobinary Laves phases as related to the atomic fraction, x, of the M2 component.
Reproduced from [23].

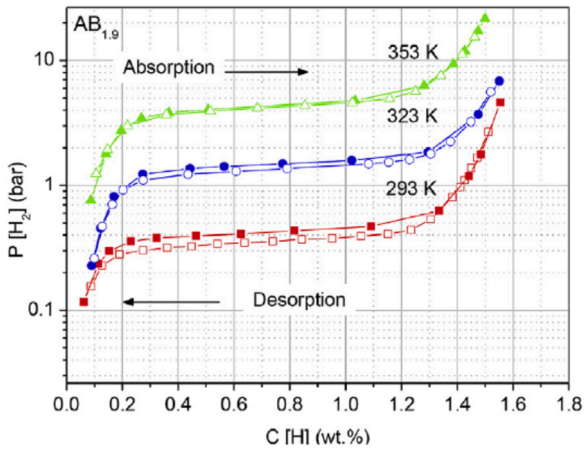

Fig. 6. Temperature-dependent variation of the PCT curves for the $AB_{1.9}$ Laves type hydride showing several beneficial features, including (i) negligible hysteresis between absorption and desorption; (ii) flat single-plateau isotherms; (iii) merging of the isotherms of abs-des at 353 K thus indicating a proximity of the critical temperature.
Reproduced from [125].

1990 s–early 2000s [62–64], and optimised compositions of the alloys were patented [66,68].

$Ti(V,M)_{2+x}$ alloys (M=Mn, Ni, Cr) show benefits of combining hydrogen storage capacities above 2 wt.% H with easy activation and fast hydrogenation/dehydrogenation kinetics. These alloys are multiphase consisting of a BCC solid solution and a Laves phase intermetallic with each phase contributing to the hydrogenation performance. This class of promising hydrogen storage materials,"Laves phase related BCC solid solutions", was described by Akiba (see [65] and references therein for further details).

A partial replacement of Zr by Ti or vise versa, reduces the stability of the hydrides for the Ti→Zr replacement while achieving an opposite effect stabilising the hydrides for the Zr→Ti replacement. A ratio between Ti and Zr forming a solid solution on the A side defines the thermodynamic properties and stabilities of the AB_2H_x hydrides. Ti and Zr have similar chemistry, however, are significantly different in their atomic sizes (Ti-1.462 Å; Zr-1.602 Å). Increasing the content of Ti and replacing Zr in the AB_2 the intermetallics (normally limited by a maximum value of 22%, $Ti_{0.22}Zr_{0.78}$) results in a gradual contraction of the unit cells of the intermetallics, which causes a destabilization of the corresponding hydrides [70,71].

Creation of the multicomponent Laves phase compositions containing a mixture of the components on both A and B sites proved to be efficient in optimising the hydrogenation-dehydrogenation performance particularly when applied as the metal hydride anode electrodes of the Ni-MH batteries.

In the multi-element $AB_{2\pm x}$ alloys, the constituting elements contribute to the H storage performance in a variable way. Indeed, Ti, Zr, and V are the hydride-forming elements, Ni has a high catalytic activity facilitating splitting of the molecular hydrogen, Co and Mn provide surface activity relevant for the improvement of hydrogen exchange, while Cr, Al, and Fe increase alloys stability in hydrogen on cycling. Choice of elements and their relative content contributing on the B side (Fe, Co, Ni, Mn, Cr, V, and Al) can be optimised using empirically defined optimal ratio of mixing of four transition metals on the B side - $Ni_{10}Mn_{5.83}VFe$ – which allows to achieve excellent reversibility of hydrogen absorption and desorption with extremally small hysteresis between the isotherms of hydrogen absorption and desorption. This allows to achieve energy efficient compression of hydrogen gas by using such alloys and to decrease an overpotential of the metal hydride anodes utilising the alloys [70,71].

Changing the ratio of B and A between $AB_{1.9}$ (see Fig. 6) and $AB_{2.1}$ while keeping a single phase Laves type structure unchanged appears to be very useful in modifying their behaviours. Increase of the B/A ratio in the alloys causes a gradual contraction of the unit cells and a corresponding destabilization of the hydrides allowing to finely tune their stability.

Effect of Ti replacing Zr in the AB_2 alloys is very distinct as can be concluded from the data presented in Fig. 7(a) showing that hydrogen desorption pressure is more than 2 orders of magnitude higher for $TiMn_2$ based hydride as compared to $ZrMn_{2\pm x}$ based hydrides. Simultaneous doping on both A and B sites allows to finely tune hydrogen desorption pressures conveniently making them being close to 1 bar H_2 Fig. 7(b).

Relatively high hydrogen storage capacities of the Laves phases on the basis of Ti and Zr (up to ~2 wt.% H) along with fast hydrogenation / dehydrogenation kinetics and extremely wide range of stabilities of their hydrides which can be effectively controlled by the variation of the alloy's composition (see Section 5) makes these materials very promising for the various applications covering a broad range of operating temperatures and hydrogen pressures (Section 6). At the same time, disadvantages of these hydrogen storage materials include: (a) metallurgical difficulties of their large-scale preparation associated with high melting temperatures and increased high-temperature reactivity of Ti and Zr because of the high affinity to oxygen; (b) difficulties in activation to initiate the hydrogenation; (c) sensitivity to the impurities of active gases when present in H_2; and (d) pyrophoricity of the activated hydrogenated / dehydrogenated alloy powders. These features will be later considered in the Sections 4.1 and 4.5 of this review.

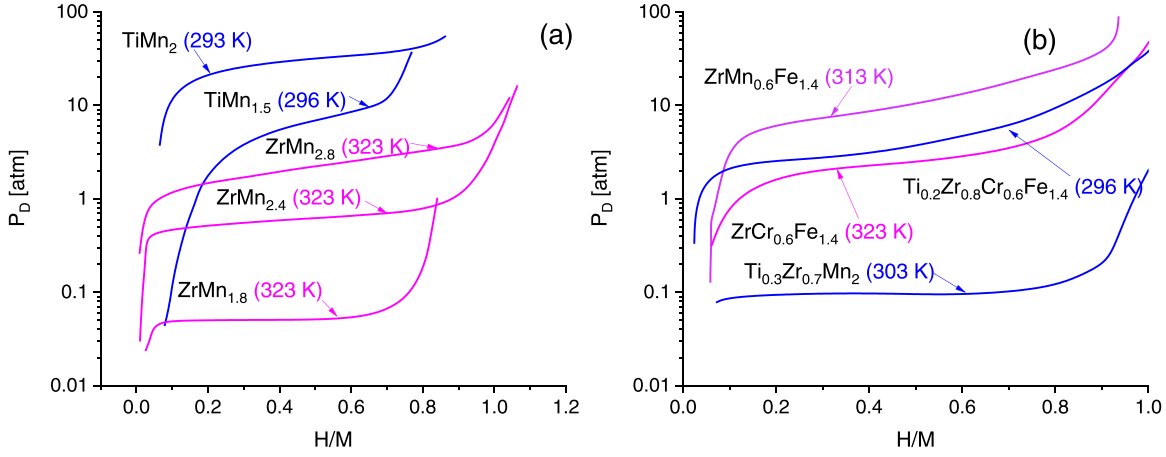

Fig. 7. Hydrogen desorption isotherms for some C14 Laves phase intermetallics. (a) Binary $AB_{2\pm x}$ [46,60,72]. (b) Ternary and quaternary AB_2 [50,51,73].

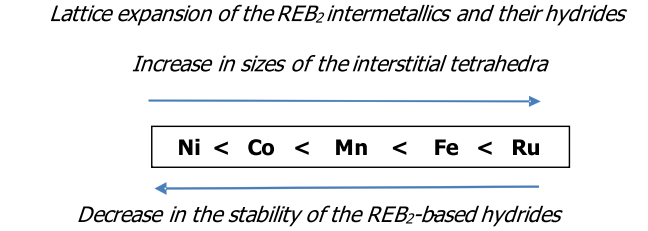

Fig. 8. Influence of the nature of transition metal (TM) component with the rare-earth metals (RE) in the Laves type intermetallic compounds $RETM_2$ on the crystal structure features of the intermetallics and their hydrides and the stability of the hydrides.

3.2. Rare earth-based $RETM_2$, $REAl_2$ and $REMg_2$ intermetallics

3.2.1. $RETM_2$ based hydrides

$RETM_2$ intermetallics are formed by all rare earth metals and a large variety of transition metals including but not limited to Mn, Fe, Co, Ni, Ru together with nontransition elements Al and Mg.

Hydrogen interaction with this group of intermetallic alloys proceeds via three alternative mechanisms:

(a) Formation of insertion type hydrides with hydrogen atoms filling the available interstitials in the structures of the initial intermetallics. This insertion is always accompanied by a volume expansion, 10–30%. Its extent is determined by the nature of the RE and TM components and maximum hydrogen storage capacity, most frequently being in a range between $RETM_2H_3$ and $RETM_2H_4$. The expansion amounts 2–4 Å^3/at.H, with the most frequent value close to 3 Å^3/at.H. For the isostructural intermetallic hydrides a gradual change proceeds in the following sequence presented in the Scheme (Fig. 8):

One typical example is $ErFe_2$-H_2 system. The PCT diagram for this system is shown in Fig. 9 [74]. One can see multi-ptateau equilibria between 6 individual phases resulting in a step-by-step synthesis of $ErFe_2H_{4-5}$.

For the Sc-based intermetallics $ScNi_2$, $ScCo_2$ and $ScFe_2$ H storage capacity and stability of the crystalline insertion type hydrides increases in a sequence Ni < Co < Fe [75].

(b) Disproportionation of the intermetallics during their interaction with hydrogen resulting in the formation of the binary hydrides of rare earth metals and enriched with B component phase constituents or individual elements B. One example is presented in [76]:

$$CeFe_2 + 3/2H_2 \rightarrow CeH_3 + 2\ \alpha\text{-}Fe \quad (6)$$

(c) Hydrogen Induced Amorphisation (HIA) of the metal lattice takes place for many C15 Laves compounds $RETM_2$ (TM = Fe, Co, Ni) during their hydrogenation at 130–230 °C. The atomic size ratio is the most important feature determining the HIA reaction of the C15 Laves compounds, and the compounds with the ratio above 1.37 become amorphous on hydrogenation. When the temperature of the hydrogenation is further increased, a crystallisation of the binary hydrides of the rare earth metals together with enriched with transition metal intermetallics / their hydrides (normally, $RETM_5$) takes place [77,78].

3.2.2. Hydrides of $RENi_2$ Laves type alloys

C15 cubic Laves type $RENi_2$ (RE = rare earth metal) compounds are formed for the whole series of the rare earth metals, including vacancy-free stoichiometric alloys of heavy rare earths or slightly RE-deficient and containing vacancies ordered at the empty RE sites thus causing a doubling of the FCC unit cells of intermetallics of light rare earths.

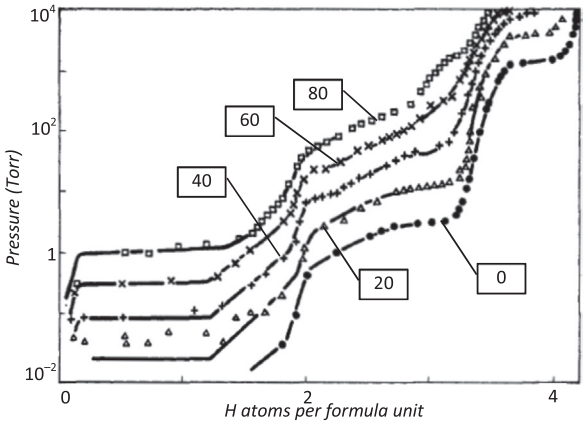

Fig. 9. Desorption isotherm in the $ErFe_2$–H_2 system, at various temperatures (°C) shown as curve labels. The full curves are model calculations based on the multi plateau Lacher-Kierstead model.
Adopted from [74].

The mechanism of the hydrogenation of the $RE_{1-x}Ni_2$ Laves phases is defined by the type of the rare earth metal. Compounds of light rare earth metals have the highest H storage capacity forming tetrahydrides $RENi_2H_{3.6-4.2}$ (RE=Y, La,Ce, Pr), while for the heavy rare earth metals the hydrogenation yields trihydrides $RENi_2H_{2.9-3.1}$ (RE=Sm,Er) with a lower hydrogen content [79–85]. During the heating to 400–470 K, a partially reversible hydrogen desorption occurs for the all studied $RENi_2$-hydrides.

However, in general saturated hydrides are prone to disproportionation, and saturated $RENi_2H_{3-4}$ hydrides (RE=La, Ce, Pr and Sm) when heated to 650–670 K, decompose to form REH_{2-3} binary hydrides and $RENi_5$ intermetallics. At higher temperatures, a gradual, step-by-step (through the formation of intermediate IMCs RE_2Ni_7 and $RENi_3$) regeneration of the parent REM_2 occurs. While Er- and Y-based hydrides can be formed as crystalline hydrides with expanded unit cells (with $\Delta V/V_0$~14.2% for $ErNi_2H_{3.1}$ and 17.7% for $YNi_2H_{3.6}$ [85]), their amorphization occurs during the hydrogenation at high H_2 pressures and high temperatures.

Degradation of the $RENi_2$ hydrides takes place at ca. 550–600 K and results in the formation of amorphous binary hydrides $REH_{\sim 2-3}$ and hydrides of nonstoichiometric Laves phases accommodating extra Ni on the sites depleted by the rare earth metal, $(RE_{1-y}Ni_y)Ni_2H_x$ (y ~0.05 for Er, ~0.1 for Y; x ~1) [84]. Similar transformation occurs at 700 K in the amorphous $PrNi_2D_{3.6}$ [83].

Hydrogen induced amorphization of various $RENi_2$ intermetallics has been studied for the various intermetallics in [78].

3.2.3. $REAl_2$ hydrides

When transition metals in $RETM_2$ Laves type alloys are replaced by aluminium, the formed $REAl_2$ intermetallics crystallise with C15 cubic Laves type structures. Even though their crystal lattice expands as compared to $RE(Fe,Co,Ni)_2$ because Al has a larger atomic size as compared to Fe/Co/Ni, and interstitial sites become larger in size, no insertion type hydrides are formed by any of the $REAl_2$ intermetallics. The hydrogenation at 50 bar H_2/500 °C results in a disproportionation yielding binary hydrides of rare earth metals and a variety of enriched by Al binary intermetallics (La_3Al_{11}, $EuAl_4$ or $YbAl_3$) [86].

3.2.4. $REMg_2$ hydrides with Mg as a B component

When the hydrogenation temperature is below 100 °C, cubic C15 type $LaMg_2$ and $CeMg_2$ form tetragonal heptahydrides $REMg_2H_7$ [87]. The hydride formation results in a volume expansion of appr. 15 % and gives a completely ordered distribution of hydrogen atoms filling RE_2Mg_2, Mg_4 and RE_2Mg interstitial sites.

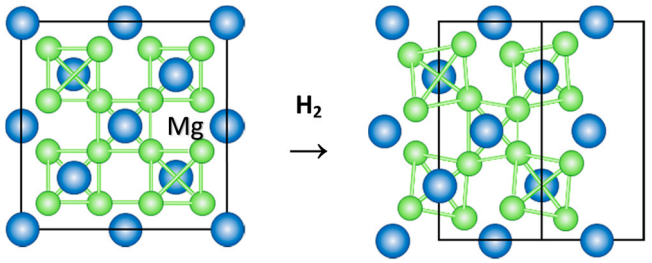

Fig. 10. Metal sublattice of the parent (left) and hydrogenated (right) $NdMg_2$ IMC with C15 Laves type structure.
Adopted from [88].

The metal sublattice and a framework of corner-sharing Mg_4 tetrahedra undergo a deformation on the hydrogenation, see Fig. 10 [88].

Hexagonal C14 type $EuMg_2$ forms an orthorhombic unit cell of $EuMg_2Hx$ where a similar to the C15 type matrix deformation of the metal sublattice takes place (Fig. 11).

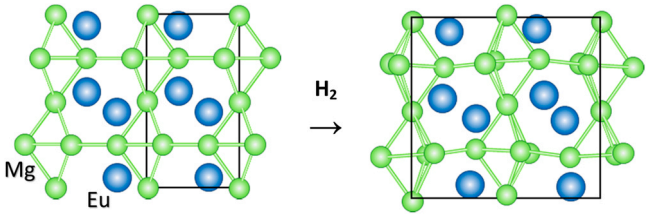

Fig. 11. Metal sublattice of the parent (left) and hydrogenated (right) $EuMg_2$ IMC with C14 Laves type structure.
Adopted from [88].

Hydrogenation at high temperatures of 673–723 K and hydrogen pressure of 50 bar H_2 results in a disproportionation to form binary hydrides of the rare earth metals and magnesium hydride (RE=La, Ce, Pr, Nd, Sm, Eu, Gd, Tb, Ho, Er, Tm, Yb) [88].

3.3. Hydrides of magnesium-containing $MgTM_2$ (TM=Ni, Co) intermetallics: $MgNi_2$, $MgCo_2$ and $Mg(Ni,Co)_2$

3.3.1. $MgNi_2$-H_2

$MgNi_2$ intermetallic alloy crystallises with the hexagonal C36 type of Laves phase structure. It does not absorb hydrogen at normal P-T conditions. However, at 300 °C during interaction with hydrogen (deuterium) gas compressed to 2.8–7.4 GPa, a trihydride $MgNi_2H(D)_{3.2}$ was formed. The trihydride remained metastable at ambient conditions allowing its structure, stability and magnetic properties to be studied. The formation of $MgNi_2H_3$ is associated with a complete rebuilding of the initial hexagonal structure into the orthorhombic distorted $MoSi_2$-type sublattice. Neutron diffraction of the $MgNi_2D_{3.2}$ demonstrated that D atoms fill sites having octahedral Mg_4Ni_2 and planar Ni_2 coordination (see Fig. 12). DFT and phonon calculations showed that the *Cmca* structure of $MgNi_2D_3$ is the most stable, both from the electronic structure and the lattice dynamics arguments. The calculated gross heat of formation for the *Cmca* phase of $MgNi_2H_3$ is −37.3 kJ/mol H_2. The stability of the orthorhombic crystal structure of $MgNi_2H_3$ is enhanced by the formation of the directional Ni–H covalent bonds supplemented by the electron transfer from Mg to both Ni and H. The Bader charge analysis indicates an electron transfer from Mg ($-1.59e^-$) to Ni ($+0.21e^-$), H1 ($+0.55e^-$) and H2 ($+0.31e^-$) [90].

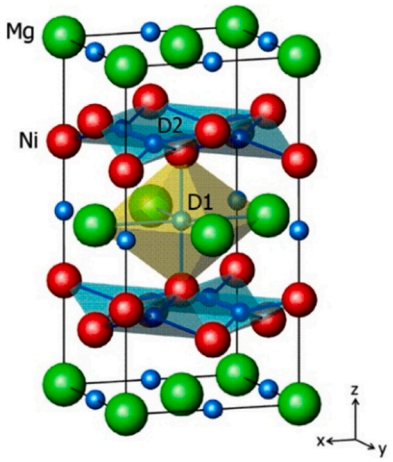

Fig. 12. Crystal structure of $MgNi_2D_3$. Two types of sites occupied by deuterium include a Mg_4Ni_2 octahedron for H1(D1) and a chair Ni_4 configuration for H2(D2) located within the buckled Ni–H nets containing bended spirals –Ni–H2–Ni–H2–. [89]. (Reproduced with permission from Elsevier.)

3.3.2. $MgCo_2$-H_2 and MgNiCo-H_2

$MgCo_2$ and MgNiCo crystallise with hexagonal Laves type intermetallic structures of the C14 type and do not form hydrides at ambient hydrogen pressures. However, applying high hydrogen pressures in the GPa range forces the hydrogen absorption and leads to the formation of multi-phase compositions, which contain approximately 2.5 atoms H per formula unit of $MgCo_2$ or MgNiCo and remain thermally stable under normal conditions. The hydrogenation of $MgCo_2$ results in its decomposition to a ternary Mg_2CoD_5 deuteride and metallic cobalt. In situ neutron powder diffraction study showed a complete recovery of the initial $MgCo_2$ intermetallic via a Hydrogenation-Disproportionation-Desorption-Recombination process on heating. At 300 °C, the Mg_2CoD_5 deuteride first decomposed to elementary Mg and hexagonal Co. At 400 °C, a MgCo phase was formed by interaction between Mg and Co. At the highest processing temperature of 500 °C, a solid-state interaction of MgCo and Co resulted in the recovery of the initial $MgCo_2$. The interaction of MgNiCo with deuterium under the synthesis conditions of 2.8 GPa and 200 °C proceeded in a more complex way. A very stable ternary deuteride $MgNi_2D_3$ was leached away while Co was separated in the form of Mg_2CoD_5 and the remaining nickel formed a solid solution with Co with the approximate composition $Ni_{0.7}Co_{0.3}$ [43].

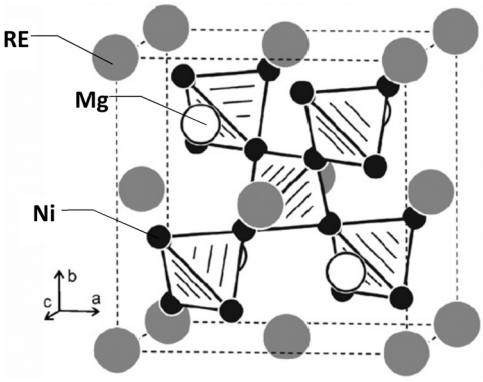

Fig. 13. The FCC crystal structure of the $REMgNi_4$ intermetalic alloy featuring an ordered replacement of half of the RE atoms by Mg atoms.
Adopted from [91].

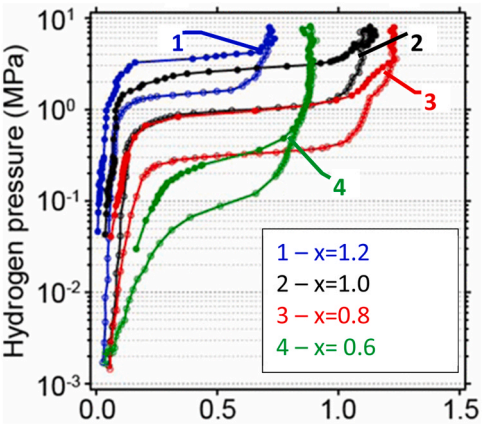

Fig. 14. PCT hydrogen absorption-desorption curves (323 K) measured for $Y_{2-x}Mg_xNi_4$ ($0.6 \leq x \leq 1.2$) alloys.
Adopted from [92].

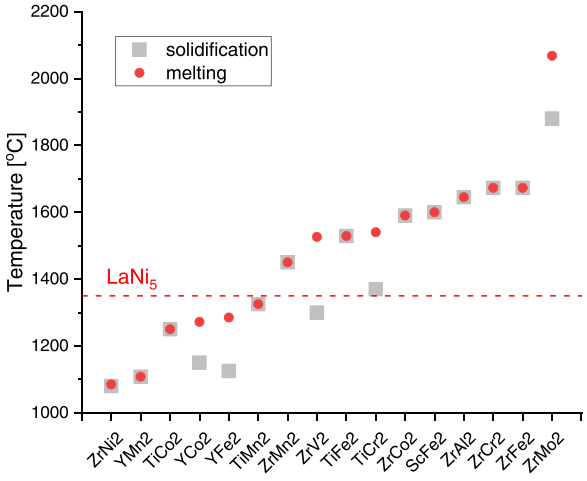

Fig. 15. Melting and solidification (for eutectoid or peritectoid intermetallics) temperatures for a series of binary Laves phases. The dashed line shows as a reference point the melting temperature of $LaNi_5$ [39].

3.4. Hydrides of Mg-containing $REMgNi_4$ and related alloys

Mg can replace RE in the C15 $MgCu_2$-type FCC Laves structures forming $RE_{2-x}Mg_xNi_4$ intermetallics. Following a replacement of RE by Mg or Ni, $MgCu_4Sn$ / $AuBe_5$ FCC superstructures are formed, and these are formed by an ordered filling by RE and Mg of the 8*a* sites of the initial structure, as for $PrMgNi_4$ shown in Fig. 13 as an example.

Magnesium content in the $RE_{2-x}Mg_xNi_4$ intermetallics can change in a broad range, between $0.6 \leq x \leq 1.2$ as for $Y_{2-x}Mg_xNi_4$. Increase of Mg content causes a gradual decrease of the unit cell parameter *a* reaching 0.83% when the composition changes from $Y_{1.4}Mg_{0.6}Ni_4$ to $Y_{0.8}Mg_{1.2}Ni_4$. The stability of the hydrides significantly decreases, while $P_{eq}(H_2)$ in the PCT diagrams increases by one order of magnitude when x increases from 0.6 to 1.2 (see Fig. 14) [92]. Hydrogen storage capacity is smaller for the intermetallics with the lowest and the highest content of Mg, while it reaches its maximum of 1.23 wt% H for $Y_{1.2}Mg_{0.8}Ni_4$ (see Fig. 14).

Compounds of light rare earth metals – $LaMgNi_4$ and $NdMgNi_4$ – reversibly absorb up to 4 hydrogen atoms per formula unit (at 7 bar H_2 and 323 K) which is equivalent to the hydrogen storage capacity of 0.99 wt.% H for the $NdMgNi_4$-based hydride [93]. When content of Mg in the La-based intermetallic alloy decreases (a continuous solid solution of Mg replacing La in $LaNi_2$ with the C15 structure exists from $LaNi_2$ to $La_{0.33}Mg_{0.67}Ni_2$), the alloys form pseudo-amorphous ($LaNi_2$) or well-crystalline for the magnesium-containing alloys hydrides. However, these hydrides are prone to a disproportionation into LaH_3, MgH_2 and Ni at increased temperatures [94].

In general, increased magnesium content in $RE_{1-x}Mg_xNi_4$ stabilises the alloys and makes possible a reversible cycling of hydrogen absorption and desorption which is suitable for H storage applications. However, hydrogen storage capacity remains relatively modest.

Hydrides of $REMgNi_4$ and $RE_{0.6}Mg_{1.4}Ni_4$ C15b Laves phase intermetallics (RE = La, Pr, Nd, Sm, and Gd) were studied in [95]. Their PCT diagrams contain one ($RE_{0.6}Mg_{1.4}Ni_4$) or two ($REMgNi_4$) plateaux with maximum storage capacities from 0.6 to 1.0 H/M.

Intermetallic compounds $LaMgNi_{3.6}M_{0.4}$ (M = Ni, Co, Mn, Cu, Al) form the hydrides with initial H storage capacity reaching 1.7 wt.% H. However, the hydrogen storage capacities of the alloys rapidly decrease with increasing the cycle number because of the H-induced amorphization. The discharge capacities of the hydrides used as anode electrodes of the metal hydride batteries decrease in the order Co > Ni > Al > Cu > Mn [96].

3.5. Ca-based Laves type intermetallics

3.5.1. $CaLi_2$

$CaLi_2$ C14 Laves type intermetallic shows a very quick hydrogen absorption kinetics, however, the hydrogenation is irreversible as the formed mixture contains CaH_2 and LiH with a storage capacity of 7 wt.% H. [97].

3.5.2. $CaMg_2$

$CaMg_2$ does not form a hydride at ambient temperature and hydrogen pressure. However, when Ni was added to partially replace Mg forming $CaMg_{1.8}Ni_{0.2}$ (C14 Laves phase structure remains), it absorbed 6.0 wt.% H at room temperature. $CaMg_{1.8}Ni_{0.2}$ decomposed into the hydrides of Mg and Ca on the hydrogenation, thus H storage is irreversible [98].

The mechanism of interaction has changed when small amount of La was introduced to form $(Ca_{0.8}La_{0.2})Mg_{2.2}Ni_{0.1}$. The latter alloy absorbed 5.1 mass% hydrogen with H/M ratio of 1.8. After the hydrogenation, the lattice of the Laves phase expands with the volume expansion of 13 %. The interstitial hydride of $(Ca_{0.8}La_{0.2})Mg_{2.2}Ni_{0.1}$ decomposed above 470 K following the temperature increase and hydrogen was released from the hydride above 610 K [98].

Because of irreversible hydrogen storage or too high decomposition temperatures, calcium compounds are not considered as a viable option for the applications in the reversible hydrogen storage.

4. Fundamentals of hydride formation by the Laves phase intermetallic compounds

4.1. Preparation routes

The preparation routes of Ti- and Zr-based AB_2-type hydride-forming Laves phase intermetallic compounds include conventional metallurgical (melting) and powder metallurgical (sintering, mechanical alloying) methods. The post-processing aimed at homogenisation of the alloys includes annealing, rapid solidification, and plastic deformation (cold rolling, equal channel angular pressing, high-pressure torsion). The methods of preparation and post-processing of hydrogen storage alloys based on Ti and Ti+Zr have been recently reviewed by Liang et al. [99].

Fig. 15 shows the melting and solidification temperatures of several binary Laves phases [39] which can form the hydrides either individually, or when modified to form substituted multi-component alloys. It is clearly seen that the melting temperatures for the

majority of the Laves phase alloys (mostly between 1500 and 1650 °C) is significantly higher than the melting temperature for the AB_5-type hydride-forming alloys (1350 °C for a typical representative, $LaNi_5$, as shown in Fig. 15). Thus, the preparation of the AB_2-type hydride forming Laves phase alloys is more demanding from the metallurgical point of view. Furthermore, specific difficulties are associated with high reactivity of the principal components (Ti, Zr), as well as high vapour pressures of some B-metals (Mn) [18].

For the small, up to 100 g, ingot sizes, the commonly used preparation method is arc melting of the alloy components in inert gas using non-consumable electrode and water-cooled copper hearth. The homogeneity of the ingots is achieved by their turning over and re-melting several times, and additional purification of the process atmosphere is provided by a pre-melting of a getter metal (e.g., Ti) [100–102].

For the larger ingot sizes (up to 100 kg), vacuum induction melting or induction melting in inert atmosphere is the most flexible and cost-efficient preparation method [29,103,104]. The main problem of this preparation route is a crucible – melt interaction resulting in the contamination of the product and shortening the crucible service time. The main ways to overcome this challenge include elimination of a contact of the melt with the wall of the cooled crucible (levitation melting), increase of the resistance of the crucible material to the interaction with the melt (for example, by using protective coatings), or application of crucible-less technologies like induction scull melting [104]. The modifications of the latter approach (e.g., plasma scull melting) are used for the large-scale manufacturing (up to 10 tons) of the AB_2-type hydrogen storage alloys [105]. The manufacturing routes also include pre-melting of several alloy components (e.g., Fe, V and Mn) to improve homogeneity of the final product. Adding deoxidiser (Mischmetal) to the charge is also necessary to reduce oxygen content thus improving the hydrogen storage performance. As it was shown in [106], the controlled introduction of oxygen (1.67 at.%) into C14-(Ti,Zr)(Mn,Ni,Cr,V,Fe)$_2$ reduces reversible H storage capacity due to formation of η-phase $(Ti,Zr)_4Fe_2O_{1-x}$ because of the formation of a stable hydride with smaller H storage capacity than the parent Laves phase. Introducing rare earth metal (La) into C14-(Ti,Zr)(V,Cr,Mn,Co,Ni,Al)$_{2-x}$ results in the formation of a LaNi secondary phase which significantly improves the activation performance and high-rate dischargeability and suppresses the formation of other Ti- and Zr-based secondary phases thus preserving high H storage capacity of the material [107]. Adding minor (below 1 at.%) additives of La, to (Ti,Zr)(Ni,Mn,V,Fe)$_{2\pm x}$ alloys has been shown to improve the performance of their hydrogen charge-discharge in gas-phase and electrochemical systems [108]. Studies of the alloys $Ti_{1.02}Cr_{1.1}Mn_{0.3}Fe_{0.6}RE_{0.03}$ (RE=La, Ce, Ho) showed appearance of the rare-earth oxides along with the major C14-type intermetallic. The increase of the unit cell volume of the latter phase by 0.3–0.4 % as compared to the pristine C14-$Ti_{1.02}Cr_{1.1}Mn_{0.3}Fe_{0.6}$ indicated a small solubility of the rare-earth component in the major C14 phase. The RE-modified alloys had a higher hydrogen storage capacity and lower hydrogen desorption plateau pressures than the pristine alloy [109,110].

Though Ti- and Zr-based hydrogen storage Laves phases do not contain significant amounts of expensive rare-earth metals, their costs can even extend the values for the RE-based AB_5-type alloys due to the metallurgical challenges of their preparation and use of expensive V along with high-purity Ti and Zr. The costs, however, can be decreased by a replacement of V with a less expensive Ferrovanadium and the use of Ti and Zr sponge instead of the bulk metals [18,29,105,111].

Along with metallurgical routes, several methods of direct preparation of the Laves phase hydride forming alloys from the oxide feedstock are of a special interest due to a potential cost decrease of the final product. The methods include metallothermic [105] and related routes [112], as well as electrochemical reduction of the mixture of oxides of the alloy components in a molten salt electrolyte [113].

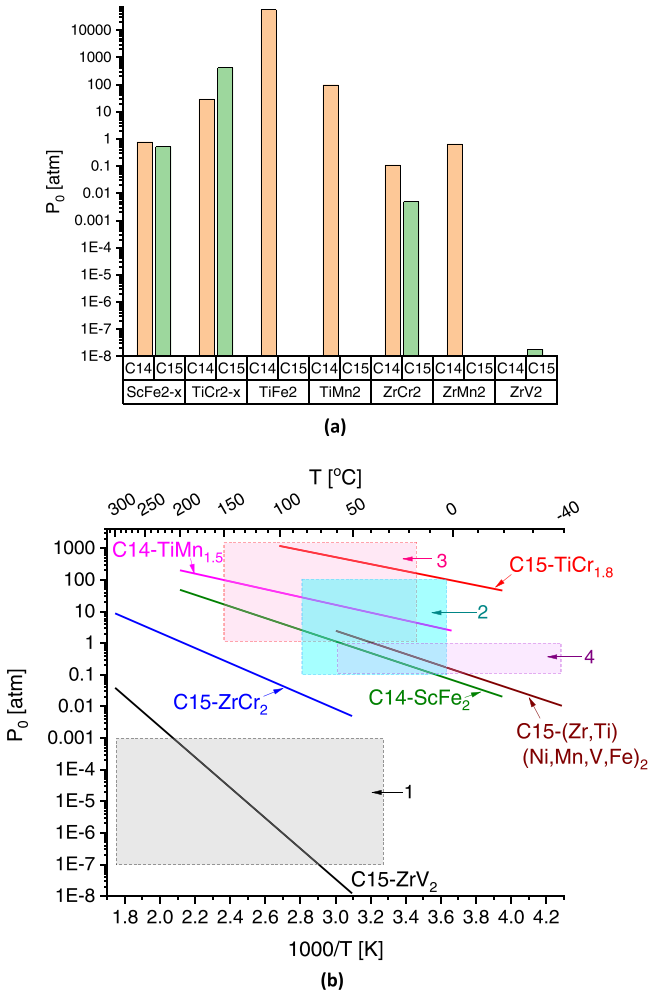

Fig. 16. (a): plateau pressures (H_2 desorption) for some binary Laves phase intermetallics at T = 323 K; $ScFe_{2-x}$ [118,119], $TiCr_{2-x}$ [120,121], $TiFe_2$ (simulated data) [122], $TiMn_2$ [46], $ZrCr_2$ [23,41,44], $ZrMn_2$ [53,55] and ZrV_2 [41,123]. (b): van't Hoff plots (H_2 desorption) for the selected binary Laves phases (see Appendix A for the detailed data). The coloured rectangular regions correspond to the operating conditions of the typical applications: **1** – hydrogen getters (T = 50–300 °C, P = 10^{-7}–10^{-3} bar H_2); **2** – hydrogen storage (T = 20–100 °C, P = 0.1–100 bar H_2); **3** – hydrogen compression (T = 15–150 °C, P = 1–1000 bar H_2); **4** – Metal Hydride Battery anodes (T = −40 – °60 C; P = 0.1–1 bar H_2).

Preparation of multicomponent Laves phase compositions containing a mixture of the components on both A and B sites has been successfully employed by Ovshinsky et al. [114] and proved to be efficient in achieving an advanced hydrogenation-dehydrogenation performance particularly when the applied alloys were used as the metal hydride anode electrodes of the Ni-MH batteries. Compositional and structural disorder is established in the MH materials on three different length scales through the use of elemental composition and processing techniques of alloys and electrodes. The length scales over which disorder is created can be designated as atomic, which comprises regions with dimensions up to a few nearest-neighbour atomic distances; intermediate range, regions from 10 to 20 nm extending up around 100 nm, and long range, with regions exceeding 100 nm. Disorder on each of these length scales is used to achieve different performance parameters of the hydrogen storage alloys.

The most efficient route allowing to control the phase composition, microstructure and, in turn, hydrogen sorption and electrochemical properties of the Laves phases is rapid solidification including melt spinning and gas atomisation. This preparation route allows to obtain very fine in size crystallites, reduce compositional segregation, and significantly improves performance of hydrogen

storage materials including reaching of high discharge capacity and cycle stability during their electrochemical applications [115–117].

4.2. Thermodynamics of interaction with H_2 gas

H_2 desorption plateau pressures (top; T = 50°C) and van't Hoff plots (bottom) for some representative binary Laves phases are shown in Fig. 16. Depending on the particular A and B constituents, equilibrium in H–AB_2 systems is reached at very variable pressure/temperature conditions, while the changes of the hydrogen equilibrium pressures cover incredibly high, nearly 10 orders of magnitude, range - from 10^{-6} to 10^3 bar H_2. Such great variations in the stability of the Laves phase-based hydrides allow selection of the compositions providing H_2 desorption pressure of 1 bar H_2 when used in the temperature range between 20 and 200 °C, thus being specifically suitable for their application in H_2 storage systems and as metal hydride battery anodes.

For the most promising studied AB_2 Laves phases where A=Zr, Ti, the strongest influence on the increase of the hydrides stability (i.e., decrease of the equilibrium pressure at a given temperature or increase of an absolute value of the hydrogenation enthalpy) was observed for ZrV_2 (A=Zr; B═V). Conversely, introduction of Ti on the A-side and Fe on the B-side results in a significant decrease of the hydride stability. An increase of the B/A ratio also decreases stability of the intermetallic hydrides, though this effect is less pronounced (see Fig. 7).

As suggested in [23], the origins of the variations of both stability and hydrogen storage capacity of the Laves-type hydrides include the atomic size effects, changes in electronic properties and a chemical affinity of the constituents to hydrogen. However, limited available at that time quantitative data did not allow a detailed analysis.

Subsequent systematic studies of hydrogen sorption properties of the Laves-type hydrides characterized the behaviours of hundreds of binary and multicomponent parent intermetallic compounds. Mostly, these studies were focused on [Ti,Zr]$B_{2\pm x}$ intermetallics with a hexagonal C14 structure, as such a type of the materials is the most flexible in tailoring the hydrogen storage performance to meet the specific requirements of the gas-phase applications [11,13,124]. In the recent years, the growing attention was also paid to the C15 cubic Laves phases which were shown to be particularly promising in applications as metal hydride anodes [13,36,125].

Significant attention has been recently paid to the application of the multi-principal element or high-entropy alloys (HEAs) as hydrogen storage materials. Indeed, HEAs frequently exhibit unusual hydrogen storage properties exceeding in H storage density the conventional hydrogen storage alloys [126,127]. HEAs frequently consist of several (5 and more) metallic components with atomic fractions between 0.05 and 0.35 and are characterised by the high values of entropy of their mixing exceeding 1.5 R= 12.47 J/(mol K) [128]. Quite frequently, HEAs form simple-phase solid solution structures (with, e.g., BCC type of structure) containing the components having strong affinities to hydrogen (Ti, V, Zr, etc.). Such alloys are characterised by a poor reversibility of the hydrogenation/dehydrogenation process, as thermal decomposition of their hydrides in vacuum or inert atmosphere takes place only above 200 °C that makes impossible many applications [129]. At the same time, some hydride forming HEAs may crystallise as Laves phase intermetallics. A recent example is a hydride of an equiatomic C14-type TiZrFeMnCrV alloy showing hydrogen equilibrium pressures above 0.1 bar at T > 30 °C [130]. We note that several hydride forming multi-component Laves phases studied by the authors of the present review are characterised by significantly lower hydride stabilities [29,70,125], though they were not called high-entropy alloys, but show high values of the mixing entropies of the components (12.1–14 J/(mol K)) that is close to or exceeds the above-mentioned HEA criterion of 12.47 J/(mol K). Consequently, these latter alloys belong to the Laves-type hydride-forming HEAs.

Further details on the analysis of interrelation between the composition and thermodynamics of the interaction in the systems of H_2 gas with the Laves-type intermetallics are presented in this review later.

4.3. Kinetics of interaction with H_2 gas

When properly activated, Laves-phase intermetallics are characterised by very fast hydrogen absorption / desorption kinetics, with characteristic reaction time between ca 10 s and 10 min and activation energies of hydrogen absorption-desorption been in the range 20–40 kJ/ mol H_2 [18,131–134].

A recent detailed study on the kinetics of interaction of hydrogen gas with the Ti/Zr-based Laves phase alloys [135] was focused of the kinetics study of $Ti_{0.15}Zr_{0.85}La_{0.03}Ni_{1.126}Mn_{0.657}V_{0.113}Fe_{0.113}$ alloy, containing additions of La for the improvement of the activation performance and the cycling stability. The alloy was selected based on in-house research performed at IFE on $AB_{2\pm x}$ C15 Laves-type alloys for their application as hydrogen storage and battery electrode materials. Studies of hydrogen absorption and desorption kinetics in this C15 type Laves type alloy were performed using a single-step and stepwise H_2 absorption-desorption methods. The kinetics modelling used a generic Johnson-Mehl-Avrami-Kolmogorov (JMAK) model approach which has been advanced by introducing pressure- and temperature-dependent rate terms describing the phase-structural transformations during the hydrogenation and dehydrogenation. The overall rate constant considered contributions of a pressure-dependent term K(P) and a temperature-dependent term K(T) into the rate of the process K = K(P)*K(T). The temperature-dependent rate constant shows a well-known classical Arrhenius type dependence while the pressure-dependent term is directly related to the mechanism of transformation during the hydrogenation/dehydrogenation and varies as related to the rate limiting step of the process. As both hydrogen absorption and desorption proceed faster with increasing temperature the temperature rate term K(T) also increases. The modelling showed excellent agreement between the experimental data and fitting results.

The modelling shows that the reaction follows the Johnson-Mehl-Avrami-Kolmogorov (JMAK) model, with the value of exponent n = 1–1.25 for the H_2 absorption and 1 for the H_2 desorption. This concludes that the rate-limiting hydrogen absorption and desorption steps are jointly governed by hydrogen diffusion and grain boundary nucleation of alpha-solid solution and beta-hydride. The activation energies for both hydrogen absorption and desorption decrease along with increasing hydrogen content in the hydride.

4.4. Structure – H storage properties relationship

Laves type hydrides belong to the IMC hydride structures formed by "isotropic" expansion of the unit cells of the initial alloys on their hydrogenation. Crystal structures of the Laves type intermetallic alloys, independent of their type - C14/C15/C36 – all contain three types of tetrahedral interstitial sites, A_2B_2, AB_3 and B_4. Their relative numbers are always 12 (A_2B_2): 4 (AB_3): 1 (B_4) per formula unit of AB_2. If all available sites will be occupied by H atoms, the maximum H storage capacity will reach AB_2H_{17}. This never happens because H atoms cannot simultaneously occupy the tetrahedra sharing common triangular sides, and because of that the $A_2B_2/AB_3/B_4$ sites are filled partially and statistically (as the blocking of the occupancy of the neighbouring sites is taking place) or in an ordered way when some sites are preferably filled to achieve the shortest H…H separation longer than 1.8–2.0 Å and a decrease in the symmetry of the crystal lattice takes place because of that.

When the metal lattice expands because of hydrogen absorption, the filling of the particular tetrahedral interstitials takes place as

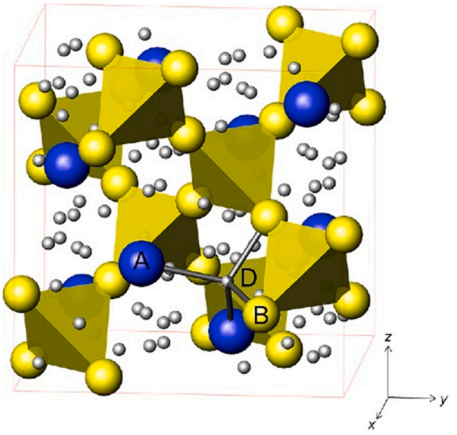

Fig. 17. The crystal structure of the cubic $AB_2D_{2.9}$ deuteride [142]. D atoms partially fill 96*g* sites are shown as small spheres. A, B and D represent Zr/Ti/V (8*a*), Ni/Mn/Fe/V (16*d*), and D atoms, respectively. A spatial framework of the B_4 tetrahedra is shown. (Reprinted with permission from Elsevier.)

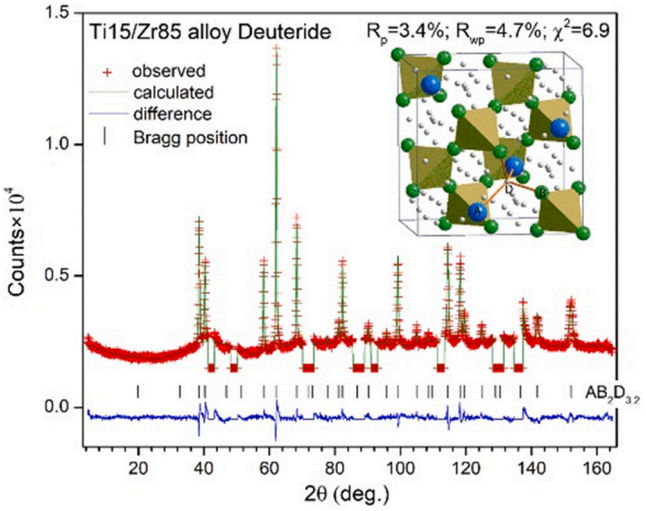

Fig. 18. Whole profile Rietveld refinements of the neutron powder diffraction pattern of the Ti15/Zr85 alloy deuteride $AB_2D_{3.2}$ [71], The peaks of the stainless-steel sample container were eliminated from the refinements. Neutron diffraction pattern were measured in situ at D_2 pressure of 5 bar. Insert: The crystal structure of the FCC $AB_2D_{3.2}$ deuteride. A, B, and D represent Ti/Zr/V (8*a*), Ni/Mn/Fe/V (16*d*), and D(H) (96 g) atoms, respectively.

soon as they become larger in size than 0.4 Å (then the distances Me-H for each of the metal atoms in the surrounding of the occupied by H interstitial sites become larger than $d_{Me-H} - r_{Me} \geq 0.4$ Å).

Hydride structures based on the Laves phases of composition $(Sc,Ti,Zr)T_2$ (T = transition metal of the first row) with the $MgCu_2$, $MgZn_2$ and $MgNi_2$ structure types share common features [42,136–142]. Neutron diffraction studies showed that the A_2B_2 tetrahedral sites with maximum number of A atoms in their surrounding are first filled by H atoms. When the hydrogen content in the hydrides does not exceed $H/AB_2 = 3.2$, the A_2B_2 sites are the only ones being occupied by H atoms ($TiFe_{1.16}V_{0.84}D_{2.1}$ [136], $ZrMoFeD_{2.6}$ [137], $ZrCr_2D_{3.5}$ [138], λ_1-$ScFe_2D_{2.5}$ [139], λ_3-$ScFe_2D_{2.9}$ [140], λ_2-$ZrV_2D_{1.5}$ [141], $ZrFe_{1.98}Al_{0.02}D_{2.9}$ [42], $(Ti,Zr,V)(Ni,Mn,Fe,V)_2D_{2.9}$ with Ti/Zr= 0.2/0.8 [142], $(Ti,Zr,V)(Ni,Mn,Fe,V)_2D_{3.2}$ with Ti/Zr= 0.15/0.85 [71]). One typical example of such a structure – the structure of the $(Ti,Zr,V)(Ni,Mn,Fe,V)_2D_{2.9}$ C15 type deuteride is shown in Fig. 17 [142]. Fig. 18 shows that an excellent agreement has been reached during the Rietveld full-profile refinements of the neutron powder diffraction pattern of the $(Ti,Zr,V)(Ni,Mn,Fe,V)_2D_{2.9}$ deuteride measured for a crystal structure model assuming an exclusive filling of the A_2B_2 sites at D_2 pressure of 5 bar.

When the hydrogen content is close to reaching a saturation limit, the hydrogen atoms also become accommodated in the AB_3 and B_4 interstices, which are smaller in size and less suitable for the accommodation of H because of their surrounding (less A component). Thus, in the $ZrV_2D_{2.8}$ deuteride [141], a partial filling of the ZrV_3 interstices (5 % of the total number of D atoms) was observed. In the $ZrV_2D_{4.5}$ deuteride, the main part of the deuterium atoms in excess of the composition $D/ZrV_2 = 2.8$ is located in the ZrV_3 interstices, and this raises the fraction of filled ZrV_3 interstices up to ~ 1/3. The reason for this may be in the expansion of the unit cell up to a = 7.68 Å, which causes the calculated values of the radii of the ZrV_3 interstices to exceed 0.4 Å (for $ZrV_2D_{2.8}$: a ~ 7.77 Å). This creates chemical conditions suitable for the formation of a stable metal hydride: $d_{M-i} > r_M + 0.4$ Å [143].

For the C14-type $ZrVFeD_{3.6}$, $ZrVCuD_{4.0}$ and $ZrVNbD_{5.4}$ deuterides [144], in addition to the preferentially occupied $Zr_2(V,T)_2$ interstices, their structures contain partially filled $Zr(V,T)_3$ and $(V,T)_4$ interstices: 3% and 0%, 4% and 7%, 3% and 0%, respectively, of the total hydrogen content. In this case all filled interstices also have radii exceeding 0.4 Å.

Ordering of hydrogen atoms in the C15 type Laves type hydrides is taking place when lowering the temperature. Various types of ordering have been systematically reviewed in [145]. Below and including hydrogen content of 4 at.H / f.u. tetrahedra A_2B_2 are filled. However, for $ZrTi_2D_4$ only $ZrTi_3$ tetrahedra are completely filled at low temperatures 11–300 K [145], while a trend of populating 96 *g* sites at the expense of 32*e* sites persists at high temperatures [146]. When the maximum hydrogen storage capacity of 6 at. H / f.u. ZrV_2 is reached in the ordered structure of ZrV_2H_6, it is described as 3 at. H in Zr_2V_2 + 3 at. H in ZrV_3 showing an equal overall ordered filling of these sites by H atoms [147].

4.5. Activation, poisoning tolerance and pyrophoric properties

The activation of the Laves AB_2-type hydride forming alloys is generally more difficult than that for the AB_5-type ones but easier than that for the TiFe and its derivatives. The alloys based on A=Zr and B=Mn can be activated without vacuum heating while addition of Ti to the A-side and Cr to the B-side results in hardening of the activation conditions requiring an increase of the activation temperature and/or long-time exposure of the virgin alloys to the high-pressure hydrogen [18].

Surface analysis of the commercial AB_2-type alloy ($Ti_{0.96}Zr_{0.04}Mn_{1.43}V_{0.45}Fe_{0.08}$; Japan Steel Works) showed [148] that after a long-term exposure to air its surface was completely oxidised to form a 15 nm-thick layer consisting of TiO_2, $MnO/Mn_2O_3/Mn_3O_4$ and VO_2; the layer was enriched by the segregated manganese oxides. The air-exposed alloy activated by 4–5 cycles of vacuum heating to 120 °C followed by an exposure to hydrogen at 18 bar pressure and T = 0 °C absorbed up to 2.7 at. H per formula unit in 10–15 min. During such processing, the alloy flakes disintegrate into a fine powder, with the particle size of ~20 μ. The powder was found to be highly pyrophoric and sensitive to oxygen as re-activation of the material shortly exposed to air (P = 0.1 bar at RT for 3 min) did not allow to achieve H sorption capacity higher than 0.7 at. H/f.u.

There is a lack of the reported data describing pyrophoric properties of the Laves phase hydrides. At the same time, it was noted that the activated AB_2-type alloys rich in Zr and Mn are highly pyrophoric, in contrast to the Ti- and Cr-rich alloys [18].

Recent XPS studies of Ti–Zr–Fe alloys (33.3–50 at.% Fe, 25–28.6 at. % Zr) which form under-stoichiometric C14-$(Zr,Ti)(Fe,Ti)_2$ major phases and additionally contain minor phase of $(Ti,Zr)_2Fe$ [149], showed a preferential surface oxidation of Zr and Ti. The authors assumed a formation of a mixed oxide of Zr, Ti and Fe which may

facilitate initial activation of the hydrogen uptake. Indeed, the alloys could be easily hydrogenated at room temperature and P = 30 bar. We note that observed effect can be caused by the phase identified in [149] as $(Ti,Zr)_2Fe$ having the Ti_2Ni-type structure which is stabilised by oxygen (η-$(Ti,Zr)_4Fe_2O_{1-x}$) and facilitates hydrogenation reactions in the H – AB_2 systems [106].

Degradation of hydrogen sorption performance of (Zr,Ti)(Ni,Mn,VFe)$_2$ intermetallic when operating in hydrogen contaminated by water vapours was eliminated by doping the pristine alloy with 1 at% La [150].

Significant improvement of the activation performance and poisoning tolerance of the Laves phases (A=Ti, Zr) during their gas-phase or electrochemical H charge can be achieved by the surface modification including hot alkaline treatment [151], fluorination [152], or coating with Platinum Group Metals including Pd and its alloys [153,154].

4.6. Electrochemical hydrogenation / dehydrogenation performance

Recent studies of the Zr- and Ti- containing Laves-type intermetallics [36,71,108,125,142,155–157] showed their excellent high rate performance with electrochemical storage capacities reaching 495 mAh/g and possibilities to optimise electrochemical behaviours as related to a) Type of structure - C15/C14; b) Ratio between Zr and Ti; c) Selection of chemical composition of B (Mn, Ni, Fe, V, Sn, Al) and B/A ratio; d) Presence of catalytic additive - small amounts of La promoting an easy activation of the alloys; e) Metallurgical route of the alloy's preparation with benefits of increased H diffusion rates created by the rapid solidification processing of the alloys.

5. Statistical data analysis for the Laves phase based hydrides

Large volume of the accumulated to date experimental data strongly motivates a need for establishing the regularities in an interrelation between the alloy's composition and its hydrogenation/dehydrogenation properties. One prospective approach is based on the statistical analysis of the data for the $AB_{2\pm x}$ Laves phases and has been applied in the early studies [29], [70], [112], [158], [159]. This approach has been further developed during analysis of the data in the present review. The results are presented in the current section.

5.1. Input information and data processing

The reference data describing the properties of the $AB_{2\pm x}$ hydride-forming intermetallics, all introduced into the Microsoft Access database, included:

- Type of intermetallic alloy – C14 or C15.[1] For the multiphase materials, their classification is based on the type of the majority phase, while the other (minor) phase constituents are all specified as well.
- Elemental composition. If available, the data on the elemental analysis (by EDX or other relevant techniques), instead of the target alloy composition, were used in the database. The compositions were normalised as $[A1_{x1}A2_{x2}\ldots](B1_{y1}B2_{y2}\ldots)_z$, where the elements in square brackets represent A components, the elements in round brackets – the B ones, the values of x_i and y_i represent atomic fractions of the i-th A and B-component, respectively, and $z = \frac{n_B}{n_A}$ (see Tables A.1, A.2).
- Specific unit cell volume, V_0, for the parent intermetallic per one formula unit of AB_2 (crystallographic unit cells contain 4 f.u. for C14 and 8 f.u. for the C15 types intermetallics).

[1] As only a very few reference publications describe hydrogen storage properties of C36 Laves phases, these data were not considered during the analysis.

Table 2
Summary information in the database of hydride-forming Laves phase intermetallics (see Tables A.1, A.2 of the Appendix).

Modification	*Number of entries*		
	All	*Single phase*	*Accounted during regression analysis*
C14	275	238	230
C15	67	52	44
Total	342	290	274

- Maximum hydrogen content in the intermetallic hydride in H atoms per one metal atom in the $AB_{2\pm x}$ unit.
- Relative volume increase upon hydrogenation, $\Delta V/V_0$.
- Absolute values of the standard hydrogen desorption enthalpy (ΔH^o) and entropy changes (ΔS^o).
- Hysteresis energy loss, $RT\ \ln(P_A/P_D)$ where indexes A and D are related to H_2 absorption and desorption, respectively.
- Plateau slope, $d(\ln P_D)/d(H/M)$.

In case the original data for the thermodynamic parameters, ΔH and ΔS, were given at different H concentrations, the values included in the database were taken for the plateaux midpoint. When numerical data on hydrogen sorption properties were not given, they were obtained by digitalising the original figures showing pressure – composition isotherms. The values for hysteresis were taken from H absorption/desorption isotherms at the lowest experimental temperature, while the plateau slope was deduced from the desorption isotherms taken at the temperature closest to the ambient conditions (300 K).

The corresponding data are summarised in the Table 2 and are presented in Tables A.1 and A.2 (Appendix A).

The correlations between the composition and hydrogen sorption properties were deduced by the applying a linear regression equation:

$$Y = A_0 + \sum_{i=1}^{n} A_i X_i \tag{7}$$

where Y is a response parameter, X_i are the atomic fractions of the i-th component ($i = 1.n\text{-}1$). The fractions for the A- and B-components were considered separately. In doing so, one component from both A- and B-side was considered as belonging to a "base" AB_2 intermetallic for which the fraction balanced other fractions of the A- and B-components to yield 1 in total, and the calculated response parameter Y was equal to A_0. For example, when considering C14 intermetallics (A=Ti,Zr; B=Al,Co,Cr,Cu,Fe,Mn,Mo,Ni,V,W), the "base" was assumed to be $TiMn_2$, so as:

$$X_{Ti} = 1 - X_{Zr};$$
$$X_{Mn} = 1 - X_{Al} - X_{Co} - X_{Cr} - X_{Cu} - X_{Fe} - X_{Mo} - X_{Ni} - X_V - X_W \tag{8}$$

For C15 intermetallics, the "base" intermetallic was assumed as $ZrFe_2$ where the fractions X_{Zr} and X_{Fe} were calculated similar to Eq. (8). In other cases (e.g., for common datasets C14 +C15), $TiFe_2$ was selected as the "base".[2]

The n-th independent variable in Eq. (7) was a deviation of B/A ratio from the exact AB_2 stoichiometry:

$$X_n = \frac{n_B}{n_A} - 2 \tag{9}$$

where n_B and n_A correspond to the sums of the stoichiometric coefficients in the formula.

[2] Selection of the "base" intermetallic does not significantly influence the fitting results but it allows to exclusively use independent composition variables. It also provides clarity of the free term (A_0) of Eq.(7) ascribing it to the response parameter Y which corresponds to the "base" intermetallic composition.

Table 3
List of the composition-dependent variables in the database of hydride-forming Laves phases. The shaded boxes contain the variables accounted during the regression analysis.

Type	*Component*	*C14*			*C15*			*Total # of entries*
		Entries	*Xmin*	*Xmax*	*Entries*	*Xmin*	*Xmax*	
A	Sc	2	0.50	1.00	3	0.20	1.00	5
	Ti	37	0.05	1.00	6	0.15	1.00	43
	Y	0	-	-	6	0.09	0.39	6
	Zr	36	0.01	1.00	13	0.20	1.00	49
B	Al	16	0.00	0.40	9	0.03	0.20	25
	Co	17	0.02	0.75	6	0.08	0.12	23
	Cr	81	0.02	1.00	2	0.1	1.00	83
	Cu	6	0.00	0.29	1	0.10	0.10	7
	Fe	78	0.02	1.00	23	0.06	1.00	101
	Mn	97	0.05	1.00	8	0.09	0.33	113
	Mo	8	0.01	0.50	0	-	-	9
	Ni	34	0.05	0.65	8	0.10	0.56	42
	Sn	6	0.00	0.01	1	0.01	0.01	7
	V	53	0.02	0.52	9	0.02	1.00	62
	W	3	0.01	0.05	0	-	-	3
	$\frac{n_B}{n_A} - 2$	68	-0.50	1.80	21	-0.20	0.50	89

During the regression analysis of the composition – properties relationships, in most cases the data for the single-phase intermetallics were taken (second column of Table 2). Furthermore, the entries containing less than 3 different composition-dependent parameters for the parent intermetallic (*X min* and *X max* correspond to the minimum and maximum values of the variables X_i in Eq.(7) – see Table 3) were omitted. The resulting number of entries accounted in the regression analysis is presented in the Table 2 (third column).

5.2. General statistics

Fig. 19 shows statistical data for a complete dataset of the hydride-forming Laves phases presented as histograms of the particular hydrogen sorption properties.

The maximum hydrogen capacity, see Fig. 19(A), mostly varies between 0.5 and 0.6 and 1.2–1.3 $(H/M)_{max}$ with the highest number of entries being between 0.8 and 1.2. Please, note that pressure – temperature conditions of the hydrogenation experiments affect the data and should be consulted in the reference works for the details (see end notes (1) and (2) to Tables A.1 and A.2, respectively). The highest maximum H concentration (H/M=1.6–2.0) was observed for C15-ZrV_2 [41,123,147].

Typical volume expansion of the crystal lattice on the hydrogenation of the Laves type intermetallics is 20–25% volume (Fig. 19B). Most frequently this is equivalent to 2–4 Å^3/at.H for both C14 and C15 intermetallics. Please, note that for some of the hydrides no reliable data is available because of the experimental challenges when performing the X-ray diffraction experiments for the unstable hydride samples releasing hydrogen at ambient conditions.

Both maximum H storage capacity and the relative volume increase upon the hydrogenation are characterised by a Gaussian distribution of the histograms data.

The distributions of the data on hydrogenation enthalpies and entropies show maxima in the ranges 19–29 kJ/mol H_2 and 90–120 J/(mol H_2 K), for ΔH^o and ΔS^o, respectively. The enthalpy distribution histogram (Fig. 19C) can be satisfactory fitted by a logarithmic normal distribution while the entropy one (Fig. 19D) is well described by the Weibull distribution.

A rather surprising fact is that for many of the studied systems the hysteresis appears to be close to zero. This is because many H – AB_2 systems have low critical temperatures (see below), and when the data for the studied systems are collected at the temperatures close to or exceeding the critical temperature, the hysteresis vanishes.

The histograms of the data on hysteresis (Fig. 19E) and plateau slope (Fig. 19F) can be characterised by the Weibull and logarithmic normal distributions, respectively.

5.3. Composition-dependent thermodynamics of H – $AB_{2\pm x}$ interaction

The interrelation between the stability of the multicomponent intermetallic hydrides and composition of the parent alloys was analysed already in 1970 s. Miedema et al. [160,161] proposed a simple to apply "rule of reversed stability" (related to the Hess law) when the enthalpy of the formation of a ternary hydride, $AB_nH_{2\,m}$, can be calculated as a sum of the formation enthalpies of the binary hydrides of its components minus the enthalpy of the formation of the parent intermetallic compound, AB_n:

$$\Delta \boldsymbol{H}(\mathbf{AB_nH_{2m}}) = \Delta \boldsymbol{H}(\mathbf{AH_m}) + \Delta \boldsymbol{H}(\mathbf{B_nH_m}) - \Delta \boldsymbol{H}(\mathbf{AB_n}). \quad (10)$$

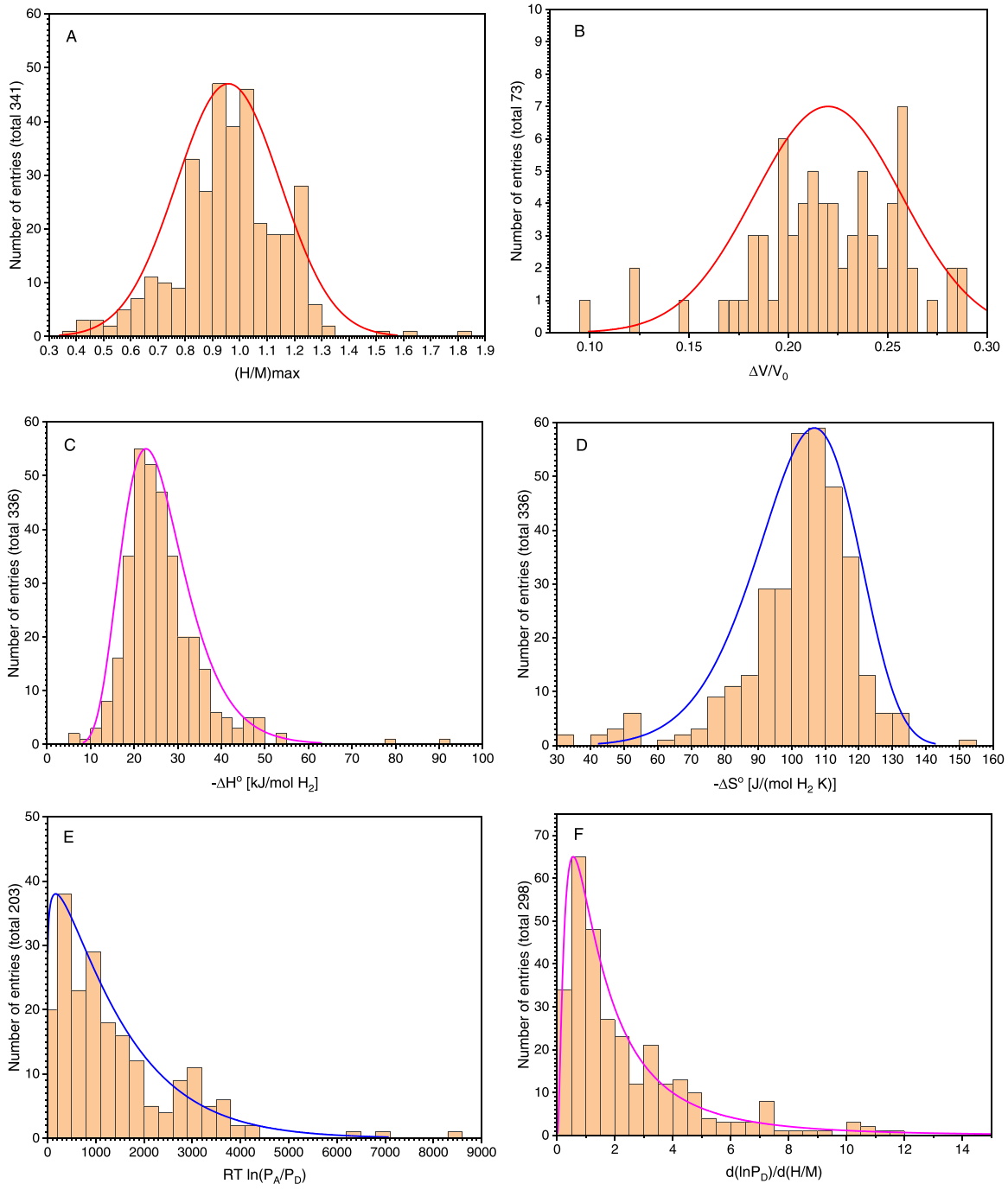

Fig. 19. Distribution histograms of maximum hydrogen concentration (A), volume increase upon hydrogenation (B), hydrogenation enthalpy (C) and entropy (D), hysteresis (E) and plateau slope (F). The estimated distribution functions are shown as lines: normal / Gaussian (red), logarithmic normal (magenta) and Weibull (blue). (For interpretation of the references to colour in this figure legend, the reader is referred to the web version of this article.)

Application of Miedema's model [162–164] results in reaching a qualitative agreement between the model predictions and the experimental data on the stabilities of the Laves type AB_2 alloys [23,44,165]. The related "imaginary binary hydrides" model [162] is also able to predict the hydrogen site occupancies from which are derived the hydrogen sorption capacities [163].

However, the quantitative correlations do not appear to be equally successful. Indeed, an application of the Miedema's model to quaternary Laves phases $(Zr,Ti)(Cr,Fe)_2$ [166] showed discrepancies between the reference data and the calculation results, $(|\Delta H_{CALC}| - |\Delta H_{EXP}|)/|\Delta H_{EXP}|$, ranging between −21 and +15%. These discrepancies correlate with the values of $|\Delta H_{EXP}|$ (see Supplementary Information, Fig. S1).

The main reasons for the discrepancies between the experimental data and the model predictions include (i) Uncertainties in the values of the formation enthalpies for the unstable binary hydrides of the B-components and (ii) Incomplete breaking of the A–B bonds in the intermetallic hydrides which normally have the structure closely related to the original metallic matrix. The latter aspect can be accounted by utilising a more general form of the Eq. (10):

Table 4
Fitting results for Ts= $\Delta H^o/\Delta S^o$ for the single-phase C14 and C15 intermetallics with Eq. (7).

C14			C15		
Component type	Fitted Coefficient		Component type	Fitted Coefficient	
	Variable	Value		Variable	Value
–	A_0:*Y* ($TiMn_2$)	182.86	–	A_0: *Y* ($ZrFe_2$)	161.71
A	A_1: X_1(Zr)	221.12	A	A_1: X_1(Sc)	153.96
B	A_2: X_2(Al)	203.35		A_2: X_2(Ti)	-158.62
	A_3: X_3(Co)	-172.41		A_3: X_3(Y)	308.83
	A_4: X_4(Cr)	38.05	B	A_4: X_4(Al)	456.55
	A_5: X_5(Cu)	205.90		A_5: X_5(Mn)	257.28
	A_6: X_6(Fe)	-149.84		A_6: X_6(Ni)	74.90
	A_7: X_7 (Mo)	-47.86		A_7: X_7(V)	718.07
	A_8: X_8(Ni)	-125.76	–	A_8: X_8 (n_B/n_A-2)	-31.40
	A_9: X_9(V)	312.35			
	A_{10}: X_{10}(W)	-760.66			
–	A_{11}: X_{11}(n_B/n_A-2)	-75.12			
Number of points		230	*Number of points*		44

$$\Delta H(\mathbf{A_xB_yH_{u+v}}) = \frac{x}{x+y}\Delta H(\mathbf{AH_u}) + \frac{y}{x+y}\Delta H(\mathbf{BH_v}) - (1-F)\cdot\Delta H(\mathbf{A_xB_y}) \quad (11)$$

Here *F* depends on the number of A–B bonds which correlates with a *y*/*x* ratio [164]. In other words, the enthalpy of the formation of the multicomponent intermetallic hydride is assumed to be proportional to the sum of the formation enthalpies of the existing or expected to be formed hydrides of its components multiplied by their atomic fractions in the intermetallic alloy.

Other not accounted by the Miedema model factors are related to the structural features of the intermetallic structure as a potential host to accommodate hydrogen atoms. These include criterium of minimum interstitial hole size suitable to be occupied by H atoms and a lower limit of the H–H distances in the structures of the hydrides [167], the decrease of the hydride stability with the decrease of the unit cell volume [165], as well as the factors describing the electronic structure of the parent intermetallics and their hydrides [168–171].

As it can be seen from the data listed in the Tables A.1 and A.2, the formation entropies of the Laves phase hydrides exhibit significant deviations from the "ideal" value of −130.52 J/(mol H_2 K) which corresponds to the standard entropy change for molecular hydrogen when transformed into atomic H and was adopted during the estimations of the hydride stability in the reference publications [160–164].

As is well known, in the plateau region of the Me-H phase diagram, the equilibrium between the H_2 gas and the mixture of α-solid solution in the metal matrix and β-hydride can be determined by the change of the standard Gibbs energy, ΔG^o, during the α–β transition [172][3]:

$$\Delta G^o = \Delta H^o - T\Delta S^o = RT\ln P_0, \quad (12)$$

where P_0 is the plateau pressure [atm] received using the van't Hoff equation by a division of both sides of Eq. (12) by *RT*:

$$\ln P_0 = \frac{\Delta G^o}{RT} = -\frac{\Delta S^o}{R} + \frac{\Delta H^o}{RT} \quad . \quad (13)$$

As a complimentary approach, Kojima et al. considered a contribution of strain energy originating from the H atoms-induced lattice expansion into the Gibbs free energy of the solid during the hydride formation. They showed that ΔG^o (or $\ln P_0$ at T = Const) is directly proportional to the bulk modulus of the initial intermetallic compound and to its reciprocal unit cell volume [26,173].

Application of the above-mentioned approaches to the quantification of the composition – stability relationships in the Laves phase hydrides is not simple as it requires knowledge of the several input parameters which are frequently not known and are taken as rough estimates only. This includes the value of the bulk modulus of intermetallic compound which is approximated as a weighted sum of bulk moduli of its components; this simplified approach results in underestimations in a range from 7.3 % to 15.3 % when comparing the experimentally determined values and approximation results [26]. As a result, the modelling of the stabilities of intermetallic hydrides which utilises stabilities of the binary hydrides of the components of the parent intermetallic, bulk moduli and unit cell volumes, as well as the combination of these factors yields rather poor agreements with the data. Further details can be found in Supplementary Information (Section S2).

Thus, it would be useful to analyse the composition – stability correlations empirically, by using a regression analysis of a vast in its volume reference data collected during the last five decades (Tables A.1, A.2).

Direct processing of the data on the hydrogenation enthalpy (Y=−ΔH^o) by Eq. (7) and, particularly, on entropy (Y=−ΔS^o), yields a rather poor correlation with the reference data as the squared Pearson correlation coefficients (R^2) appeared to be 0.7 and 0.4 for ΔH^o and ΔS^o, respectively (see example in Supplementary Information; Table S1 and Figs. S5, S6).

In contrast, fitting of the Y= $\Delta H^o/\Delta S^o$ ratio, which is equal to the temperature *Ts* corresponding to the equilibrium plateau pressure of 1 atm, yields very good results (see Table 4, Fig. 20[4]), as the Pearson correlation coefficient between the calculated and reference data (linear fit) exceeds 0.99. This feature is related to the frequently discussed issue concerning enthalpy – entropy correlation in the metal–hydrogen systems [11], which is manifested by the disappearance of the difference in the changes of the hydrogenation Gibbs energy for the bulk and nanostructured materials at Ts= $\Delta H^o/\Delta S^o$ [174].

If to consider hydride formation as a first-order phase transition, the values of ΔH^o, ΔS^o and *Ts* can be considered as the latent heat, entropy and temperature of the transition at a standard pressure (1 atm).[5] Equilibrium of the phase transformation is described by the following equation [175]:

$$\Delta H^o = Ts\Delta S^o \quad (14)$$

[3] Here and below, we consider the quantities ΔG^o, ΔH^o and ΔS^o as the values at the standard temperature (298 K) per 1 mol H_2. Accordingly, ΔG^o is equal to the chemical potential of the reaction (1a) where M is α-solid solution of hydrogen in the parent metal.

[4] The labelled points in Fig. 17 and Fig. 18 correspond to the intermetallics exhibiting minimum ($TiFe_2$) and maximum (ZrV_2) values of $\Delta H^o/\Delta S^o$, as well as C14 Laves phases which showed maximum deviations from the general trend.

[5] This is an approximation as ΔH^o and ΔS^o correspond to a standard temperature (298 K), while the temperature dependence of the ΔH and ΔS should be considered for the accurate calculations.

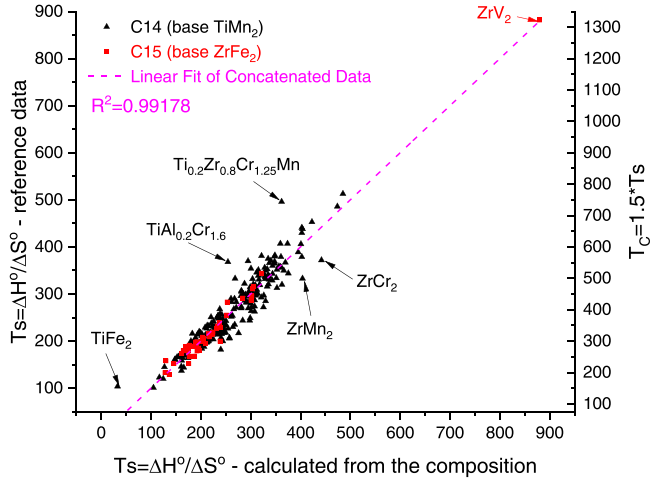

Fig. 20. Comparison of results of the regression analysis (Eq. (7)) for single-phase C14 (black triangles) and C15 (red squares) intermetallics assuming Y= $\Delta H^o/\Delta S^o$ with the data taken from the references. The trend line was calculated for the overall dataset.

and

$$Ts = \frac{\Delta H^o}{\Delta S^o} \quad (15)$$

Recently, Zhou et al. [176] showed that the values of *Ts* for the systems of hydride-forming metals and intermetallics with H_2 gas well correlate with their critical temperatures, T_C, according to the empirical Guldberg rule for liquids where *Ts* defines the boiling point at 1 atm.:

$$T_C = 1.5Ts \quad (16)$$

The established correlation $Ts = \Delta H^o/\Delta S^o$ (Table 4, Fig. 20) when combined with Eq. (16) is very useful for the estimation of the critical temperatures for the H–$AB_{2\pm x}$ systems in case the experimental measurements are difficult. Analysis of the data of Fig. 20 shows that in most cases the values of *Ts* vary between 150 and 360 K that gives the range of critical temperatures T_C= 225–540 K. Thus, the critical temperatures for the H_2 interaction with $AB_{2\pm x}$ Laves phases are significantly lower than the T_c for the AB_5-type intermetallics [177] indicating that attractive interactions between the H atoms filling the interstitials in the structure of the parent intermetallic compounds are weaker [178].

The influence of the compositional parameters, i.e., type of the components and n_B/n_A ratio, on $Ts = \Delta H^o/\Delta S^o$ shows the following dependencies (see the data of the Table 4 for further details):

- For the C14 type intermetallics, the influence of the elemental composition on the decrease of *Ts* and, in turn, critical temperature, T_C, is strengthened in a series Mo < (n_B/n_A-2) < Ni < Fe < Co < < W. In turn, *Ts* and T_C increase in a series Cr < < Al≈Cu≈Zr < V.
- For the C15 type intermetallics, the decrease of *Ts* and T_C is caused by the increase of (n_B/n_A-2) and, to a larger extent, by the changes in the atomic fraction of Ti. *Ts* and T_C increase is observed when increasing the fractions of other components, i.e., the influence is strengthened in a series Ni < Sc < Mn < Y < Al < V.

Fig. 21 shows the correlations between the values of ΔG^o calculated using Eq. (12) from the experimental reference data (ΔH^o and ΔS^o) at T = 298 K, and the values of $Y = \Delta G^o$ calculated from the composition of the alloys fitted using Eq. (7). The top X- and right Y-axes show the corresponding values of plateau pressures at T = 298 K (Eq. (13)) varying between approximately 10^{-9} to 10^5 atm for ZrV_2 and $TiFe_2$, respectively. Both C14 and C15 intermetallics exhibit very

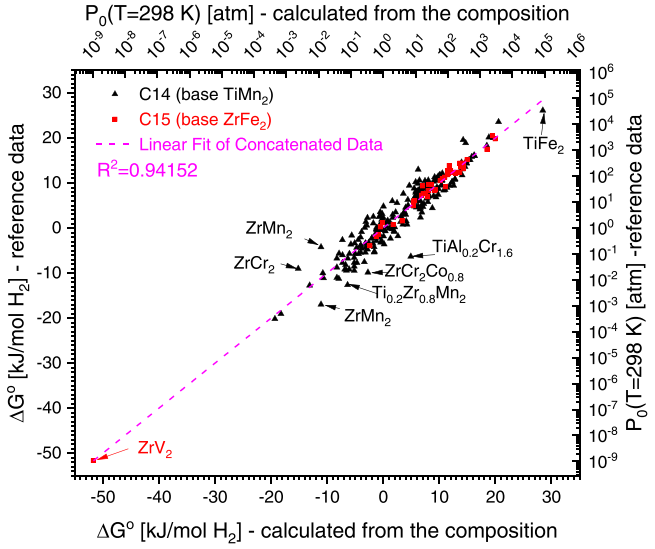

Fig. 21. Comparison of the data of the regression analysis (Eq. (7)) for the single-phase C14 (black triangles) and C15 (red squares) intermetallics assuming Y= ΔG^o with the data calculated from the reference values (Eq. (12)). The trend line was calculated for the overall dataset.

good correlations with $R^2 > 0.94$ for the common linear fit of the calculated and reference data. When the multi-phase alloys are included into the starting dataset (C14 +C15), this retains a rather high R^2 value being close to 0.9 (see Fig. 22), even though R^2 slightly decreases.

Analysis of the data listed in Table 5 allows to quantify the influence of elemental compositions on the stability of Laves phase hydrides. Three trends can be observed:

- For the single-phase C14 intermetallics, the hydride stability (as compared to the base $TiMn_2$ intermetallic) increases stronger with the increase of the atomic fraction of the components in the series: Cr < Cu < Al≈Zr < V. The effect of components on the decrease of hydride stability becomes stronger in the series: Mo < (n_B/n_A-2) < Ni < Fe < Co < < W.[6]
- For the single-phase C15 Laves phases (base $ZrFe_2$), the effect of components follows the series V < Al < Mn≈Y < Sc < Ni < < (n_B/n_A-2) < Ti, where the deviation from stoichiometry and increase in the content of Ti increases the hydride stability while other parameters decrease it.
- For the C14 +C15 multi-phase alloys where $TiFe_2$ was selected as a base intermetallic, the increase of hydride stability while the effect of the components follows the series Sn < < V < Y≈Al < Sc < Cu≈Cr≈Zr≈Mo≈Mn < Ni < Co < (n_B/n_A-2) < < W.

The observed regularities show that the "elemental composition – hydride stability" correlations are strongly related to the chemical potential of hydrogen which is equal to ln P_0 multiplied by RT (Eqs. (12),(13)), rather than to the conventionally considered hydrogenation enthalpies. The reason for that is in a significant variation of the hydrogenation entropies for the Laves phase hydrides (see Fig. S6) which are usually lower (by their absolute values) than the standard entropy of H_2 gas (130.52 J/(mol K)) being the main contributor to the entropy change during the hydride formation. The main factor is related to the changes of configurational entropy originating from the statistical distribution of hydrogen atoms over the interstitials of

[6] The strongest effects observed for Sn and W can be explained by a small number of entries available for these components and a very narrow variation of their atomic fractions at the B-side (0.0045–0.0056 and 0.01–0.05 for Sn and W, respectively).

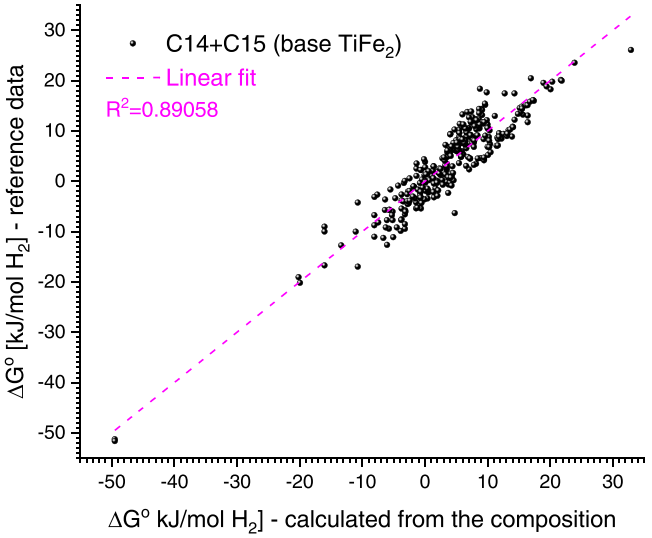

Fig. 22. Comparison of the data of the regression analysis (Eq. (7)) for the single-phase and multi-phase C14 intermetallics (combined datasets) assuming Y= ΔG° with the data calculated from the reference values (Eq. (12)).

the metal matrix [179]. Hydride-forming Laves phases, particularly, multicomponent and non-stoichiometric ones, are characterised by a very high configurational entropy contribution originating from the high level of disorder of the metal matrix including presence of a large number of chemically equivalent hydrogen-accommodating interstitial sites [25,57,180]. A strong entropy – enthalpy correlation (see Fig. 20) has been established and is manifested by a good agreement between the values of the chemical potentials calculated from the reference data and the corresponding values derived by accounting the chemical composition of the intermetallic alloys (Fig. 21, Fig. 22).

A good correlation between the calculated (Eq. (7)) and the reference data on ΔG^o, accordingly, provides a nice agreement between the values of $\ln P_0$ calculated using Eq. (13) from the experimental reference data (ΔH^o and ΔS^o) in the temperature range 300–450 K, and the corresponding values of $\ln P_0$ calculated from the composition of the alloys fitted using Eq. (7). Both C14 and C15 intermetallics exhibit $R^2 \approx 0.96$ for C14 (Fig. S7, Table S3) and R^2 close to 1 for C15 (Fig. S8, Table S4).

Since ln P_0 linearly depends on $1/T$ (Eq. (13)) and the regression analysis uses a linear Eq.(7), the values of the fitted coefficients A_i linearly depend on the reciprocal temperature (Figs. S9, S10). The effect of most of the composition parameters increases with the temperature (more pronounced for V and Y) while decreasing for Ti and approximately constant with changing temperature for Sc and (n_B/n_A-2).

6. Applications of the hydrides of Laves-type intermetallics

Advantages of the AB_2-type hydrogen storage materials on the basis of Laves phase intermetallics used for various applications include:

(a) Higher hydrogen storage capacity and lower cost of the raw materials as compared to the AB_5-type hydrogen storage alloys;
(b) Extremely wide range of stabilities of the AB_2-based hydrides allowing to operate at hydrogen pressures from << 1 mbar to > 1000 bar;
(c) Brittleness of the AB_2-type alloys (in contrast to the hard and ductile solid solution type BCC hydrogen storage alloys) assisting in preparation of their powders from ingots [18].

At the same time, high pyrophoricity, challenges in performing activation and sensitivity to the impurities of active gases present as admixtures in the commercial hydrogen gas require appropriate handling of the alloys/hydrides during operation and service of the hydrogen energy systems based on use of AB_2-type hydrides.

A short overview of the key applications of the hydride-forming Laves-type intermetallics is given below.

6.1. Hydrogen storage

"Low-temperature" AB_2-type hydrides are characterised by hydrogen storage densities reaching 1.9 wt% H/100 g_H/L and low heat effects of hydrogen absorption, as low as 20–25 kJ/mol H_2, that allows to develop weight-, volume- and energy-efficient hydrogen storage systems on their basis [21,29]. As these systems provide compact hydrogen storage at convenient ambient temperature-hydrogen pressure conditions, they are frequently used in integrated energy systems proving hydrogen fuel to a low-temperature polymer exchange membrane fuel cell (LT-PEMFC) [9]. Apart from the stationary [181–183] and portable [184] applications where the system weight is either not critical or has flexible margins of tolerance due to a small amount of the stored H_2 and thus utilising a low amount of the H storage material, AB_2-type alloys showed promising performance in on-board hydrogen storage in some special mobile

Table 5
Results of fitting of ΔG° for C14 and C15 intermetallics with Eq. (7).

C14 (single phase)			C15 (single phase)			C14 +C15 (incl. multi-phase)		
Component type	Fitted Coefficient		Component type	Fitted Coefficient		Component type	Fitted Coefficient	
	Variable	Value		Variable	Value		Variable	Value
–	A_0:*Y* ($TiMn_2$)	12.56	–	A_0: *Y* ($ZrFe_2$)	14.95	–	A_0: *Y* ($TiFe_2$)	32.91
A	A_1: X_1(Zr)	-23.66 A		A_1: X_1(Sc)	-15.89 A		A_1: X_1(Sc)	-34.47
B	A_2: X_2(Al)	-22.73		A_2: X_2(Ti)	17.84		A_2: X_2(Y)	-36.84
	A_3: X_3(Co)	18.09		A_3: X_3(Y)	-33.04		A_3: X_3(Zr)	-23.26
	A_4: X_4(Cr)	-4.06	B	A_4: X_4(Al)	-58.00	B	A_4: X_4(Al)	-36.71
	A_5: X_5(Cu)	-11.44		A_5: X_5(Mn)	-34.27		A_5: X_5(Co)	-0.47
	A_6: X_6(Fe)	15.89		A_6: X_6(Ni)	-6.46		A_6: X_6(Cr)	-25.67
	A_7: X_7 (Mo)	3.88		A_7: X_7(V)	-66.65		A_7: X_7(Cu)	-28.52
	A_8: X_8(Ni)	11.3	–	A_8: $X_8(n_B/n_A$-2)	7.15		A_8: X_8(Mn)	-20.34
	A_9: X_9(V)	-32.36					A_9: X_9 (Mo)	-20.77
	A_{10}: X_{10}(W)	75.77					A_{10}: X_{10}(Ni)	-5.02
–	A_{11}: $X_{11}(n_B/n_A$-2)	7.62					A_{11}: X_{11}(Sn)	-537.85
							A_{12}: X_{12}(V)	-59.16
							A_{13}: X_{13}(W)	62.63
						–	A_{14}: $X_{14}(n_B/n_A$-2)	6.22
Number of points		230	*Number of points*		44	*Number of points*		329

applications, like weight efficient fuel cell vehicles [185] and materials handling units / forklifts [70,186,187]. Unstable Laves phase hydrides are also suitable for their use in hybrid hydrogen storage tanks combining advantages of compressed gas (unlimited rate of H_2 supply) and metal hydride based hydrogen storage methods (compactness, low H_2 working pressure and high volumetric density of H) [28,102,109,188].

6.2. Hydrogen compression

AB_2-type hydrides on the basis of C14-Laves phase intermetallics allow thermal compression of hydrogen gas to very high pressures (above 1 kBar H_2) while utilising moderate heating - up to 150–170 °C. Their particular important advantage related to this application is in a higher cycling stability as compared to AB_5-type and BCC solid solution alloys for hydrogen compression, which both suffer from a decayed performance on cycling [4]. Thus, the development, preparation and characterisation of the C14-AB_2 high-pressure hydrogen compression alloys all intensified in the recent years [29–31,189–192]. The associated research activities also include modelling and design of the MH compressors utilising the Laves phase alloys [11,193–196], as well as a development of the various prototype units some capable of compressing hydrogen to 450–900 bar H_2 [11,13,70,197–199].

6.3. Heat management

Applications based on use of the Reaction (1a) for cooling, heating, heat upgrade and heat storage are realised in the heat engines which operate as inverted metal hydride compressor units, when the difference in hydrogen pressure is used as a driving force of the processes of heat absorption (cooling) and release (heating) associated with a decomposition or formation of the metal hydride, respectively [1,3,6, 200–203] while providing a maximum specific heating/cooling power per unit weight and volume based on the high reversible hydrogen sorption capacity in the operating pressure/temperature range of the selected material. Since the efficiency of the intermetallic hydrides is inferior to the light-weight "high-temperature" hydrides on the basis of Mg and Ca, the latter ones are mainly considered as the candidates for the heat management applications at the operating temperatures above 300–350 °C [13,204]. However, at low operating temperatures use of intermetallic hydrides including Laves phases remains as the only option.

Heat pumps utilising metal hydrides use two different MH with tailored thermodynamics of the metal-hydrogen interactions functioning at the hot and cold sides of the heat pump. The vast majority of the MH heat pumps use the pairing between an AB_5 hydride (hot side) and AB_2 Laves type hydride (cold side) [207]. To achieve efficient operation, the selected AB_2 Laves type hydride should have high heat effects of H_2 absorption (approx. above 30 kJ/mol H_2) and low absolute values of the hydrogenation entropy changes on the hydrogenation, < 110 J/(mol H_2 K) [15]. As it can be seen from the Tables A.1 and A.2, many of the studied Laves phase hydrides well fit these criteria and are suitable for the heat management applications at low-temperatures. Already 40 years ago, at the end of 1980s, Laves phase hydrides were used in applications as heat pumps in the metal-hydride-based coolers and heat transformers [205]. Detailed studies of the Laves-type AB_2 alloys (A=Ti, Ti+Zr; B=Cr,Mn,Fe,V)) which cover possible range of their operation in the MH heat pumps: T = –80…+ 60 °C, P = 5–300 bar are described in [206]. Analysis of the properties of 336 (pseudo)binary, complex and intermetallic hydrides (with > 100 000 available hydride pairs) for the heat management applications showed that > 700 pairs comprising the AB_2-type MH on the cold side can provide the static Coefficient of Performance (COP) above 1 (showing their suitability for this application) when operating in a temperature range 20 (cooling) – 50 (heat sink) – 150 °C (heating) and $P(H_2)$ < 150 bar.

Further detailed data describing the performance of the prototype heat pumps utilising AB_2-type Laves phase hydrides can be found in the reviews [6, 202,203], and in the original publications [34,201, 208,209].

6.4. Getters and low-pressure sources of hydrogen

Among the studied Laves phases, C15-ZrV_2 forms the most stable hydride, with H_2 equilibrium pressure about 10^{-5} mbar at T = 50 °C (see Fig. 16) and ~1 mbar at T = 300 °C (Fig. 2). Thus, this intermetallic and its related derivatives are promising for their use as reversible getters of hydrogen and its heavy isotopes, D and T.

Cuevas and Latroche [210] have recently published a comprehensive review on the intermetallic-based materials for hydrogen gettering. One type of getters contain Laves phases $Zr(V,Fe)_2$ and $(Ti,Zr)(V,Fe)_2$ while the commercial getter Zr–V–Fe and Zr–Ti–V–Fe alloys are multi-phase and contain α-Zr in addition. In spite at ambient temperature hydrogen absorption by ZrV_2-based alloys is strongly passivated by small impurities of air present in H_2 (1%), the passivation effect, however, can be significantly reduced by the surface modification of the alloy particles via fluorination followed by electroless deposition of Pd–Ag coating [211]. On the other hand, introducing oxygen into Zr–V getter alloys during their preparation (from either gas phase or oxide additive in the charge) is accompanied by the formation of an oxygen-stabilised intermetallic η-$Zr_3V_3O_{1-x}$ phase which significantly improves the rates of hydrogen absorption at low applied pressures [212].

Hydrogen release from $Zr(V_{0.75}Fe_{0.25})_2$ hydrogenated at pressures below 10^{-2} Pa takes place at T = 327–737 °C. The rates of hydrogen desorption increase with an increase of the applied H_2 exposure dose when varied between 10 and $1.3{\cdot}10^4$ Langmuir[7] [213].

Hydrogen thermodesorption behaviour [214] is strongly influenced by the residual hydrogen concentration in the hydrogenated Zr–V–(O) alloy (0.1–0.5 wt% O; ~40% ZrV_2 and η-$Zr_3V_3O_{1-x}$ each, balance – α-Zr). A decrease of H/M from 1.00 to 0.32 results in a gradual increase of onset temperature of H_2 desorption from 100 to 350 °C. At T > 400 °C the desorption rate linearly increases with temperature until reaching its maximum at T = 590 °C and quickly drops with a completion of H desorption at T = 650 °C.

Nearly uniform and well-controlled hydrogen desorption from the hydrogenated Zr–V based getter type alloys during their heating allows to use these materials in vacuum-plasma technologies utilising hydrogen, deuterium and tritium. In such technologies reversible Zr–V–(Fe) getters can combine functions of a getter and are a source of the working gas with controlled hydrogen flow rate thus providing the required for the efficient system operation conditions [215].

6.5. NiMH batteries

Rechargeable Nickel-Metal Hydride (Ni-MH) batteries serve as commercial power sources for portable applications, stationary energy storage and automotive transportation. While having the same operational voltage as primary alkaline batteries, 1.2 V, Ni-MH batteries are superior in reaching high energy densities and high power performance, while operating in a broad temperature range, from subzero, down to – 40 °C, to the increased temperatures as high as 60–70 °C. Long cycle and calendar life allow to use them in stand-alone, operating for many years applications, as they are able to keep the battery's functionality and to maintain stable in time

[7] One Langmuir corresponds to the exposure of a getter to the adsorbate at a pressure of $P = 10^{-6}$ Torr for one second.

performance. Particularly successful is application of the MH batteries in the hybrid vehicles where their use saves fuel and dramatically reduces CO_2 emissions with more than 10 M vehicles used worldwide and Toyota standing as the main technology developer. Recent large-scale applications include battery systems for buses, ships and trams [216].

Electrochemical discharge capacities of the Ti/Zr-based Laves type alloys (400–495 mAh/g) are superior to the conventional Co-containing AB_5 type alloys of the rare earth metals (320 mAh/g), and they together with Mg-substituted alloys of rare earth metals with a capacity of 420 mAh/g increasingly replace AB_5 type anodes. Various options to tune the performance of the anode materials to suit specific applications include: (a) Variation of the ratio between Ti and Zr; (b) Changes of the stoichiometry between understoichiometric (B/A < 2.0), stoichiometric AB_2 and overstoichiometric (B/A > 2.0) compositions; (c) Surface treatment, adding catalytic additives (La) and microstructure modification (nanostructuring) by rapid solidification to achieve improved battery anode performance at high current densities [217].

7. Concluding remarks

Laves type hydrides will continue to remain in focus of research and development of intermetallic hydrides. The present review will guide the future work in the areas of fundamental research and also in advancing the applications of the hydrides of Laves type intermetallics, based on the performed systematic comprehensive overview of the past and current activities in the field. A great advantage of utilising Laves type hydrides is in a fact that the crystal lattices of Zr/Ti-based alloys are very stable towards the cycling in hydrogen gas, withstanding thousands of cycles, and are not prone to degradation because of the disproportionation process even at elevated working temperatures, 100–200 °C, and hydrogen pressures up to several hundred bar H_2. Thus, they are used to build hydrogen storage and compression systems allowing a long-term operation without a need for the maintenance. What is even more important – is a unique opportunity to finely adjust their hydrogen storage performance because of the presence of the extended homogeneity ranges of the intermetallics allowing to tune equilibrium pressures of hydrogen desorption in a range spanning ten orders of magnitude. Thus, Laves type hydrides fit the requirements for many applications including hydrogen getters, materials for hydrogen storage operating at ambient conditions, materials for the efficient compression of hydrogen gas with an output pressure of several hundred bar and anode materials for the metal hydride batteries operating from subzero temperatures (down to −40 °C) and also at extreme heat, at 60–70 °C. Pseudo-binary and more complex multi-element in composition Laves type intermetallics achieve a continuous variation of hydrogen sorption properties, based on an interplay between the stability and crystal structure features of the original alloys. An excellent flatness and high length of the hydrogen absorption plateau pressure can be achieved and optimised based on the intrinsic behaviours of the alloys, including a contribution from elastic and electronic H–H interactions. One promising, yet insufficiently explored feature is in the fact that many Laves type alloys in fact belong to the high entropy materials offering a reversibility of hydrogen storage at convenient for the customer conditions in contrast to the traditional high entropy compositions forming too stable and thus non-reversible hydrides. The fundamentals of Laves phases regarding their structure and properties need to be better understood, even though new important findings have been recently reported. Taking into consideration that rare earth metals belong to the critical raw materials, replacement of their alloys by the Laves phase compounds not containing rare earths will proceed at increasing scale and a future progress in this direction is anticipated.

CRediT authorship contribution statement

V.A. Yartys: Conceptualization; Writing – review & editing; Funding acquisition. **M.V. Lototskyy:** Conceptualization; Writing – review & editing; Funding acquisition.

Declaration of Competing Interest

The authors declare that they have no known competing financial interests or personal relationships that could have appeared to influence the work reported in this paper.

Acknowledgements

This work has received a support from EU Horizon 2020 programme in the frame of the H2020-MSCA RISE-2017 action, HYDRIDE4MOBILITY project, with Grant Agreement 778307. VAY acknowledges a support from the Institute for Energy Technology. MVL acknowledges financial support from the South African Department of Science and Innovation (DSI), Key Programme KP6 “Metal Hydride Materials and Technologies” and South African National Research Foundation (NRF), grant number 132454. VAY is grateful to Arif Hariyadi for his help.

Appendix A

See Appendix Table A1 and Table A2 here.

Table A1
Properties of C14 Laves phases and their hydrides. The stoichiometric coefficients are rounded to 2 decimal digits.

#	Composition	V_0/Z [Å^3]	(H/M) max	$\Delta V/V_0$ [%]	$-\Delta H^o$ [kJ/mol H_2]	$-\Delta S^o$ [J/ (mol H_2 K)]	RT ln (P_A/P_D) [J/mol]	d ($\ln P_D$)/ d (H/M)	Refs
1	$[Sc](Fe)_2$	42.96	1.07	24.21	35.2	106.7			[119]
2	$[Sc_{0.5}Ti_{0.5}](Fe)_2$ [1a]	41.14	1.03	22.04	17.7	103.8		2.578	[119]
3	$[Ti](Al_{0.02}Cr_{0.98})_2$ [1a],[2]	41.99	1.07		22.8	112	2390	3.525	[218]
4	$[Ti](Al_{0.03}Cr_{0.97})_{1.8}$ [1a]	42	1		24	116	50	4.189	[218]
5	$[Ti](Al_{0.11}Cr_{0.89})_{1.8}$ [1]	41.99	1.04		33.4	90.8	175	10.184	[218]
6	$[Ti](Al_{0.11}Cr_{0.89})_{1.9}$ [1]	42.25	1.09		28.1	128.5	100	11.04	[218]
7	$[Ti](Cr)_{1.9}$ [2],[7]	41.84	1.21	17.86	22.58	97.8	0	5.04	[121]
8	$[Ti](Cr)_{1.9}$ [2],[7]	42.06	1.3		26.5	122		4.997	[120]
9	$[Ti](Cr_{0.46}Mn_{0.54})_{1.72}$		1		21.56	102.98	1511	3.278	[26]
10	$[Ti](Cr_{0.48}Mn_{0.15}Fe_{0.38})_{1.96}$		0.96		18.7	116.4	3193	1.661	[189]
11	$[Ti](Cr_{0.52}Mn_{0.15}Fe_{0.32})_{1.96}$		0.96		19.8	117.1	2744	0.963	[189]
12	$[Ti](Cr_{0.52}Mn_{0.15}Fe_{0.34})_{1.96}$		0.96		19.3	115.5	3143	1.501	[189]
13	$[Ti](Cr_{0.53}Mn_{0.47})_{1.96}$ [3]		1.04		22	113.3			[26]
14	$[Ti](Cr_{0.55}Mn_{0.15}Fe_{0.3})_{1.96}$	40.65	0.84		16.47	103.75	1161	0.205	[109]
15	$[Ti](Cr_{0.55}Mn_{0.15}Fe_{0.3})_{1.96}$		0.94		20.2	117.6	2968	0.963	[189]
16	$[Ti](Cr_{0.5}Fe_{0.5})_2$ [1a]		0.97		17.2	119	349	0.519	[219]
17	$[Ti](Cr_{0.5}Mn_{0.12}Fe_{0.38})_{1.96}$		0.97		19	117.9	3193	1.208	[189]
18	$[Ti](Cr_{0.5}Mn_{0.15}Fe_{0.35})_{1.96}$		0.97		19.9	119.8	3492	1.111	[189]
19	$[Ti](Cr_{0.5}Mn_{0.5})_{1.67}$ [1a,b]	41.01	1.05		25.52	111.29	306	0.659	[220]
20	$[Ti](Cr_{0.5}Mn_{0.5})_{1.82}$	40.68	0.84		22.9	114.7		0.917	[28]
21	$[Ti](Cr_{0.5}Mn_{0.5})_{1.9}$ [1a]	41.25	1.05		22.8	114.9	1472		[218]
22	$[Ti](Cr_{0.5}Mn_{0.5})_2$	40.67	0.87		19.6	106.5		0.192	[120]
23	$[Ti](Cr_{0.62}Mn_{0.38})_2$	40.85	1		19.9	106.1		0.438	[120]
24	$[Ti](Cr_{0.6}Mn_{0.1}Fe_{0.3})_{1.82}$	40.74	0.89		14.98	91.25	453	2.038	[221]
25	$[Ti](Cr_{0.6}Mn_{0.1}Fe_{0.3})_{1.9}$	40.65	0.86		17.46	103.51	308	0.662	[221]
26	$[Ti](Cr_{0.6}Mn_{0.1}Fe_{0.3})_{1.96}$	40.62	0.84		16.67	101.51	303	0.629	[221]
27	$[Ti](Cr_{0.6}Mn_{0.1}Fe_{0.3})_2$	40.55	0.72		13.7	94.14	250	1.193	[221]
28	$[Ti](Cr_{0.6}Mn_{0.4})_{1.54}$ [1b],[4e]	41.33	0.98		25.1	108.37	44	1.785	[220]
29	$[Ti](Cr_{0.6}Mn_{0.4})_{1.67}$ [1b],[4e]	41.3	1		25.94	117.99	109	1.296	[220]
30	$[Ti](Cr_{0.6}Mn_{0.4})_{1.82}$ [1b],[4e]	41.48	0.94		25.1	114.64	306	1.011	[220]
31	$[Ti](Cr_{0.75}Mn_{0.25})_2$ [2]	41.12	1.53		21.4	108.6		0.657	[120]
32	$[Ti](Cr_{0.85}Mn_{0.15})_2$ [1a,b]	41.26	1.2				1270		[218]
33	$[Ti](Cr_{0.85}Ni_{0.15})_2$ [1a],[5b,c]	41.41	0.99		21.7	106.7	748	7.554	[218]
34	$[Ti](Cr_{0.89}Mn_{0.11})_{1.8}$ [1a]	41.64	0.98		28	129	75		[218]
35	$[Ti](Cr_{0.95}Mn_{0.05})_{1.67}$ [1b]	41.71	0.91		20.08	100.42	22	2.611	[220]
36	$[Ti](Cr_{0.99}Mo_{0.01})_{1.91}$ [1a]	41.51	1		24.8	113	2968	3.393	[218]
37	$[Ti](Fe)_2$ [6]	39.1			14	134.5			[122]
38	$[Ti](Mn)_{1.5}$ [4c]	40.91	0.84	25.95	23.6	94		2.369	[60]
39	$[Ti](Mn)_2$ [1a]	39.51	1		24.6	114.1	6339	0.27	[46],[222]
40	$[Ti](V_{0.02}Cr_{0.5}Mn_{0.42}Fe_{0.05})_2$ [1b]		0.95		20.6	107	1330	0.6	[223]
41	$[Ti](V_{0.05}Cr_{0.5}Mn_{0.35}Fe_{0.1})_2$ [1b]		0.97		20.6	107	1100	0.6	[223]
42	$[Ti](V_{0.05}Cr_{0.5}Mn_{0.35}Fe_{0.1})_2$	40.91	0.93		19.6	101.2	421	0.784	[32]
43	$[Ti](V_{0.08}Cr_{0.5}Mn_{0.28}Fe_{0.15})_2$ [7]		0.85		20.9	106	470	0.24	[223]
44	$[Ti](V_{0.1}Cr_{0.2}Fe_{0.7})_2$ [1a]		0.9		14	114	125	1.713	[219]
45	$[Ti](V_{0.1}Cr_{0.5}Mn_{0.2}Fe_{0.2})_2$ [1b]		1		22	109		0.72	[223]
46	$[Ti](V_{0.26}Cr_{0.07}Mn_{0.67})_{2.92}$ [5b,c]	40.49	0.58		27.73	103.97	433	0.884	[224]
47	$[Ti](V_{0.26}Mn_{0.68}Nb_{0.06})_{2.84}$ [5b,c]	41.32	0.83		23.68	104.48	340	1.589	[224]
48	$[Ti](V_{0.26}Mn_{0.68}Ta_{0.06})_{2.84}$ [5b,c],[8]	41.73	0.68						[224]
49	$[Ti](V_{0.27}Mn_{0.67}Mo_{0.06})_{2.92}$ [5b,c]	40.82	0.63		19.81	93.58	469	1.384	[224]
50	$[Ti](V_{0.29}Mn_{0.67}Nb_{0.04})_{2.85}$ [5b,c]	42.42	0.67		25.71	109.73	433	1.686	[224]
51	$[Ti](V_{0.2}Mn_{0.67}Nb_{0.13})_{2.92}$ [5b,c],[8]	41.88	0.7						[224]
52	$[Ti](V_{0.32}Mn_{0.68})_{3.11}$ [4c]	40.87	0.83		25.4	100.28	1597	0.87	[225]
53	$[Ti](V_{0.34}Mn_{0.66})_{3.02}$ [5b,c]	40.75	0.86		26.63	117.16	1758	0.375	[225]
54	$[Ti](V_{0.3}Fe_{0.7})_2$ [1a]		0.83		21.5	121	100	6.648	[219]
55	$[Ti_{0.05}Zr_{0.95}](Cr_{0.4}Fe_{0.6})_2$	44.76	1.05		32.55	101.67	1367	0.225	[180]
56	$[Ti_{0.15}Zr_{0.85}](Cr_{0.4}Fe_{0.6})_2$		0.95		30.12	98.74	437	2.412	[180]
57	$[Ti_{0.1}Zr_{0.9}](Cr_{0.35}Fe_{0.65})_2$	44.4	1.01		32.05	106.27	1490	0.255	[180]
58	$[Ti_{0.1}Zr_{0.9}](Cr_{0.3}Fe_{0.7})_2$	44.16	0.95		29.79	104.18	1571	0.315	[180]
59	$[Ti_{0.1}Zr_{0.9}](Cr_{0.45}Fe_{0.55})_2$	44.53	1.03		34.73	105.02	1155	0.183	[180]
60	$[Ti_{0.1}Zr_{0.9}](Cr_{0.4}Fe_{0.6})_2$	44.92	1.02		32.43	104.18	1321	0.339	[180]
61	$[Ti_{0.1}Zr_{0.9}](Cr_{0.5}Fe_{0.5})_2$	44.74	1.03		36.02	105.02	962	0.381	[180]
62	$[Ti_{0.1}Zr_{0.9}](Cr_{0.5}Mn_{0.5})_2$ [4d]	41.16	1.19		37.7	92.91	2760	1.677	[226]
63	$[Ti_{0.1}Zr_{0.9}](Mn)_2$	45.13	1.13	24.50					[49]
64	$[Ti_{0.1}Zr_{0.9}](V_{0.15}Fe_{0.85})_{1.92}$	44.34	1.12		28.5	103.9		1.227	[227]
65	$[Ti_{0.21}Zr_{0.79}](Mn_{0.5}Fe_{0.5})_{2.02}$	43.52	0.94		33	111.4	3570	1.318	[228]
66	$[Ti_{0.25}Zr_{0.75}](Mn_{0.55}Fe_{0.45})_2$ [4b],9		1		30.2	98.45	800		[57]
67	$[Ti_{0.2}Zr_{0.8}](Al_{0.08}Fe_{0.92})_2$ [1a]		0.97		20.4	112	150	1.641	[219]
68	$[Ti_{0.2}Zr_{0.8}](Al_{0.15}Fe_{0.85})_2$ [1a]		0.67		16.8	118	100	1.992	[219]
69	$[Ti_{0.2}Zr_{0.8}](Cr_{0.08}Mn_{0.42}Fe_{0.5})_2$	43.91	0.92		31.51	97.91	2803	0.441	[229]

(continued on next page)

Table A1 (*continued*)

#	Composition	V_0/Z [Å^3]	(H/M) max	$\Delta V/V_0$ [%]	$-\Delta H^o$ [kJ/mol H_2]	$-\Delta S^o$ [J/ (mol H_2 K)]	RT ln (P_A/P_D) [J/mol]	d ($\ln P_D$)/ d (H/M)	Refs
70	$[Ti_{0.2}Zr_{0.8}](Cr_{0.12}Mn_{0.38}Fe_{0.5})_2$	43.91	0.92		33.39	111.71	2435	0.561	[229]
71	$[Ti_{0.2}Zr_{0.8}](Cr_{0.25}Mn_{0.25}Fe_{0.5})_2$		0.91		30.71	103.93	1138	0.771	[229]
72	$[Ti_{0.2}Zr_{0.8}](Cr_{0.35}Fe_{0.65})_2$	44.08	0.98	19.96					[51]
73	$[Ti_{0.2}Zr_{0.8}](Cr_{0.38}Mn_{0.12}Fe_{0.5})_2$		0.95		32.76	103.85	946	0.891	[229]
74	$[Ti_{0.2}Zr_{0.8}](Cr_{0.3}Fe0._7)_2$ **(4d)**	43.76	1.06	21.28	26.89	100.45		1.219	[51]
75	$[Ti_{0.2}Zr_{0.8}](Cr_{0.4}Fe_{0.6})_2$	44.12	0.9		30.67	102.09	2091	2.454	[180]
76	$[Ti_{0.2}Zr_{0.8}](Cr_{0.56}Mn_{0.44})_{2.25}$	44.54	1.1		20.53	41.42		2.947	[22]
77	$[Ti_{0.2}Zr_{0.8}](Cr_{0.5}Fe_{0.5})_2$	48.39	0.97		31	93.3	527	2.88	[180], [229]
78	$[Ti_{0.2}Zr_{0.8}](Mn)_2$	44.78	1.2	25.31	47.2	115.9		2.289	[46], [49],[23]
79	$[Ti_{0.2}Zr_{0.8}](Mn_{0.5}Fe_{0.5})_2$		0.9		29.62	101.25	1782	0.381	[229]
80	$[Ti_{0.36}Zr_{0.64}](Al_{0.01}V_{0.15}Cr_{0.07}Mn_{0.2}Ni_{0.57}Sn_{0.01})_{1.98}$	42.92	0.98	21.97	25.77	80	0	3.262	[230]
81	$[Ti_{0.36}Zr_{0.64}](Al_{0.01}V_{0.15}Cr_{0.11}Mn_{0.12}Ni_{0.48}Co_{0.12}Sn_{0.01})_{1.98}$ **(5a,c)**	42.91	0.91		32	104	101	4.28	[36]
82	$[Ti_{0.37}Zr_{0.63}](Al_{0.01}V_{0.15}Cr_{0.05}Mn_{0.06}Ni_{0.6}Co_{0.12}Sn_{0.01})_{1.89}$ **(5a,c)**	43.22	0.82		27	90	593	6.23	[231],[177]
83	$[Ti_{0.37}Zr_{0.63}](Al_{0.01}V_{0.15}Cr_{0.06}Mn_{0.06}Ni_{0.6}Co_{0.12}Sn_{0.01})_{1.81}$ **(5a,c)**	43.51	0.73		28	87	312	7.426	[231],[177]
84	$[Ti_{0.37}Zr_{0.63}](Al_{0.01}V_{0.15}Cr_{0.08}Mn_{0.08}Ni_{0.61}Co_{0.07}Sn_{0.01})_{1.8}$ **(5a,c)**	43.72	0.82		26	77	1065	7.279	[231],[177]
85	$[Ti_{0.37}Zr_{0.63}](Al_{0.01}V_{0.15}Cr_{0.08}Mn_{0.08}Ni_{0.61}Co_{0.08}Sn_{0.01})_{1.98}$ **(5a,c)**	43.26	0.72		22	75	321	4.659	[231],[177]
86	$[Ti_{0.37}Zr_{0.63}](Al_{0.01}V_{0.15}Cr_{0.09}Mn_{0.07}Ni_{0.61}Co_{0.07}Sn_{0.01})_{1.88}$ **(5a,c)**	43.43	0.83		24	75	919	7.328	[231],[177]
87	$[Ti_{0.37}Zr_{0.63}](Al_{0.01}V_{0.15}Cr_{0.13}Mn_{0.08}Ni_{0.61}Co_{0.02}Sn_{0.01})_{1.8}$ **(5a,c)**	43.98	0.83		29	77	1630	10.89	[231],[177]
88	$[Ti_{0.37}Zr_{0.63}](Al_{0.01}V_{0.15}Cr_{0.13}Mn_{0.09}Ni_{0.61}Co_{0.02}Sn_{0.01})_{1.88}$ **(5a,c)**	43.75	0.91		28	81	1912	6.87	[231],[177]
89	$[Ti_{0.37}Zr_{0.63}](Al_{0.01}V_{0.15}Cr_{0.13}Mn_{0.09}Ni_{0.61}Co_{0.02}Sn_{0.01})_{1.98}$ **(5a,c)**	43.6	0.88		24	77	633	6	[231],[177]
90	$[Ti_{0.37}Zr_{0.63}](Al_{0.01}V_{0.15}Cr_{0.13}Mn_{0.09}Ni_{0.6}Co_{0.02}Sn_{0.01})_{2.11}$ **(5a,c)**	43.21	0.82		23	76	516	6.39	[231],[177]
91	$[Ti_{0.37}Zr_{0.63}](Al_{0.01}V_{0.15}Cr_{0.13}Mn_{0.09}Ni_{0.6}Co_{0.02}Sn_{0.01})_{2.2}$ **(5a,c)**	43.02	0.69		21	71	547	7.309	[231],[177]
92	$[Ti_{0.39}Zr_{0.61}](Mn_{0.38}Fe_{0.62})_{1.86}$	42.9	0.97		25.69	103.66	3556	0.738	[232]
93	$[Ti_{0.3}Zr_{0.7}](Cr_{0.3}Fe_{0.7})_2$ **(4c)**	43.71	0.96	20.89	22.03	89.35		1.955	[51]
94	$[Ti_{0.3}Zr_{0.7}](Cr_{0.5}Fe_{0.5})_2$ **(4d)**	43.97	1.07	19.74	29.7	97.5	360	3.159	[180],[52]
95	$[Ti_{0.3}Zr_{0.7}](Cr_{0.5}Mn_{0.5})_2$ **(4d)**	42.47	1.17		33.64	93.65	1701	3.452	[226]
96	$[Ti_{0.3}Zr_{0.7}](Mn)_2$ **(4d)**	44.06	1.2	25.78	29.346	80.26		0.039	[49]
97	$[Ti_{0.3}Zr_{0.7}](Mn)_2$ **(4c)**		1		32.5	96.3		2.856	[73]
98	$[Ti_{0.3}Zr_{0.7}](Mn_{0.71}Fe_{0.29})_{2.8}$ **(4a)**	43.13	0.63		13.5	53.2		4.181	[23],[54]
99	$[Ti_{0.3}Zr_{0.7}](V_{0.15}Fe_{0.85})_{1.92}$	43.39	0.97		26.1	102.8		1.383	[227]
100	$[Ti_{0.3}Zr_{0.7}](V_{0.1}Fe_{0.9})_{1.92}$	43.07	0.96		23.5	105.9		0.794	[227]
101	$[Ti_{0.3}Zr_{0.7}](V_{0.25}Fe_{0.75})_{1.92}$	44.03	1.04		33.1	103.8		1.767	[227]
102	$[Ti_{0.41}Zr_{0.59}](Mn_{0.44}Fe_{0.56})_{1.88}$	42.96	0.98		26.91	104.26	3899	0.966	[232]
103	$[Ti_{0.45}Zr_{0.55}](V_{0.18}Mn_{0.54}Ni_{0.28})_{2.48}$	41.66	0.97		28.3	107.9		1.392	[233]
104	$[Ti_{0.45}Zr_{0.55}](V_{0.22}Mn_{0.35}Ni_{0.42})_2$	42.09	1.24		32.8	112		1.701	[233]
105	$[Ti_{0.45}Zr_{0.55}](V_{0.22}Mn_{0.44}Ni_{0.34})_{2.05}$	42.27	1.24		32.3	108.6		2.019	[233]
106	$[Ti_{0.45}Zr_{0.55}](V_{0.24}Mn_{0.38}Ni_{0.38})_{1.86}$	42.73	1.15	20.89	35.6	108.1		2.182	[233]
107	$[Ti_{0.45}Zr_{0.55}](V_{0.25}Mn_{0.29}Ni_{0.46})_{1.83}$	42.73	1.13		36.4	113.3		2.445	[233]
108	$[Ti_{0.45}Zr_{0.55}](V_{0.26}Mn_{0.16}Ni_{0.58})_{1.73}$	42.93	1.16	19.70	36.9	104.4		7.486	[233]
109	$[Ti_{0.45}Zr_{0.55}](V_{0.27}Mn_{0.12}Ni_{0.61})_{1.64}$	43.19	1.13	19.89	39	105		10.011	[233]
110	$[Ti_{0.45}Zr_{0.55}](V_{0.27}Mn_{0.32}Ni_{0.42})_{1.68}$	43.29	1.05	23.60	54.8	153		10.883	[233]

(*continued on next page*)

Table A1 (*continued*)

#	Composition	V_0/Z [Å^3]	(H/M) max	$\Delta V/V_0$ [%]	$-\Delta H^o$ [kJ/mol H_2]	$-\Delta S^o$ [J/ (mol H_2 K)]	RT ln (P_A/P_D) [J/mol]	d ($\ln P_D$)/ d (H/M)	Refs
111	$[Ti_{0.45}Zr_{0.55}](V_{0.28}Mn_{0.2}Ni_{0.52})_{1.63}$	43.02	1.07		44.2	125.7		4.518	[233]
112	$[Ti_{0.45}Zr_{0.55}]$ $(V_{0.29}Mn_{0.06}Ni_{0.65})_{1.54}$	43.54	1.13	18.40	41.7	109.1		11.984	[233]
113	$[Ti_{0.45}Zr_{0.55}]$ $(V_{0.29}Mn_{0.15}Ni_{0.56})_{1.53}$	43.21	1.25	18.70	47.6	133.8		5.245	[233]
114	$[Ti_{0.49}Zr_{0.51}](Mn_{0.45}Fe_{0.55})_{1.97}$	42.23	0.9		24.91	107.43	3697	1.873	[232]
115	$[Ti_{0.4}Zr_{0.6}](Fe)_2$ **(1a),(5a)**	41.27	0.87	23.80	18.3	127	873	0.864	[218], [219]
116	$[Ti_{0.4}Zr_{0.6}](Mn)_2$	43.64	1.1		35.94	102.51		2.577	[46]
117	$[Ti_{0.4}Zr_{0.6}](Mn)_2$	43.68	0.93	25.69	34.81	102.62		0.408	[49]
118	$[Ti_{0.4}Zr_{0.6}](Mn_{0.34}Fe_{0.66})_{1.92}$	42.84	0.92		24.57	106.09	3415	1.302	[232]
119	$[Ti_{0.51}Zr_{0.49}](V_{0.02}Mn_{0.5}Fe_{0.48})_{1.89}$	42.6	0.99		26.42	104.39	3758	2.297	[232]
120	$[Ti_{0.55}Zr_{0.45}]$ $(Cr_{0.42}Mn_{0.19}Fe_{0.27}Ni_{0.1}Cu_{0.01})_2$		0.94		18.46	78.1	624	0.541	[29]
121	$[Ti_{0.5}Zr_{0.5}](Al_{0.05}Fe_{0.95})_2$		0.9		16	117	349	1.725	[219]
122	$[Ti_{0.5}Zr_{0.5}](Al_{0.2}Fe_{0.8})_2$		0.67		23.3	108	75	3.408	[219]
123	$[Ti_{0.5}Zr_{0.5}](Cr_{0.5}Fe_{0.5})_2$ **(4d)**	42.98	1	16.75	24.3	96.7		4.104	[234]
124	$[Ti_{0.5}Zr_{0.5}](Cr_{0.5}Mn_{0.5})_2$	43.43	1.15		29.82	96.47	1924	3.922	[226]
125	$[Ti_{0.5}Zr_{0.5}](Mn)_2$	42.72	0.6	25.89					[49]
126	$[Ti_{0.5}Zr_{0.5}](Mn_{0.5}Fe_{0.5})_{1.91}$	42.27	0.96		25.13	103.65	4202	1.859	[232]
127	$[Ti_{0.5}Zr_{0.5}](V_{0.15}Fe_{0.85})_{1.92}$	42.4	0.84		21.9	103.1		1.49	[227]
128	$[Ti_{0.5}Zr_{0.5}]$ $(V_{0.25}Cr_{0.25}Fe_{0.25}Ni_{0.25})_2$ **(9)**		0.96		38	109.94	6984	10.23	[235]
129	$[Ti_{0.65}Zr_{0.35}]$ $(Cr_{0.42}Mn_{0.14}Fe_{0.32}Ni_{0.1}Cu_{0.01})_2$		0.81		21.74	102.44	536	0.27	[29]
130	$[Ti_{0.65}Zr_{0.35}](Cr_{0.4}Mn_{0.5}Fe_{0.1})_{1.86}$		1.21		26	96	1440		[134]
131	$[Ti_{0.65}Zr_{0.35}](Cr_{0.4}Mn_{0.5}Fe_{0.1})_{1.9}$		1.18		29	100	1060	2.364	[134]
132	$[Ti_{0.65}Zr_{0.35}](Cr_{0.4}Mn_{0.5}Fe_{0.1})_{1.98}$		1.27		28	99	1704		[134]
133	$[Ti_{0.65}Zr_{0.35}](Cr_{0.4}Mn_{0.5}Fe_{0.1})_2$		1.15		29	100			[134]
134	$[Ti_{0.6}Zr_{0.4}](Mn)_2$	42.29	0.9		25.69	90.79		1.935	[46]
135	$[Ti_{0.6}Zr_{0.4}](V_{0.2}Fe_{0.5}Ni_{0.3})_2$		0.77		26.8	112.66	370	4.951	[32]
136	$[Ti_{0.72}Zr_{0.28}]$ $(Cr_{0.42}Mn_{0.12}Fe_{0.34}Ni_{0.1}Cu_{0.01})_{1.9}$		0.96		19.26	93.66	455	1.088	[29]
137	$[Ti_{0.72}Zr_{0.28}]$ $(Cr_{0.42}Mn_{0.14}Fe_{0.32}Ni_{0.1}Cu_{0.01})_2$		0.91		24.847	115.33	698	2.641	[29]
138	$[Ti_{0.78}Zr_{0.22}]$ $(Cr_{0.42}Mn_{0.19}Fe_{0.27}Ni_{0.1}Cu_{0.02})_{2.02}$		0.9		23.989	108.94	274	0.604	[29]
139	$[Ti_{0.7}Zr_{0.3}]$ $(Cr_{0.42}Mn_{0.12}Fe_{0.34}Ni_{0.1}Cu_{0.01})_{2.03}$	41.47	0.91	23.18	23.03	108.96	1198	0.836	[29]
140	$[Ti_{0.7}Zr_{0.3}](Cr_{0.5}Fe_{0.5})_2$	41.75	0.4	19.63	22.87	106.81		4.225	[234]
141	$[Ti_{0.7}Zr_{0.3}](V_{0.3}Fe_{0.7})_2$ **(1a)**	42.59	1.2	18.01	31.1	116	499	3.75	[218]
142	$[Ti_{0.81}Zr_{0.19}](V_{0.05}Cr_{0.48}Fe_{0.48})_{1.96}$	41.52	0.88		21.38	103.41	0	1.825	[31]
143	$[Ti_{0.83}Zr_{0.17}](Cr_{0.6}Fe_{0.4})_{1.96}$	41.52	0.88		20.49	102.79	0	1.182	[31]
144	$[Ti_{0.83}Zr_{0.17}](V_{0.05}Cr_{0.48}Fe_{0.48})_{1.96}$	41.4	0.83		20.38	102.84	0	1.3	[31]
145	$[Ti_{0.83}Zr_{0.17}](V_{0.05}Cr_{0.55}Fe_{0.4})_{1.96}$	41.63	0.9		22.67	104.16	0	2.424	[31]
146	$[Ti_{0.83}Zr_{0.17}](V_{0.05}Cr_{0.6}Fe_{0.35})_{1.96}$	41.79	0.49		24.42	106.69	0	2.262	[31]
147	$[Ti_{0.83}Zr_{0.17}](V_{0.1}Cr_{0.5}Fe_{0.4})_{1.96}$	41.68	0.89		24.41	104.84	0	3.352	[31]
148	$[Ti_{0.85}Zr_{0.15}]$ $(Cr_{0.42}Mn_{0.5}Fe_{0.07})_{1.82}$		0.82		22.2	103.9		1.451	[31]
149	$[Ti_{0.85}Zr_{0.15}]$ $(Cr_{0.42}Mn_{0.5}Mo_{0.08})_{1.82}$	42	0.94		21.7	100.9		0.853	[28]
150	$[Ti_{0.85}Zr_{0.15}]$ $(Cr_{0.45}Mn_{0.15}Fe_{0.29}Ni_{0.1}Cu_{0.02})_{2.02}$		0.92		22.035	110.3	424	0.423	[29]
151	$[Ti_{0.85}Zr_{0.15}]$ $(Cr_{0.45}Mn_{0.5}Fe_{0.05})_{1.82}$		0.87		24.7	112.4		1.674	[236]
152	$[Ti_{0.85}Zr_{0.15}]$ $(Cr_{0.45}Mn_{0.5}Mo_{0.05})_{1.82}$	41.87	0.99		23.7	106.4		0.922	[28]
153	$[Ti_{0.85}Zr_{0.15}]$ $(Cr_{0.45}Mn_{0.5}W_{0.05})_{1.82}$	41.82	0.79		22.6	106.2		1.216	[28]
154	$[Ti_{0.85}Zr_{0.15}]$ $(Cr_{0.46}Mn_{0.5}Fe_{0.04})_{1.82}$		0.87		25.4	112.7		1.104	[236]
155	$[Ti_{0.85}Zr_{0.15}]$ $(Cr_{0.47}Mn_{0.5}Fe_{0.02})_{1.82}$		0.87		26.7	115		1.197	[236]
156	$[Ti_{0.85}Zr_{0.15}]$ $(Cr_{0.47}Mn_{0.5}Mo_{0.03})_{1.82}$	41.63	1.04		26.2	115.2		0.957	[28]
157	$[Ti_{0.85}Zr_{0.15}]$ $(Cr_{0.47}Mn_{0.5}W_{0.03})_{1.82}$	41.73	0.81		24.3	109.2		0.536	[28]
158	$[Ti_{0.85}Zr_{0.15}]$ $(Cr_{0.49}Mn_{0.5}W_{0.01})_{1.82}$	41.68	0.84		26.3	113.8		0.879	[28]
159	$[Ti_{0.85}Zr_{0.15}](Cr_{0.5}Mn_{0.5})_{1.82}$	41.61	0.98		26.6	112.1		0.837	[28]
160	$[Ti_{0.85}Zr_{0.15}](Cr_{0.5}Mn_{0.5})_{1.82}$		0.92		26.6	112.1		0.868	[236]
161	$[Ti_{0.85}Zr_{0.15}](Cr_{0.5}Mn_{0.5})_2$		1		25.3	112.1	1990	1.701	[223]
162	$[Ti_{0.85}Zr_{0.15}](Cr_{0.6}Mn_{0.4})_2$		1.1		26.2	114	800	1.71	[223]
163	$[Ti_{0.85}Zr_{0.15}](V_{0.05}Cr_{0.48}Fe_{0.48})_{1.96}$	41.31	0.8		19.62	101.91	0	1.329	[31]

(*continued on next page*)

Table A1 (*continued*)

#	Composition	V_0/Z [Å^3]	(H/M) max	$\Delta V/V_0$ [%]	$-\Delta H^o$ [kJ/mol H_2]	$-\Delta S^o$ [J/ (mol H_2 K)]	RT ln (P_A/P_D) [J/mol]	d ($\ln P_D$)/ d (H/M)	Refs
164	$[Ti_{0.85}Zr_{0.15}](V_{0.15}Cr_{0.1}Mn_{0.6}Fe_{0.03}Ni_{0.11}Cu_{0.01})_2$		1.02		26.61	109.68	873	0.225	[29]
165	$[Ti_{0.85}Zr_{0.15}](V_{0.18}Cr_{0.08}Mn_{0.6}Fe_{0.03}Ni_{0.11}Cu_{0.01})_2$		0.72		21.17	102.63	574	0.075	[29]
166	$[Ti_{0.8}Zr_{0.2}](Cr_{0.4}Mn_{0.6})_2$		1.1		28.87	112.97		1.14	[45]
167	$[Ti_{0.8}Zr_{0.2}](Cr_{0.5}Mn_{0.5})_{1.82}$	41.87	1.05		28.3	111.8		1.083	[28]
168	$[Ti_{0.8}Zr_{0.2}](Cr_{0.5}Mn_{0.5})_2$ **(4c)**		1.17		21.45	91.61		1.358	[29]
169	$[Ti_{0.8}Zr_{0.2}](Cr_{0.5}Mn_{0.5})_2$	45.08	0.86		21.54	98.63	2266	2.099	[226]
170	$[Ti_{0.8}Zr_{0.2}](V_{0.2}Fe_{0.8})_2$ **(1a)**	41.19	1.01	20.60	17.85	99.25	299	3.678	[32]
171	$[Ti_{0.8}Zr_{0.2}](V_{0.2}Fe_{0.8})_2$ **(1a)**	41.26	1.01	20.66	19.7	109.9	100	3.528	[218]
172	$[Ti_{0.93}Zr_{0.07}](V_{0.1}Cr_{0.35}Mn_{0.55})_2$	41.37	0.97		22.86	100.41	907	0.876	[238]
173	$[Ti_{0.94}Zr_{0.06}](V_{0.1}Cr_{0.35}Mn_{0.55})_2$	41.27	0.97		22.36	99.61	907	1.034	[238]
174	$[Ti_{0.95}Zr_{0.05}](Cr_{0.5}Mn_{0.5})_2$ **(1b)**		1		20.8	105	2100	0.801	[223]
175	$[Ti_{0.95}Zr_{0.05}](Cr_{0.6}Mn_{0.4})_2$		0.92		21.9	108.1	900	0.18	[223]
176	$[Ti_{0.95}Zr_{0.05}](V_{0.19}Cr_{0.1}Mn_{0.58}Fe_{0.03}Ni_{0.1}Cu_{0.01})_{2.07}$		0.89		25	112.3	414	0.101	[29]
177	$[Ti_{0.95}Zr_{0.05}](V_{0.1}Cr_{0.25}Mn_{0.65})_2$	41.11	0.98		21.18	97.25	1462	0.678	[238]
178	$[Ti_{0.95}Zr_{0.05}](V_{0.1}Cr_{0.35}Mn_{0.55})_2$	41.24	0.96		21.27	96.88	882	0.737	[238]
179	$[Ti_{0.95}Zr_{0.05}](V_{0.1}Cr_{0.45}Mn_{0.45})_2$	41.36	0.94		21.64	97.34	353	0.767	[238]
180	$[Ti_{0.95}Zr_{0.05}](V_{0.2}Mn_{0.7}Fe_{0.05}Ni_{0.05})_{2.15}$		0.95		28.11	112.34	1559	0.362	[29]
181	$[Ti_{0.96}Zr_{0.04}](V_{0.2}Cr_{0.02}Mn_{0.73}Fe_{0.05})_{1.91}$ **(5c)**	40.99	0.87		25.8	110	798	1.268	[30]
182	$[Ti_{0.97}Ce_{0.03}](Cr_{0.55}Mn_{0.15}Fe_{0.3})_{1.91}$ **(1b),(5d)**	40.79	0.87		19.27	112.11	1268	0.536	[109]
183	$[Ti_{0.97}Ho_{0.03}](Cr_{0.55}Mn_{0.15}Fe_{0.3})_{1.91}$ **(1b),(5d)**	40.76	0.89		19.39	111.29	1164	0.9	[109]
184	$[Ti_{0.97}La_{0.03}](Cr_{0.55}Mn_{0.15}Fe_{0.3})_{1.91}$ **(1b),(5d)**	40.82	0.91		16.63	104.17	1428	0.149	[109]
185	$[Ti_{0.98}Zr_{0.02}](V_{0.16}Cr_{0.06}Mn_{0.72}Fe_{0.06})_{2.41}$ **(5c)**	40.87	0.74		24.8	111.3	1272	0.624	[30]
186	$[Ti_{0.98}Zr_{0.02}](V_{0.19}Cr_{0.02}Mn_{0.74}Fe_{0.04})_{2.11}$ **(5c)**	40.89	0.81		24.7	109.3	1347	0.854	[30]
187	$[Ti_{0.98}Zr_{0.02}](V_{0.21}Cr_{0.02}Mn_{0.72}Fe_{0.05})_{2.21}$ **(5c)**	40.91	0.8		24.2	107.1	1098	1.078	[30]
188	$[Ti_{0.98}Zr_{0.02}](V_{0.21}Cr_{0.02}Mn_{0.73}Fe_{0.04})_{2.06}$ **(4c)**		0.79		24.06	101.56		1.469	[29]
189	$[Ti_{0.98}Zr_{0.02}](V_{0.23}Cr_{0.02}Mn_{0.71}Fe_{0.04})_{2.28}$ **(5c)**	40.88	0.85		24.3	109.5	1422	0.434	[30]
190	$[Ti_{0.98}Zr_{0.02}](V_{0.23}Cr_{0.02}Mn_{0.71}Fe_{0.05})_{2.13}$ **(5c)**	40.92	0.71		24	107.8	1297	0.532	[30]
191	$[Ti_{0.98}Zr_{0.02}](V_{0.23}Cr_{0.03}Mn_{0.67}Fe_{0.07})_{1.94}$ **(5c)**	41.03	0.68		28.7	117.5	574	1.831	[30]
192	$[Ti_{0.98}Zr_{0.02}](V_{0.25}Cr_{0.03}Mn_{0.67}Fe_{0.05})_{1.9}$ **(5c)**	41.43	0.84		27.8	108.5	574	3.369	[30]
193	$[Ti_{0.98}Zr_{0.02}](V_{0.27}Cr_{0.02}Mn_{0.66}Fe_{0.05})_{1.82}$ **(5c)**	41.52	0.69		29.9	110.2	624	4.177	[30]
194	$[Ti_{0.98}Zr_{0.02}](V_{0.2}Cr_{0.02}Mn_{0.65}Fe_{0.05}Ni_{0.09})_{2.19}$ **(5c)**	41	0.87		26.3	111.1	748	1.313	[30]
195	$[Ti_{0.98}Zr_{0.02}](V_{0.34}Cr_{0.02}Mn_{0.6}Fe_{0.03})_{2.09}$ **(5c)**	41.32	0.87		27.2	105.9	698	1.968	[30]
196	$[Ti_{0.99}Zr_{0.01}](V_{0.52}Cr_{0.02}Mn_{0.43}Fe_{0.03})_{1.87}$ **(5b,c)**	42.29	0.91		32.7	99.2			[30]
197	$[Ti_{0.9}Zr_{0.1}](Cr_{0.42}Mn_{0.55}Mo_{0.02})_{1.6}$	41.41	0.81		24	110	1100	1.09	[102]
198	$[Ti_{0.9}Zr_{0.1}](Cr_{0.5}Mn_{0.5})_{1.82}$	41.2	0.9		25.5	112.6		0.687	[28]
199	$[Ti_{0.9}Zr_{0.1}](Cr_{0.5}Mn_{0.5})_2$ **(10)**		0.67		22.5	104.9			[33]
200	$[Ti_{0.9}Zr_{0.1}](V_{0.15}Fe_{0.85})_2$ **(1a)**	40.36	0.98	22.22	13.5	112.9	199	1.254	[218]
201	$[Ti_{0.9}Zr_{0.1}](V_{0.1}Cr_{0.18}Mn_{0.7}Fe_{0.02})_2$		1.03		25.89	106.9			[15]
202	$[Ti_{0.9}Zr_{0.1}](V_{0.1}Cr_{0.32}Mn_{0.4}Fe_{0.02}Ni_{0.15}Cu_{0.01})_2$		0.9		25.29	110.11	324	0.21	[29]
203	$[Ti_{0.9}Zr_{0.1}](V_{0.1}Cr_{0.35}Mn_{0.55})_2$	41.53	1.01		22.92	97.9	857	0.477	[238]
204	$[Ti_{0.9}Zr_{0.1}](V_{0.1}Fe_{0.75}Ni_{0.15})_2$ **(1a)**	40.01	0.99	20.38	12.08	119.5	168	2.166	[218]
205	$[Ti_{0.9}Zr_{0.1}](V_{0.35}Mn_{0.65})_2$ **(4d),(9)**		0.93		30	99.56	1046	2.379	[239]
206	$[Zr](Al_{0.4}Fe_{0.6})_2$	47.07	0.63	9.83	47.6	122.4		36.205	[178]
207	$[Zr](Cr)_2$ **(4e)**		1.2		45.19	121.34		3.555	[41]
208	$[Zr](Cr_{0.11}Mn_{0.44}Fe_{0.44})_{2.25}$ **(4d)**	44.61	1.19		25.6	75		0.66	[22]
209	$[Zr](Cr_{0.25}Fe_{0.75})_2$		0.9		32.3	112.97	1690	1.089	[180]
210	$[Zr](Cr_{0.25}Fe_{0.75})_2$		0.95		24.27	92.05			[23], [44]

(*continued on next page*)

Table A1 (*continued*)

#	Composition	V_0/Z [Å^3]	(H/M) max	$\Delta V/V_0$ [%]	$-\Delta H^o$ [kJ/mol H_2]	$-\Delta S^o$ [J/ (mol H_2 K)]	RT ln (P_A/P_D) [J/mol]	d ($\ln P_D$)/ d (H/M)	Refs
211	$[Zr](Cr_{0.2}Fe_{0.8})_2$ [4d]		1		28.4	100.8	2138	1.131	[240]
212	$[Zr](Cr_{0.36}Fe_{0.36}Co_{0.29})_{2.8}$ [4a]	43.39	0.74	20.11	20.02	88.14		3.96	[59]
213	$[Zr](Cr_{0.36}Fe_{0.36}Cu_{0.29})_{2.8}$ [4c]	44.58	0.78	21.52	29.78	93.05		2.288	[59]
214	$[Zr](Cr_{0.36}Fe_{0.36}Ni_{0.29})_{2.8}$ [4b]	43.52	0.69	21.19	20.73	88.29		4.857	[59]
215	$[Zr](Cr_{0.36}Fe_{0.64})_{2.8}$ [4b]	44.05	0.81	21.23	19.51	77.54		3.733	[59]
216	$[Zr](Cr_{0.36}Mn_{0.29}Fe_{0.36})_{2.8}$ [4c]	44.62	0.9	21.51	29.5	94.8		4.497	[59]
217	$[Zr](Cr_{0.38}Fe_{0.62})_{2.6}$		0.72		29.1	107.6	1010	2.455	[228]
218	$[Zr](Cr_{0.38}Fe_{0.62})_{2.6}$ [4c]	44.29	1.2	18.93	25.2	92.2		2.317	[59]
219	$[Zr](Cr_{0.3}Fe_{0.7})_2$ [4d]	44.47	1.04	20.21	26.92	89.43		1.044	[51]
220	$[Zr](Cr_{0.3}Fe_{0.7})_2$		1		28.5	94.7	851	0.915	[57],[23],[47], [241]
221	$[Zr](Cr_{0.3}Fe_{0.7})_2$ [4d]		1		29.8	100.3	2980	0.378	[240]
222	$[Zr](Cr_{0.42}Fe_{0.58})_{2.4}$ [4d]	44.15	1.28		20	65.6		2.558	[22]
223	$[Zr](Cr_{0.4}Fe_{0.6})_2$		1.02		32.97	99.16	1300	1.131	[180]
224	$[Zr](Cr_{0.4}Fe_{0.6})_2$ [4d]		1		36.2	103.3	1068	0.819	[240]
225	$[Zr](Cr_{0.4}Fe_{0.6})_{2.5}$ [4d]	44.27	1.14		22.7	80.3		1.234	[22]
226	$[Zr](Cr_{0.5}Co_{0.5})_2$		1.07		40.17	121.34			[44]
227	$[Zr](Cr_{0.5}Fe_{0.5})_2$	45.03	1.13		49.37	133.89			[23],[44]
228	$[Zr](Cr_{0.5}Fe_{0.5})_2$ [4d]		1		39.4	103.6	3100	0.648	[240]
229	$[Zr](Cr_{0.5}Fe_{0.5})_2$ [4d]	45.12	1.1	19.39	36.1	99		0.802	[52],[59]
230	$[Zr](Cr_{0.5}Mn_{0.5})_2$ [4d]	46.32	1.27		37.21	82.12	2190	0.572	[226],[22]
231	$[Zr](Cr_{0.71}Co_{0.29})_{2.8}$ [4a]	44.72	0.84	21.55	45.3	118.9		0.132	[242]
232	$[Zr](Cr_{0.71}Fe_{0.29})_{2.8}$ [4a]	45.36	1	22.96	46.5	130.7		0.456	[242]
233	$[Zr](Cr_{0.71}Ni_{0.29})_{2.8}$ [4c]	44.83	1.17	22.35	37.9	101.2		3.214	[242]
234	$[Zr](Fe_{0.5}Mo_{0.5})_2$ [4d]		0.99		40.74	127.08		2.412	[48]
235	$[Zr](Fe_{0.9}Mo_{0.1})_2$ [1a],(2)	44.81	1.18	23.61	25.9	112.5	2993	1.107	[218],[219]
236	$[Zr](Mn)_2$	45.16	1.2	28.57	53.14	121.34			[46], [44],[53]
237	$[Zr](Mn)_2$ [4b],(9)	45.16	1.2	28.57	40.4	121.34	2400		[49], [23],[55]
238	$[Zr](Mn)_{2.5}$		1.2		18	51.5			[23]
239	$[Zr](Mn)_{2.7}$	43.72	0.85		33.6	100.6	2650	3.375	[228]
240	$[Zr](Mn)_{2.8}$ [4a],(9)	44.5	0.95	25.79	32.9	91.3	3000	0.583	[57],[53]
241	$[Zr](Mn)_{3.8}$ [4b]	43.03	0.75	28.44	17	51	1.3974		[23],[53]
242	$[Zr](Mn_{0.2}Fe_{0.8})_2$ [4e]		0.62		26.7	109.6		3.382	[50]
243	$[Zr](Mn_{0.3}Fe_{0.7})_2$ [4d]		0.93		24.5	98.3		2.689	[50]
244	$[Zr](Mn_{0.48}Fe_{0.52})_{2.33}$		0.77		18.3	51.7	8410		[23]
245	$[Zr](Mn_{0.48}Fe_{0.52})_{2.33}$	43.57	0.85		29.4	104.9	3580	0.902	[228]
246	$[Zr](Mn_{0.52}Fe_{0.48})_{2.36}$	43.76	0.82		31	106	4070	1.161	[228]
247	$[Zr](Mn_{0.55}Fe_{0.45})_{2.8}$		0.9		9.4	43.3			[23]
248	$[Zr](Mn_{0.5}Co_{0.5})_2$		1.03		34.73	108.78		0.99	[23],[44]
249	$[Zr](Mn_{0.5}Fe_{0.35}Co_{0.15})_2$ [4b]	44.16	0.82		23.73	87.22		3.228	[243]
250	$[Zr](Mn_{0.5}Fe_{0.5})_2$	44.37	0.97		30.12	89.54			[44]
251	$[Zr](Mn_{0.5}Fe_{0.5})_2$ [4c]	44.43	1	18.58	36.9	109.3		2.624	[50]
252	$[Zr](Mn_{0.62}Fe_{0.37})_{3.2}$ [4a]	43.86	0.48	12.34	6.8	32.8		4.988	[55]
253	$[Zr](Mn_{0.6}Co_{0.4})_2$		1.03		35.98	105.44			[23],[44]
254	$[Zr](Mn_{0.6}Fe_{0.4})_2$		1.07		33.05	96.23			[23],[44]
255	$[Zr](Mn_{0.71}Co_{0.29})_{2.8}$ [9]		0.55		23.8	84	2900		[57]
256	$[Zr](Mn_{0.71}Co_{0.29})_{2.8}$ [4b]	43.17	0.6	22.32	18.5	50		3.81	[58]
257	$[Zr](Mn_{0.71}Cu_{0.29})_{2.8}$ [4a],(9)		0.92		35.9	83.4	4300		[57]
258	$[Zr](Mn_{0.71}Cu_{0.29})_{2.8}$ [4a]		0.92		31.6	83.4			[57],[23]
259	$[Zr](Mn_{0.71}Cu_{0.29})_{2.8}$ [4d]	45.04	0.94	25.74	27	61.2		0.302	[58]
260	$[Zr](Mn_{0.71}Fe_{0.29})_{2.79}$	43.35	0.76		29.3	107.6	3310	4.531	[228]
261	$[Zr](Mn_{0.71}Fe_{0.29})_{2.8}$ [9]	44.17	1.13	21.35	25	83		5.453	[57], [23],[55]
262	$[Zr](Mn_{0.71}Ni_{0.29})_{2.8}$ [4c]	43.76	0.85	18.44	18.6	70.8		4.45	[58]
263	$[Zr](Mn_{0.71}Ni_{0.29})_{2.8}$ [4c],(9)		0.87		26.4	92.1	1400		[57]
264	$[Zr](Mn_{0.75}Co_{0.25})_2$		1.13		44.35	117.15			[23], [44]
265	$[Zr](Mn_{0.88}Fe_{0.13})_{3.2}$ [4c]	43.3	0.79	26.40	21.7	80.3		2.777	[56]
266	$[Zr](Mn_{0.88}Ni_{0.13})_{3.2}$ [4c]	43.19	0.83	23.14	15.89	65.18		4.812	[58]
267	$[Zr](Mn_{0.8}Fe_{0.2})_2$ [4b]	44.81	0.73	23.02	42.2	103.8			[50]
268	$[Zr](Mn_{0.93}Fe_{0.07})_{2.8}$ [4c]		0.92		15	47.4		2.391	[56]
269	$[Zr](Mn_{0.93}Fe_{0.07})_3$	44.25	0.9	27.05					[56]
270	$[Zr](V_{0.15}Fe_{0.85})_{1.92}$	44.89	1.16		29.1	102.2		0.244	[227]
271	$[Zr](V_{0.25}Co_{0.75})_2$		1		34.31	109.62			[23],[44]
272	$[Zr](V_{0.25}Fe_{0.75})_{1.92}$	45.21	1.23		42.5	123.6		3.496	[227]
273	$[Zr](V_{0.25}Fe_{0.75})_2$	45.26	1.07		32.22	87.86			[23],[44]
274	$[Zr](V_{0.5}Co_{0.5})_2$		1.23		49.37	101.67			[23],[44]
275	$[Zr](V_{0.5}Fe_{0.5})_2$	46.67	1.07		48.12	93.72			[23],[44]

Notes: [1] – (H/M)max measured at [a] P > 1000 bar and/or [b] T < –20 °C; [2] – thermodynamic data for the first / lower plateau; [3] – stable performances during 1000 cycles of H absorption/desorption; [4] – thermodynamic data presented for plateau midpoint corresponding to H/M about: [a] 0.25, [b] 0.33, [c] 0.4, [d] 0.5 and [e] 0.6; [5] – multiphase: [a] C14 +C15, [b] C14 + BCC, [c] C14 + FCC, [d] impurity of RE oxide; [6] – calculated thermodynamic data; [7] – critical temperature below 20°C; [8] – no plateau; [9] – thermodynamic data taken calorimetrically; [10] – (H/M)max presented as reversible H capacity between 20 and 85°C

Table A2
Properties of C15 Laves phases and their hydrides. The stoichiometric coefficients are rounded to 2 decimal digits.

#	Composition	V_0/Z [Å^3]	(H/M) max	$\Delta V/V_0$ [%]	$-\Delta H^o$ [kJ/mol H_2]	$-\Delta S^o$ [J/ (mol H_2 K)]	RT ln (P_A/P_D) [J/mol]	d ($\ln P_D$)/ d (H/M)	Refs
1	$[Sc](Fe)_{1.8}$ **(1b)**	43.99	0.91	12.38	29.6	86	3760	0.752	[119],[118]
2	$[Sc_{0.2}Zr_{0.8}](Fe)_2$ **(2a,b),(3c)**	43.86	1.23	26.01	21	117	612	0.666	[119]
3	$[Sc_{0.5}Zr_{0.5}](Fe)_2$ **(2a,b),(3a)**	43.82	1.2	23.89	19	95		2.377	[119]
4	$[Ti](Cr)_{1.8}$ **(1a)**	41.73	1.26		21.3	116		3.528	[120]
5	$[Ti](Cr_{0.93}Mo_{0.07})_{2.37}$ **(4a)**	41.34	0		17.2	117	200	3.424	[218]
6	$[Ti](Cr_{0.95}Ni_{0.05})_{1.85}$ **(2a,b),(4a,c)**	41.49	1.1		20.5	107.8	848	4.016	[218]
7	$[Ti_{0.15}Zr_{0.85}](V_{0.06}Mn_{0.33}Fe_{0.06}Ni_{0.56})_{1.96}$		1.13		33.984	107.67	374	0.355	[125]
8	$[Ti_{0.15}Zr_{0.85}](V_{0.06}Mn_{0.33}Fe_{0.06}Ni_{0.56})_{2.01}$		1.14		35.25	113.33	773	0.812	[125]
9	$[Ti_{0.15}Zr_{0.85}](V_{0.06}Mn_{0.33}Fe_{0.06}Ni_{0.56})_{2.06}$		1.01		34.538	116.61	100	0.582	[125]
10	$[Ti_{0.15}Zr_{0.85}](V_{0.06}Mn_{0.33}Fe_{0.06}Ni_{0.56})_{2.11}$ **(1b),(5a)**		1		28.129	98.06	748	0.56	[125]
11	$[Ti_{0.21}Zr_{0.78}La_{0.01}](V_{0.06}Mn_{0.32}Fe_{0.06}Ni_{0.56}Sn_{0.01})_{2.15}$	42.96	0.62		35.4	130	781	0.855	[36]
12	$[Ti_{0.21}Zr_{0.78}La_{0.01}](V_{0.06}Mn_{0.32}Fe_{0.06}Ni_{0.56}Sn_{0.01})_{2.18}$ **(4c),(5)**	42.99	1.03		31.8	119	328	0.968	[36]
13	$[Ti_{0.2}Zr_{0.8}](Fe)_2$ **(2a)**	43.5	1.16	24.20	19.8	125	1247	0.756	[218], [219]
14	$[Ti_{0.2}Zr_{0.8}](V_{0.1}Fe_{0.5}Ni_{0.4})_2$ **(2a)**	42.96	1.23	25.00	26.8	118.3	100	2.634	[218], [219]
15	$[Ti_{0.37}Zr_{0.63}](Al_{0.01}V_{0.15}Cr_{0.05}Mn_{0.06}Ni_{0.61}Co_{0.12}Sn_{0.01})_{1.98}$ **(4a,b)**		0.59		12	47	592	6.083	[177,231]
16	$[Ti_{0.37}Zr_{0.63}](Al_{0.01}V_{0.15}Cr_{0.05}Mn_{0.06}Ni_{0.6}Co_{0.12}Sn_{0.01})_{2.1}$ **(4a,b)**		0.57		11	47	1019	5.971	[177,231]
17	$[Ti_{0.37}Zr_{0.63}](Al_{0.01}V_{0.15}Cr_{0.05}Mn_{0.06}Ni_{0.6}Co_{0.12}Sn_{0.01})_{2.2}$ **(4a)**		0.39		7	32	885	7.051	[177,231]
18	$[Ti_{0.37}Zr_{0.63}](Al_{0.01}V_{0.15}Cr_{0.08}Mn_{0.08}Ni_{0.6}Co_{0.08}Sn_{0.01})_{2.1}$ **(4a,b)**		0.67		20	72	659	5.602	[177,231]
19	$[Ti_{0.37}Zr_{0.63}](Al_{0.01}V_{0.15}Cr_{0.08}Mn_{0.08}Ni_{0.6}Co_{0.08}Sn_{0.01})_{2.2}$ **(4a,b)**		0.48		14	54	1055	7.006	[177,231]
20	$[Ti_{0.4}Zr_{0.6}](Fe_{0.6}Ni_{0.4})_2$ **(2a)**	41.42	1.04	24.53	16.5	124	224	0.39	[218]
21	$[Ti_{0.8}Zr_{0.2}](V_{0.1}Fe_{0.5}Ni_{0.4})_2$ **(2a)**	42.96	1.23		15.1	117	150	3.966	[218], [219]
22	$[Y_{0.09}Zr_{0.91}](Fe)_{1.97}$ **(2b)**	44.7	0.82		23.73	119.99	424	1.624	[244]
23	$[Y_{0.14}Zr_{0.86}](Fe)_{2.04}$ **(2b)**	38.88	1.05		24.41	118.69	430	1.925	[244]
24	$[Y_{0.26}Zr_{0.74}](Fe)_{2.05}$ **(2b)**	45.33	1.11		24.05	105.01	477	4.896	[244]
25	$[Y_{0.29}Zr_{0.71}](Fe)_{2.02}$ **(2b)**	45.5	1.15		29.19	114.49	954	8.809	[244]
26	$[Y_{0.2}Zr_{0.8}](Fe)_{1.95}$ **(2b)**	45.12	1.08		25.06	116.53	428	3.131	[244]
27	$[Y_{0.39}Zr_{0.61}](Fe)_{1.98}$ **(2b)**	45.98	1.21		31.3	107.58	1592	9.406	[244]
28	$[Zr](Al_{0.03}Fe_{0.97})_{1.93}$ **(2b),(3b)**	44.59	1.02		12.64	83.13		1.688	[227]
29	$[Zr](Al_{0.05}Fe_{0.95})_{1.93}$ **(2b)**	44.59	0.88		15.2	90.6		4.422	[227]
30	$[Zr](Al_{0.07}Fe_{0.93})_{1.92}$	44.78	0.84		15.9	88.5		3.425	[227]
31	$[Zr](Al_{0.12}Fe_{0.88})_{1.92}$	45.02	0.66		19.3	90.3		5.246	[227]
32	$[Zr](Al_{0.12}Fe_{0.88})_2$ **(2b)**	44.95	0.93	21.22	19.3	92.4	0	4.138	[178]
33	$[Zr](Al_{0.15}Fe_{0.85})_{1.92}$	45.06	0.59		21.4	92.3		6.801	[227]
34	$[Zr](Al_{0.16}Fe_{0.84})_2$	45.12	0.93	19.85	23.4	97.9	0	7.077	[178]
35	$[Zr](Al_{0.1}Fe_{0.9})_{1.92}$	44.83	0.76		18.1	92.9		4.634	[227]
36	$[Zr](Al_{0.2}Fe_{0.8})_2$	45.52	0.87	17.30	28.7	101.5		8.283	[178]
37	$[Zr](Cr)_2$		1.27		46.02	98.32			[44]
38	$[Zr](Cr)_2$ **(6)**		1.3		39.2	98	2800		[23]
39	$[Zr](Cr_{0.1}Fe_{0.9})_2$ **(1b),(2a)**	44.24	1.21	23.83	22	109	1023	0.999	[218], [219]
40	$[Zr](Cr_{0.1}Fe_{0.9})_2$ **(1a),(2a)**		0.43		23.2	108	898	1.398	[219]
41	$[Zr](Fe)_{1.9}$ **(2a)**	44.46	1.27		21.8	121.4	2419	1.058	[219], [245]
42	$[Zr](Fe)_2$ **(2a)**	44.21	1.23	25.93	21.2	122	1871	0.672	[119], [219]
43	$[Zr](Fe)_{2.5}$ **(2a)**	43.89	1.19		18.3	120	998	1.074	[219], [245]
44	$[Zr](Fe_{0.6}Ni_{0.4})_2$ **(2a)**		1.23		21.7	114	3317	1.008	[219]
45	$[Zr](Fe_{0.7}Ni_{0.3})_2$ **(2a)**		1.2		21.6	114	2669	0.996	[219]
46	$[Zr](Fe_{0.8}Ni_{0.2})_2$ **(1a),(2a)**		0.5		22	115	2843	1.386	[219]
47	$[Zr](Fe_{0.8}Ni_{0.2})_2$ **(1b),(2a)**		1.2		18.7	111	1446	1.332	[219]

(*continued on next page*)

Table A2 (*continued*)

#	Composition	V_0/Z [Å^3]	(H/M) max	$\Delta V/V_0$ [%]	$-\Delta H^o$ [kJ/mol H_2]	$-\Delta S^o$ [J/ (mol H_2 K)]	RT ln (P_A/P_D) [J/mol]	d (lnP_D)/ d (H/M)	Refs
48	$[Zr](Fe_{0.9}Co_{0.1})_2$ [2a]	44.1	1.18	22.68	16.8	108.1	1746	0.666	[119], [219]
49	$[Zr](Fe_{0.9}Cu_{0.1})_2$ [1a]	43.75	1.12	25.00	19.6	112	997	1.303	[218,219]
50	$[Zr](Fe_{0.9}Ni_{0.1})_2$ [1a],[2a]		0.4		22.6	120	1770	1.32	[219]
51	$[Zr](Fe_{0.9}Ni_{0.1})_2$ [1b],[2a]	43.88	1.18	24.20	21.5	119.7	1496	0.795	[218], [219]
52	$[Zr](Mn_{0.11}Fe_{0.89})_{1.97}$	44.34	0.53		18.06	91.23	3172	3.115	[232]
53	$[Zr](Mn_{0.15}Fe_{0.85})_{1.91}$	44.4	0.81		19.06	91.76	2808	2.498	[232]
54	$[Zr](Mn_{0.1}Fe_{0.9})_2$ [2a]	44.22	1.21	28.01	21.8	115.8	1820	4.05	[218], [219]
55	$[Zr](Mn_{0.2}Fe_{0.8})_{1.92}$ [2b]	44.47	1.04		19.97	92.81	2849	2.425	[232]
56	$[Zr](Mn_{0.3}Fe_{0.7})_{1.95}$ [2b],[4a]	44.49	1.08		25.5	99.25	3212	3.391	[232]
57	$[Zr](V)_2$ [3c],[4a]	51.44	1.6	14.99	91.21	133.89	0		[41]
58	$[Zr](V)_2$		1.83		78	88.4			[123]
59	$[Zr](V_{0.02}Fe_{0.98})_{2.03}$ [2b]	44.16	1.18		20.41	113.86	899	1.133	[246]
60	$[Zr](V_{0.05}Fe_{0.95})_{1.93}$	44.87	0.92		23	115.1		3.722	[227]
61	$[Zr](V_{0.05}Fe_{0.95})_{2.06}$ [2b]	44.31	1.07		20.69	111.99	623	1.152	[246]
62	$[Zr](V_{0.05}Mn_{0.09}Fe_{0.86})_{1.92}$ [2b]	44.59	1.04		19.27	87.86	1313	3.21	[232]
63	$[Zr](V_{0.05}Mn_{0.15}Fe_{0.79})_{1.94}$ [2b],[4a]	44.68	1.08		20.75	85.58	1758	3.436	[232]
64	$[Zr](V_{0.07}Fe_{0.93})_{1.98}$ [2b],[4a]	44.34	1.12		21.86	111.61	417	1.934	[246]
65	$[Zr](V_{0.08}Fe_{0.92})_{2.01}$ [2b],[4a]	44.36	1.16		22.03	108.38	388	1.953	[246]
66	$[Zr](V_{0.1}Fe_{0.9})_{1.92}$ [4a]	44.89	1.06		24.2	105.4		4.078	[227]
67	$[Zr](V_{0.1}Fe_{0.9})_2$ [4a]	44.32	1.2	25.36	23.6	102	200	3.24	[218], [219]

Notes: [1] –thermodynamic data for the [a] first / lower and [b] second / higher plateau; [2] – (H/M)max measured at [a] P > 1000 bar and/or [b] T < −30 °C; [3] – thermodynamic data presented for plateau midpoint corresponding to H/M about: [a] 0.4, [b] 0.5 and [c] 0.8; [4] multiphase: [a] C15 +C14, [b] BCC impurity, [c] ZrNi impurity; [5] as-cast alloy; [6] – thermodynamic data taken calorimetrically

Appendix B. Supporting information

Supplementary data associated with this article can be found in the online version at doi:10.1016/j.jallcom.2022.165219.

References

[1] P. Dantzer, Metal-hydride technology: a critical review, in: H. Wipf (Ed.), Hydrogen in Metals III. Properties and Applications (Topics in Applied Physics, volume 73, Springer-Verlag, Berlin Heidelberg, 1997, pp. 279–340.

[2] J.-M. Joubert, M. Latroche, A. Percheron-Guégan, Metallic hydrides II: materials for electrochemical storage, MRS Bull. 27 (9) (2002) 694–698.

[3] G. Sandrock, R.C. Bowman Jr., Gas-based hydride applications: recent progress and future needs, J. Alloy. Comp. 356–357 (2003) 794–799.

[4] M.V. Lototskyy, V.A. Yartys, B.G. Pollet, R.C. Bowman Jr., Metal hydride hydrogen compressors: a review, Int. J. Hydrog. Energy 39 (2014) 5818–5851.

[5] V.A. Yartys, M. Lototskyy, V. Linkov, D. Grant, A. Stuart, J. Eriksen, R. Denys, R.C. Bowman Jr., Metal hydride hydrogen compression: recent advances and future prospects, Appl. Phys. A 122 (4) (2016) 415, https://doi.org/10.1007/s00339-016-9863-7

[6] M.M.H. Bhuiya, A. Kumar, K.J. Kim, Metal hydrides in engineering systems, processes, and devices: a review of non-storage applications, Int. J. Hydrog. Energy 40 (2015) 2231–2247.

[7] N.A.A. Rusman, M. Dahari, A review on the current progress of metal hydrides material for solid-state hydrogen storage applications, Int. J. Hydrog. Energy 41 (2016) 12108–12126.

[8] V. Yartys, D. Noreus, M. Latroche, Metal hydrides as negative electrode materials for Ni–MH batteries, Appl. Phys. A 122 (2016) 43, https://doi.org/10.1007/s00339-015-9538-9

[9] M.V. Lototskyy, I. Tolj, L. Pickering, C. Sita, F. Barbir, V. Yartys, The use of metal hydrides in fuel cell applications, Prog. Nat. Sci. 27 (2017) 3–20.

[10] L. Ouyang, J. Huang, H. Wang, J. Liu, M. Zhu, Progress of hydrogen storage alloys for Ni-MH rechargeable power batteries in electric vehicles: a review, Mater. Chem. Phys. 200 (2017) 164–178.

[11] J. Bellosta von Colbe, J.-R. Ares, J. Barale, M. Baricco, C. Buckley, G. Capurso, N. Gallandat, D.M. Grant, M.N. Guzik, I. Jacob, E.H. Jensen, T. Jensen, J. Jepsen, T. Klassen, M.V. Lototskyy, K. Manickam, A. Montone, J. Puszkiel, S. Sartori, D.A. Sheppard, A. Stuart, G. Walker, C.J. Webb, H. Yang, V. Yartys, A. Züttel, M. Dornheim, Application of hydrides in hydrogen storage and compression: achievements, outlook and perspectives, Int. J. Hydrog. Energy 44 (2019) 7780–7808.

[12] A. El Kharbachi, E.M. Dematteis, K. Shinzato, S.C. Stevenson, L.J. Bannenberg, M. Heere, C. Zlotea, P.Á. Szilágyi, J.-P. Bonnet, W. Grochala, D.H. Gregory, T. Ichikawa, M. Baricco, B.C. Hauback, Metal hydrides and related materials. Energy carriers for novel hydrogen and electrochemical storage, J. Phys. Chem. C. 124 (14) (2020) 7599–7607, https://doi.org/10.1021/acs.jpcc.0c01806

[13] M. Hirscher, V.A. Yartys, M. Baricco, J. Bellosta von Colbe, D. Blanchard, R.C. Bowman Jr., D.P. Broom, C.E. Buckley, F. Chang, P. Chen, Y.W. Cho, J.-C. Crivello, F. Cuevas, W.I.F. David, P.E. de Jongh, R.V. Denys, M. Dornheim, M. Felderhoff, Y. Filinchuk, G.E. Froudakis, D.M. Grant, E. MacA. Gray, B.C. Hauback, T. He, T.D. Humphries, T.R. Jensen, S. Kim, Y. Kojima, M. Latroche, H.-W. Li, M.V. Lototskyy, J.W. Makepeace, K.T. Møller, L. Naheed, P. Ngene, D. Noréus, M.M. Nygård, S.-I. Orimo, M. Paskevicius, L. Pasquini, D.B. Ravnsbækc, M.V. Sofianos, T.J. Udovic, T. Vegge, G.S. Walker, C.J. Webb, C. Weidenthaler, C. Zlotea, Materials for hydrogen-based energy storage – past, recent progress and future outlook, J. Alloy. Compd. 827 (2020) 153548.

[14] I.A. Hassan, H.S. Ramadan, M.A. Saleh, D. Hissel, Hydrogen storage technologies for stationary and mobile applications: review, analysis and perspectives, Renew. Sust. Energy Rev. 149 (2021) 111311.

[15] M. Lototskyy, B. Satya Sekhar, P. Muthukumar, V. Linkov, B.G. Pollet, Niche applications of metal hydrides and related thermal management issues, J. Alloy. Comp. 645 (2015) S117–S122, https://doi.org/10.1016/j.jallcom.2014.12.271

[16] R. Mohtadi, S.-I. Orimo, The renaissance of hydrides as energy materials, Nat. Rev. Mater. 2 (2016) 16091, https://doi.org/10.1038/natrevmats.2016.91

[17] M. Baricco, M. Bang, M. Fichtner, B. Hauback, M. Linder, C. Luetto, P. Moretto, M. Sgroi, SSH2S: Hydrogen storage in complex hydrides for an auxiliary power unit based on high temperature proton exchange membrane fuel cells, J. Power Sources 342 (2017) 853–860.

[18] G. Sandrock, A panoramic overview of hydrogen storage alloys from a gas reaction point of view, J. Alloy. Comp. 293–295 (1999) 877–888, https://doi.org/10.1016/S0925-8388(99)00384-9

[19] Hydrogen Storage Technology Materials and Applications, in: L. Klebanoff (Ed.), CRC Press / Taylor & Francis, 2016.

[20] P. Modi, K.-F. Aguey-Zinsou, Room temperature metal hydrides for stationary and heat storage applications: a review, Front. Energy Res. 9 (2021) 616115, https://doi.org/10.3389/fenrg.2021.616115

[21] M. Lototskyy, V.A. Yartys, Comparative analysis of the efficiencies of hydrogen storage systems utilising solid state H storage materials, J. Alloy. Comp. 645 (2015) S365–S373.

[22] V.K. Sinha, G.Y. Yu, W.E. Wallace, Hydrogen storage in some ternary and quaternary zirconium-based alloys with the C14 structure, J. Less Common Met. 106 (1985) 67–77, https://doi.org/10.1016/0022-5088(85)90367-4

[23] D.G. Ivey, D.O.Northwood Storing, Hydrogen in AB_2 laves-type compounds, Z. Phys. Chem. N. F. 147 (1986) 191–209, https://doi.org/10.1524/zpch.1986.147.1_2.191

[24] L.F. Chanchetti, D.R. Leiva, L.I.L. de Faria, T.T. Ishikawa, A scientometric review of research in hydrogen storage materials, Int. J. Hydrog. Energy 45 (2020) 5356–5366.

[25] F. Stein, A. Leineweber, Laves phases: a review of their functional and structural applications and an improved fundamental understanding of stability and properties, J. Mater. Sci. 56 (2021) 5321–5427, https://doi.org/10.1007/s10853-020-05509-2

[26] Y. Kojima, Y. Kawai, S.-I. Towata, T. Matsunaga, T. Shinozawa, M. Kimbara, Development of metal hydride with high dissociation pressure, J. Alloy. Comp. 419 (2006) 256–261, https://doi.org/10.1016/j.jallcom.2005.08.078

[27] L. Pickering, J. Li, Dl Reed, A.I. Bevan, D. Book, Ti–V–Mn based metal hydrides for hydrogen storage, J. Alloy. Comp. 580 (2013) S233–S237.

[28] Z. Cao, L. Ouyang, H. Wang, J. Liu, D. Sun, Q. Zhang, M. Zhu, Advanced high-pressure metal hydride fabricated via Ti-Cr-Mn alloys for hybrid tank, Int. J. Hydrog. Energy 40 (2015) 2717–2728, https://doi.org/10.1016/j.ijhydene.2014.12.093

[29] L. Pickering, M.V. Lototskyy, M.W. Davids, C. Sita, V. Linkov, Induction melted AB_2-type metal hydrides for hydrogen storage and compression applications, Mater. Today.: Proc. 5 (2018) 10470–10478, https://doi.org/10.1016/j.matpr.2017.12.378

[30] S. Nayebossadri, D. Book, Development of a high-pressure Ti-Mn based hydrogen storage alloy for hydrogen compression, Renew. Energy 143 (2019) 1010–1021, https://doi.org/10.1016/j.renene.2019.05.052

[31] Z. Cao, P. Zhou, X. Xiao, L. Zhan, Z. Li, S. Wang, L. Chen, Investigation on Ti-Zr-Cr-Fe-V based alloys for metal hydride hydrogen compressor at moderate working temperatures, Int J. Hydrog. Energy 46 (2021) 21580–21589, https://doi.org/10.1016/j.ijhydene.2021.03.247

[32] D.B. Smith, R.C. Bowman Jr, L.M. Anovitz, C. Corgnale, M. Sulic, Isotherm measurements of high-pressure metal hydrides for hydrogen compressors, J. Phys. Energy 3 (2021) 034004, https://doi.org/10.1088/2515-7655/abeab5

[33] P. Dantzer, F. Meunier, What materials to use in hydride chemical heat pumps? Mater. Sci. Forum 31 (1988) 1–18, https://doi.org/10.4028/www.scientific.net/MSF.31.1

[34] M. Linder. Automotive Cooling Systems based on Metal Hydrides, DEng Thesis, Inst. Nucl. Technol. Energy Syst. / Univ. Stuttgart, 2010. Downloaded from ⟨https://d-nb.info/1005593779/34⟩, Aug. 05, 2021.

[35] B. Bahar, W. TomHon, M. Golben, J. Zerby, M. Golben, Solid State (Metal Hydride) Refrigerant Based Air Conditioner and Freezer Systems, in: 13th IEA Heat Pump Conference, May 11–14, 2020 Jeju, Korea. Downloaded from ⟨https://www.xergyincstore.com/wp-content/uploads/2021/02/HPC2020_MHHX-HP.pdf⟩, Aug. 05, 2021.

[36] K.-H. Young, J. Nei, C. Wan, R.V. Denys, V.A. Yartys, Comparison of C14- and C15-predomiated AB_2 metal hydride alloys for electrochemical applications, Batteries 3 (2017) 22, https://doi.org/10.3390/batteries3030022

[37] C.B. Wan, X.P. Jiang, X.H. Yin, X. Ju, High-capacity Zr-based AB_2-type alloys as metal hydride battery anodes, J. Alloy. Comp. 828 (2020) 154402.

[38] D.J. Thoma, Intermetallics: Laves Phases, in: Encyclopedia of Materials: Science and Technology, 2011. ⟨https://doi:10.1016/B0–08–043152–6/00739–7⟩.

[39] P. Villars, K. Cenzual. Pearson's Crystal Data – Crystal Structure Database for Inorganic Compounds, Release 2010/11, ASM International, Materials Park, Ohio, USA.

[40] B. Chao, L. Klebanoff, Hydrogen storage in interstitial metal hydrides, in: L. Klebanoff (Ed.), Hydrogen Storage Technology, CRC Press, 2012, pp. 109–131.

[41] A. Pebler, E.A. Gulbransen, Equilibrium studies on the systems $ZrCr_2$–H_2, ZrV_2–H_2, and $ZrMo_2$–H_2 between 0 and 900°C, Trans, Met. Soc. AIME 239 (1967) 1593–1600.

[42] V.A. Yartys, R.V. Denys, C.J. Webb, J.P. Mæhlen, E. MacA. Gray, T. Blach, O. Isnard, L.C. Barnsley, High pressure in situ studies of metal-hydrogen systems, J. Alloy. Comp. 509 (Suppl. 2) (2011) S817–S822, https://doi.org/10.1016/j.jallcom.2010.12.030

[43] C. Wan, V.E. Antonov, R.V. Denys, V.I. Kulakov, V.A. Yartys, $MgCo_2$-D_2 and MgCoNi-D_2 systems synthesized at high pressures and interaction mechanism during the HDDR processing, Progr. Nat. Sci.: Mater. Int. 27 (1) (2017) 74–801, https://doi.org/10.1016/j.pnsc.2017.01.007

[44] D. Shaltiel, I. Jacob, D. Davidov, Hydrogen absorption and desorption properties of AB_2 Laves-phase pseudobinary compounds, J. Less-Common Met. 53 (1977) 117–131, https://doi.org/10.1016/0022-5088(77)90162-X

[45] Y. Machida, T. Yamadaya, M. Asanuma. Hydride formation of C14-type Ti alloy, in: Hydrides for Energy Storage. Proc. Int. Symp., Geilo, Norway, 14–19 August 1977, 1978, pp. 329–336; DOI:10.1016/B978–0–08–022715–3.50033–3.

[46] H. Oesterreicher, H. Bittner, Studies of hydride formation in $Ti_{1-x}Zr_xMn_2$, Mater. Res. Bull. 13 (1978) 83–88, https://doi.org/10.1016/0025-5408(78)90031-4

[47] L.N. Padurets, A.A. Chertkov, V.I. Mikheeva, Synthesis and properties of ternary compounds with hydrogen in the systems of Zr-M-H(M=V, Cr, Mn, Fe, Co, Ni), Izv. Akad. Nauk SSSR, Neorg. Mater. 14 (1978) 1624–1628.

[48] K.N. Semenenko, V.N. Verbetsky, S.V. Mitrokhin, V.V. Burnasheva, Investigation of the interaction with hydrogen of Zirconium intermetallic compounds crystallised in Laves phase structure types, Russ, J. Inorg. Chem. 25 (1980) 1731–1736.

[49] H. Fujii, F. Pourarian, V.K. Sinha, W.E. Wallace, Magnetic, crystallographic, and hydrogen-storage characteristics of $Zr_{1-x}Ti_xMn_2$ hydrides, J. Phys. Chem. 85 (1981) 3112–3116, https://doi.org/10.1021/j150621a021

[50] A. Suzuki, N. Nishimiya, S. Ono, Thermodynamic properties of Zr $(Fe_xMn_{1-x})_2$–H_2 systems, J. Less Common Met 89 (1983) 263–268, https://doi.org/10.1016/0022-5088(83)90278-3

[51] F. Pourarian, W.E. Wallace, Hydrogen sorption characteristics of $Zr_{1-x}Ti_x(Cr_{1-y}Fe_y)_2$ alloys, J. Less-Common Met 107 (1985) 69–78, https://doi.org/10.1016/0022-5088(85)90242-5

[52] G.Y. Yu, F. Pourarian, W.E. Wallace, The crystallographic, thermodynamic and kinetic properties of the $Zr_{1-x}Ti_xCrFe$-H_2 system, J. Less Common Met 106 (1985) 79–87, https://doi.org/10.1016/0022-5088(85)90368-6

[53] F. Pourarlan, H. FuJii, W.E. Wallace, V.K. Slnha, H. Kevin Smith, Stability and Magnetism of Hydrides of Nonstoichiometric $ZrMn_2$, J. Phys. Chem. 85 (1981) 3105–3111, https://doi.org/10.1021/j150621a021

[54] V.K. Sinha, W.E. Wallace, $Zr_{0.7}Ti_{0.3}Mn_2Fe_{0.8}$ as a material for hydrogen storage, J. Less-Common Met. 87 (1982) 297–303, https://doi.org/10.1016/0022-5088(82)90096-0

[55] V.K. Sinha, F. Pourarian, W.E. Wallace, Hydrogen absorption by $ZrMn_2Fe_x$, J. Phys. Chem. 86 (1982) 4952–4956, https://doi.org/10.1021/j100222a024

[56] F. Pourarian, V.K. Sinha, W.E. Wallace, Hydrogen absorption by $ZrMn_2Mn_yFe_x$, J. Phys. Chem. 86 (1982) 4956–4958, https://doi.org/10.1021/j100222a025

[57] A.T. Pedziwiatr, R.S. Craig, W.E. Wallace, F. Pourarian, Calorimetric entalpies of formation and decomposition of $ZrMn_2$, $ZrCr_2$ and related systems, J. Solid State Chem. 46 (1983) 336–341, https://doi.org/10.1016/0022-4596(83)90158-5

[58] F. Pourarian, V.K. Sinha, W.E. Wallace, Hydrogen sorption properties of non-stoichiometric $ZrMn_2$-based systems, J. Less-Common Met. 96 (1984) 237–248, https://doi.org/10.1016/0022-5088(84)90200-5

[59] F. Pourarian, W.E. Wallace, Hydrogenation characteristics of the hyper-stoichiometric $ZrCrFeT_x$ system (T = Mn, Fe, Co, Ni, or Cu), J. Solid State Chem. 55 (1984) 181–192, https://doi.org/10.1016/0022-4596(84)90263-9

[60] V.K. Sinha, W.E. Wallace, Hydrides of $ZrMn_2$-based alloys substoichiometric in zirconium for engineering applications, J. Less Common Met. 106 (1985) 199–210, https://doi.org/10.1016/0022-5088(85)90255-3

[61] T. Gamo, Y. Moriwaki, N. Yanagihara, T. Yamashita, T. Iwaki, Formation and properties of titanium-manganese alloy hydrides, Int. J. Hydrog. Energy 10 (1) (1985) 39–47.

[62] B.-H. Liu, D.-M. Kim, K.-Y. Lee, J.-Y. Lee, Hydrogen storage properties of $TiMn_2$-based alloys, J. Alloy. Comp. 240 (1996) 214–218.

[63] J.-L. Bobet, B. Chevalier, B. Darriet, Crystallographic and hydrogen sorption properties of $TiMn_2$ based alloys, Intermetallics 8 (2000) 359–363.

[64] J.-L. Bobet, B. Darriet, Relationship between hydrogen sorption properties and crystallography for $TiMn_2$ based alloys, Int. J. Hydrog. Energy 25 (2000) 767–772.

[65] E. Akiba, H. Iba, Hydrogen absorption by Laves phase related BCC solid solution, Intermetallics 6 (1998) 461–470.

[66] J.-Y. Lee, K.-Y. Lee, H.-H. Lee, D.-M. Kim, J.-S. Yu, J.-H. Jung, S.-G. Lee, Hydrogen-storage material employing Ti-Mn alloy system, Patent US 5888317 (1999).

[67] T. Gamo, Y. Moriwaki, T. Yamashita, M. Fukuda. Hydrogen storage material, Patent US 4195989 (1980).

[68] Y. Nakamura, H. Nakamura, M. Kamikawa, H. Watanabe, S. Fujitani, I. Yonezu. Hydrogen absorbing alloys, Patent US 5851690 (1998).

[69] R.M. van Essen, K.H.J. Buschow, Composition and hydrogen absorption of Zr-Mn compounds, Mat. Res. Bull. 15 (1980) 1149–1155.

[70] V.A. Yartys, M.V. Lototskyy, V. Linkov, S. Pasupathi, M.W. Davids, I. Tolj, G. Radica, R.V. Denys, J. Eriksen, K. Taube, J. Bellosta von Colbe, G. Capurso, M. Dornheim, F. Smith, D. Mathebula, D. Swanepoel, S. Suwarno, HYDRIDE4MOBILITY: An EU HORIZON 2020 project on hydrogen powered fuel cell utility vehicles using metal hydrides in hydrogen storage and refuelling systems, Int. J. Hydrog. Energy 46 (2021) 35896–35909, https://doi.org/10.1016/j.ijhydene.2021.01.190

[71] C. Wan, R.V. Denys, V.A. Yartys, Effects of Ti substitution for Zr on the electrochemical characteristics and structure of AB_2-type Laves-phase alloys as metal hydride anodes, J. Alloy. Comp. 889 (2021) 161655, https://doi.org/10.1016/j.jallcom.2021.161655

[72] R.M. van Essen, K.H.J. Buschow, Composition and hydrogen absorption of C14 type Zr-Mn compounds, Mater. Res. Bull. 15 (1980) 1149–1155, https://doi.org/10.1016/0025-5408(80)90079-3

[73] G. Li, N. Nishimiya, H. Satoh, N. Kamegashira, Crystal structure and hydrogen absorption of $Ti_xZr_{1-x}Mn_2$, J. Alloy. Comp. 393 (2005) 231–238, https://doi.org/10.1016/j.jallcom.2004.08.097

[74] H.A. Kierstead, A theory of multiplateau hydrogen absorption isotherms, J. Less-Common Met 71 (1980) 303–309.

[75] V.V. Burnasheva, A.V. Ivanov, V.A. Yartys, K.N. Semenenko, Intermetallic hydrides based on the scandium Laves-type compounds, Izv. AN SSSR (Bull. USSR Acad. Sci), Inorg. Mater. 17 (1981) 980–984.

[76] K. Aoki, T. Yamamoto, Y. Satoh, K. Fukamichi, T. Masumoto, Amorphization of the $CeFe_2$ Laves Phase Compound by Hydrogen Absorption, Acta Met. 35 (10) (1987) 2465-2410.

[77] K. Aoki, X.-G. Li, T. Masumoto, Factors controlling hydrogen-induced amorphization of C15 laves compounds, Acta Metal. Mater. 40 (7) (1992) 1717–1726.

[78] K. Aoki, T. Yamamoto, T. Masumoto, Hydrogen induced amorphization in RNi_2 Laves phases, Scr. Metal. 21 (1987) 27–31.

[79] A.L. Shilov, Thermodynamic instability and structure of intermetallic hydrides, Russ, J. Inorg. Chem. 36 (9) (1991) 2228–2235.

[80] K. Chattopadyhay, K. Aoki, T. Masumoto, The nature of hydrogen-induced amorphization of $SmNi_2$ Laves compound, Scr. Metal. 21 (3) (1987) 365–369.

[81] U.-I. Chung, Y.-G. Kim, J.-Y. Lee, Phase separation in amorphous $ErNi_2H_x$ prepared by hydrogenation, J. Appl. Phys. 69 (3) (1991) 1275–1278.

[82] M. Latroche, V. Paul-Boncour, A. Percheron-Guegan, Structural instability in $R_{1-x}Ni_2$ compounds and their hydrides (R=Y, rare earth), Z. Phys. Chem. 179 (1993) 261–268.

[83] A.V. Irodova, O.A. Lavrova, G.V. Laskova, P.P. Parshin, A.L. Shilov, Hydrogen-induced transformations in the $PrNi_2$-H system: from crystalline to amorphous state, Solid State Phys. 38 (1) (1996) 277–283.

[84] A.L. Shilov, L.N. Padurets, Z.V. Dobrokhotova, A.V. Gribanov, Y.D. Seropegin, Interaction of YNi_2 alloy with hydrogen, Russ. J. Inorg. Chem. 46 (2) (2001) 164–168.

[85] V.A. Yartys. Crystal Chemistry of Intermetallic Hydrides. Ph.D. Thesis, Moscow State Univ., 1980.

[86] A. Werwein, Ch Benndorf, M. Bertmer, A. Franz, O. Oeckler, H. Kohlmann, Hydrogenation Properties of $LnAl_2$ (Ln = La, Eu, Yb), $LaGa_2$, $LaSi_2$ and the Crystal Structure of $LaGa_2H_{0.71(2)}$, Crystals 9 (2019) 193, https://doi.org/10.3390/cryst9040193

[87] F. Gingl, K. Yvon, T. Vogt, A. Hewat, Synthesis and crystal structure of tetragonal $LnMg_2H_7$ (Ln = La, Ce), two Laves phase hydride derivatives having ordered hydrogen distribution, J. Alloy. Compd. 253–254 (1997) 313–317.

[88] A. Werwein, F. Maaß, L.Y. Dorsch, O. Janka, R. Pöttgen, T.C. Hansen, J. Kimpton, H. Kohlmann, Hydrogenation properties of laves phases $LnMg_2$ (Ln = La, Ce, Pr, Nd, Sm, Eu, Gd, Tb, Ho, Er, Tm, Yb), Inorg. Chem. 56 (2017) 15006–15014.

[89] V.A. Yartys, V.E. Antonov, A.I. Beskrovnyi, J.-C. Crivello, R.V. Denys, V.K. Fedotov, M. Gupta, V.I. Kulakov, M.A. Kuzovnikov, M. Latroche, Yu.G. Morozov, S.G. Sheverev, B.P. Tarasov, Hydrogen assisted phase transition in a trihydride $MgNi_2H_3$ synthesised at high H_2 pressures: thermodynamics, crystallographic and electronic structures, Acta Mater. 82 (2015) 316–327, https://doi.org/10.1016/j.actamat.2014.09.012

[90] V.A. Yartys, V.E. Antonov, D. Chernyshov, J.-C. Crivello, R.V. Denys, V.K. Fedotov, M. Gupta, V.I. Kulakov, M. Latroche, D. Sheptyakov, Structure and chemical bonding in $MgNi_2H_3$ from combined high resolution synchrotron and neutron diffraction studies and ab initio electronic structure calculations, Acta Mater. 98 (2015) 416–422, https://doi.org/10.1016/j.actamat.2015.07.053

[91] U.C. Rodewald, B. Chevalier, R. Pöttgen, Rare earth–transition metal–magnesium compounds–an overview, J. Solid State Chem. 180 (2007) 1720–1736.

[92] T. Sato, T. Mochizuki, K. Ikeda, T. Honda, T. Otomo, H. Sagayama, H. Yang, W. Luo, L. Lombardo, A. Züttel, S. Takagi, T. Kono, S.-I. Orimo, Crystal structural investigations for understanding the hydrogen storage properties of $YMgNi_4$-based alloys, ACS Omega 5 (2020) 31192–31198, https://doi.org/10.1021/acsomega.0c04535

[93] L. Guénée, V. Favre-Nicolin, K. Yvon, Synthesis, crystal structure and hydrogenation properties of the ternary compounds $LaNi_4Mg$ and $NdNi_4Mg$, J. Alloy. Comp. 348 (1–2) (2003) 129–137.

[94] H. Oesterreicher, H. Bittner, Hydride formation in $La_{1-x}Mg_xNi_2$, J. Less-Common Met 73 (1980) 339, https://doi.org/10.1016/0022-5088(80)90327-6

[95] K. Sakaki, N. Terashita, S. Tsunokake, Y. Nakamura, E. Akiba, Effect of rare earth elements and alloy composition on hydrogenation properties and crystal structures of hydrides in $Mg_{2-x}RE_xNi_4$, J. Phys. Chem. C. 116 (36) (2012) 19156–19163, https://doi.org/10.1021/jp3052856

[96] T. Yang, Z. Yuan, W. Bu, Z. Jia, Y. Qi, Y. Zhang, Effect of elemental substitution on the structure and hydrogen storage properties of $LaMgNi_4$ alloy, Mater. Des. 93 (2016) 46–52.

[97] X. Liu, K. Asano, N. Terashita, E. Akiba, Hydrogenation of C14 Laves phase alloy: $CaLi_2$, Int. J. Hydrog. Energy 34 (3) (2009) 1472–1475.

[98] N. Terashita, E. Akiba, Hydrogenation properties of $CaMg_2$ based alloys, Mater. Trans. 45 (8) (2004) 2594–2597.

[99] L. Liang, F. Wang, M. Rong, Z. Wang, S. Yang, J. Wang, H. Zhou, Recent advances on preparation method of Ti-based hydrogen storage alloy, J. Mater. Sci. Chem. Eng. (MSCE) 8 (2020) 18–38, https://doi.org/10.4236/msce.2020.812003

[100] A. Anani, A. Visintin, K. Petrov, S. Srinivasan, J.J. Reilly, J.R. Johnson, R.B. Schwarz, P.B. Desch, Alloys for hydrogen storage in nickel/hydrogen and nickel/metal hydride batteries, J. Power Sources 47 (1994) 261–275, https://doi.org/10.1016/0378-7753(94)87005-5

[101] Y.L. Zhang, J.S. Li, T.B. Zhang, R. Hu, X.Y. Xue, Microstructure and hydrogen storage properties of non-stoichiometric Zr-Ti-V Laves phase alloys, Int. J. Hydrog. Energy 38 (2013) 14675–149684, https://doi.org/10.1016/j.ijhydene.2013.09.040

[102] J. Puszkiel, J.M. Bellosta von Colbe, J. Jepsen, S.V. Mitrokhin, E. Movlaev, V. Verbetsky, T. Klassen, Designing an AB_2-Type Alloy (TiZr-CrMnMo) for the Hybrid Hydrogen Storage Concept, Energies 13 (2020) 2751, https://doi.org/10.3390/en13112751

[103] Y.-H. Zhang, G. Huang, Z.-M. Yuan, S.-H. Guo, Y. Qi, D.-L. Zhao, Electrochemical hydrogen storage behaviors of as-cast and spun RE–Mg–Ni–Co–Al-based AB_2-type alloys applied to Ni–MH battery, Rare Met 39 (2) (2020) 181–192, https://doi.org/10.1007/s12598-018-1147-2

[104] S. Fashu, M. Lototskyy, M.W. Davids, L. Pickering, V. Linkov, S. Tai, T. Renheng, X. Fangming, P.V. Fursikov, B.P. Tarasov, A review on crucibles for induction melting of titanium alloys, Mater. Des. 186 (2020) 108295, https://doi.org/10.1016/j.matdes.2019.108295

[105] B. Friedrich, Large-scale production and quality assurance of hydrogen storage (Battery) alloys, J. Mater. Eng. Perform. 3 (1) (1994) 37–46, https://doi.org/10.1007/BF02654497

[106] M.W. Davids, T. Martin, M. Lototskyy, R. Denys, V. Yartys, Study of hydrogen storage properties of oxygen modified Ti- based AB2 type metal hydride alloy, Int. J. Hydrog. Energy 46 (2021) 13658–13663, https://doi.org/10.1016/j.ijhydene.2020.05.215

[107] K. Young, D.F. Wong, T. Ouchi, B. Huang, B. Reichman, Effects of La-addition to the structure, hydrogen storage, and electrochemical properties of C14 metal hydride alloys, Electrochim. Acta 174 (2015) 815–825, https://doi.org/10.1016/j.electacta.2015.06.048

[108] A.A. Volodin, R.V. Denys, C.B. Wan, I.D. Wijayanti, B.P. Suwarno, V.E. Tarasov, V.A. Yartys, V.E. Antonov, Study of hydrogen storage and electrochemical properties of AB_2-type $Ti_{0.15}Zr_{0.85}La_{0.03}Ni_{1.2}Mn_{0.7}V_{0.12}Fe_{0.12}$ alloy, J. Alloy. Comp. 793 (2019) 564–575, https://doi.org/10.1016/j.jallcom.2019.03.134

[109] Z. Yao, L. Liu, X. Xiao, C. Wang, L. Jiang, L. Chen, Effect of rare earth doping on the hydrogen storage performance of $Ti_{1.02}Cr_{1.1}Mn_{0.3}Fe_{0.6}$ alloy for hybrid hydrogen storage application, J. Alloy. Comp. 731 (2018) 524–530, https://doi.org/10.1016/j.jallcom.2017.10.075

[110] F. Aouaini, N. Bouazizi, M.M. Almoneef, H. Al-Ghamdia, A. Ben Lamine, Absorption and desorption of hydrogen in $Ti_{1.02}Cr_{1.1}Mn_{0.3}Fe_{0.6}RE_{0.03}$: experiments, characterization and analytical interpretation using statistical physics treatment, RSC Adv. 11 (2021) 15905, https://doi.org/10.1039/d1ra00999k

[111] U. Ulmer, M. Dieterich, A. Pohl, R. Dittmeyer, M. Linder, M. Fichtner, Study of the structural, thermodynamic and cyclic effects of vanadium and titanium substitution in laves-phase AB_2 hydrogen storage alloys, Int. J. Hydrog. Energy 42 (2017) 20103–20110, https://doi.org/10.1016/j.ijhydene.2017.06.137

[112] M.W. Davids, M. Lototskyy, B.G. Pollet, Manufacturing of hydride-forming alloys from mixed titanium – iron oxide, Adv. Mater. Res. 746 (2013) 14–22, https://doi.org/10.4028/www.scientific.net/AMR.746.14

[113] J. Peng, Y. Zhu, D. Wang, X. Jina, G.Z. Chen, Direct and low energy electrolytic co-reduction of mixed oxides to zirconium-based multi-phase hydrogen storage alloys in molten salts, J. Mater. Chem. 19 (2009) 2803–2809, https://doi.org/10.1039/b820560d

[114] S.R. Ovshinsky, M.A. Fetcenko, J. Ross, A nickel metal hydride battery for electric vehicles, Science 260 (5105) (1993) 176–181, https://doi.org/10.1126/science.260.5105.176

[115] S.K. Zhang, Q.D. Wang, Y.Q. Lei, G.L. Lü, L.X. Chen, F. Wu, The phase structure and electrochemical properties of the melt-spun alloy $Zr_{0.7}Ti_{0.3}Mn_{0.4}V_{0.4}Ni_{1.2}$, J. Alloy. Comp. 330–332 (2002) 855–860, https://doi.org/10.1016/S0925-8388(01)01482-7

[116] J. Ting, U. Habel, M.W. Peretti, W.B. Eisen, R. Young, B. Chao, B. Huang, Gas atomization processing of designed dual-phase intermetallic hydrogen storage alloys, Mater. Sci. Eng. A329–331 (2002) 372–376, https://doi.org/10.1016/S0921-5093(01)01605-7

[117] Y.-H. Zhang, W. Zhang, X.-P. Song, P.-L. Zhang, Y.-G. Zhu, Y. Qi, Effects of spinning rate on structures and electrochemical hydrogen storage performances of RE–Mg–Ni–Mn-based AB_2-type alloys, Trans. Nonferrous Met. Soc. China 26 (2016) 3219–3231, https://doi.org/10.1016/S1003-6326(16)64454-0

[118] K.N. Semenenko, R.A. Sirotina, A.P. Savchenkova, V.V. Burnasheva, M.V. Lototskii, E.E. Fokina, S.L. Troitskaya, V.N. Fokin, Interactions of λ_3-$ScFe_2$ and λ_2-$ScFe_{1.8}$ with hydrogen, J. Less-Common Met 106 (1985) 349–359, https://doi.org/10.1016/0022-5088(85)90272-3

[119] T. Zotov, E. Movlaev, S. Mitrokhin, V. Verbetsky, Interaction in (Ti,Sc)Fe_2–H_2 and (Zr,Sc)Fe_2–H_2 systems, J. Alloy. Comp. 459 (2008) 220–224, https://doi.org/10.1016/j.jallcom.2007.05.027

[120] O. Beeri, D. Cohen, Z. Gavra, M.H. Mintz, Sites occupation and thermodynamic properties of the $TiCr_{2-x}Mn_x$ –H_2 ($0 < x < 1$) system: Statistical thermodynamics analysis, J. Alloy. Comp. 352 (2003) 111–122, https://doi.org/10.1016/S0925-8388(02)01155-6

[121] J.R. Johnson, Reaction of hydrogen with the high temperature (C14) form of $TiCr_2$, J. Less Common Met 73 (1980) 345–354, https://doi.org/10.1016/0022-5088(80)90328-8

[122] H. Wada, M. Hada, M. Shiga, Y. Nakamura, Low temperature specific heat of laves phase AFe_2 compounds (A=Nb, Ta and Ti), J. Phys. Soc. Jpn. 59 (1990) 701–705, https://doi.org/10.1143/JPSJ.59.701

[123] A.L. Shilov, L.N. Padurets, M.E. Kost, Thermodynamics of hydrides of intermetallic compounds of transition metals, Russ. J. Phys. Chem. 59 (1985) 1857–1875.

[124] S.-K. Chen, P.-H. Lee, H. Lee, H.-T. Su, Hydrogen storage of C14-$Cr_uFe_vMn_wTi_xV_yZr_z$ alloys, Mater. Chem. Phys. 210 (2018) 336–347, https://doi.org/10.1016/j.matchemphys.2017.08.008

[125] I.D. Wijayanti, R. Denys, A.A.Volodin Suwarno, M.V. Lototskyy, M.N. Guzik, J. Nei, K. Young, H.J. Roven, V. Yartys, Hydrides of Laves type Ti-Zr alloys with enhanced H storage capacity as advanced metal hydride battery anodes, J. Alloy. Comp. 828 (2020) 154354, https://doi.org/10.1016/j.jallcom.2020.154354

[126] M. Sahlberg, D. Karlsson, C. Zlotea, U. Jansson, Superior hydrogen storage in high entropy alloys, Sci. Rep. 6 (2016), https://doi.org/10.1038/srep36770

[127] F. Yang, J. Wang, Y. Zhang, Z. Wu, Z. Zhang, F. Zhao, J. Huot, J. Grobivć Novaković, N. Novaković, Recent progress on the development of high entropy alloys (HEAs) for solid hydrogen storage: a review, Int. J. Jydrogen Energy (2022), https://doi.org/10.1016/j.ijhydene.2022.01.141

[128] A. Amiri, R. Shahbazian-Yassar, Recent progress of high-entropy materials for energy storage and conversion, J. Mater. Chem. A. 9 (2021) 782–823, https://doi.org/10.1039/d0ta09578h

[129] M.M. Nygård, G. Ek, D. Karlsson, M. Sahlberg, M.H. Sørby, B.C. Hauback, Hydrogen storage in high-entropy alloys with varying degree of local lattice strain, Int. J. Hydrog. Energy 44 (2019) 29140–29149, https://doi.org/10.1016/j.ijhydene.2019.03.223

[130] J. Chen, Z. Li, H. Huang, Y. Lv, B. Liu, Y. Li, Y. Wu, J. Yuan, Y. Wang, Superior cycle life of TiZrFeMnCrV high entropy alloy for hydrogen storage, Scr. Mater. 212 (2022) 114548, https://doi.org/10.1016/j.scriptamat.2022.114548

[131] M. Prakash, S. Ramaprabhu, Hydrogen absorption studies in $ZrMnFe_{0.7}Co_{0.3}$, Int. J. Hydrog. Energy 25 (2000) 871–878, https://doi.org/10.1016/S0360-3199(99)00109-3

[132] F. Cuevas, B. Villeroy, E. Leroy, P. Olier, M. Latroche, Relationship between microstructure and hydrogenation properties of $Ti_{0.85}Zr_{0.15}Mn_{1.5}V_{0.5}$ alloy, J. Alloy. Comp. 446–447 (2007) 218–223, https://doi.org/10.1016/j.jallcom.2006.12.140

[133] X.-Y. Cui, Q. Li, K.-C. Chou, S.-L. Chen, G.-W. Lin, K.-D. Xu, A comparative study on the hydriding kinetics of Zr-based AB_2 hydrogen storage alloys, Intermetallics 16 (2008) 662–667, https://doi.org/10.1016/j.intermet.2008.02.009

[134] K. Manickam, D.M. Grant, G.S. Walker, Optimization of AB_2 type alloy composition with superior hydrogen storage properties for stationary applications, Int. J. Hydrog. Energy 40 (2015) 16288–16296, https://doi.org/10.1016/j.ijhydene.2015.09.157

[135] A. Hariyadi, S. Suwarno, R.V. Denys, J. Bellosta von Colbe, T.O. Sætre, V. Yartys, Modeling of the hydrogen sorption kinetics in AB_2 laves type metal hydride alloy, J. Alloy. Comp. 893 (2022) 162135, https://doi.org/10.1016/j.jallcom.2021.162135

[136] V.A. Yartys, S.V. Mitrokhin, V.N. Verbetsky, K.N. Semenenko, Crystal structure of $TiFe_{1.16}V_{0.84}D_{1.9}$, Zh. Neorg. Khim. Russ. J. Inorg. Chem. 37 (1992) 32–37.

[137] V.V. Burnasheva, V.A. Yartys, N.V. Fadeeva, S.P. Solov'ev, K.N. Semenenko, The crystal structure of $ZrMoFeD_{2.6}$ deuteride, Sov. Crystallogr. 27 (1982) 900–904.

[138] V.A. Yartys, V.V. Burnasheva, N.V. Fadeeva, S.P. Solov'ev, K.N. Semenenko, The crystal structure of $ZrCr_2D_{3.5}$ deuteride, Dokl. SSSR (Rep. USSR Acad. Sci.) 255 (1980) 582–586.

[139] V.A. Yartys, V.V. Burnasheva, N.V. Fadeeva, V.A. Sarin, L.E. Fykin, K.N. Semenenko, Neutron diffraction investigation of the crystal and magnetic structure of λ_1-$ScFe_2D_{2.5}$, Zh. Neorg. Khim. (Russ. J. Inorg. Chem. 31 (1986) 2500–2503.

[140] V.A. Yartys, V.V. Burnasheva, N.V. Fadeeva, V.A. Sarin, L.E. Fykin, K.N. Semenenko, The crystal and magnetic structure of $ScFe_2D_{2.9}$, Zh. Neorg. Khim. Russ. J. Inorg. Chem. 31 (1986) 311–317.

[141] J.-J. Didisheim, K. Yvon, P. Fischer, D. Shaltiel, The deuterium site occupation in ZrV_2D_x as a function of the deuterium concentration, J. Less-Common Met. 73 (1980) 355–362, https://doi.org/10.1016/0022-5088(80)90329-X

[142] C.B. Wan, R.V. Denys, M. Lelis, D. Milcius, V.A.Yartys, Electrochemical studies and phase-structural characterization of a high-capacity La-doped AB_2 Laves type alloy and its hydride, J. Power Sources 418 (2019) 193–201, https://doi.org/10.1016/j.jpowsour.2019.02.044

[143] V.A. Yartys, V.V. Burnasheva, K.N. Semenenko, Structural chemistry of hydrides of intermetallic compounds, Sov. Adv. Chem. 52 (1983) 529–562.

[144] V.A. Yartys, V.V. Burnasheva, K.N. Semenenko, Crystal structures of hydrides based on the $MgZn_2$ type ZrVT (T = Fe, Cu, Nb) intermetallic compounds, Zh. Neorg. Khim. (Russ. J. Inorg. Chem. (1984) 615–621.

[145] N.F. Miron, V.I. Shcherbak, V.N. Bykov, V.A. Levdik, Structural study of the quasibinary $Zr_{0.35}Ti_{0.\ 65}$-H(D) system, Sov. Phys. Crystallogr. 16 (2) (1971) 266.

[146] Y. Tokaychuk, L. Keller, K. Yvon, Deuterium site energy difference in $ZrTi_2D_{4.3}$ as studied by high-temperature neutron diffraction, J. Alloy. Comp. 394 (1–2) (2005) 126–130, https://doi.org/10.1016/j.jallcom.2004.11.018

[147] A.N. Bogdanova, A.V. Irodova, G. Andre, F. Bouree, The ZrV_2D_6 crystal structure, J. Alloy. Comp. 356–357 (2003) 50–53, https://doi.org/10.1016/S0925-8388(02)01214-8

[148] M. Schülke, H. Paulus, M. Lammers, G. Kiss, F. Réti, K.-H. Müller, Influence of surface contaminations on the hydrogen storage behaviour of metal hydride alloys, Anal. Bioanal. Chem. 390 (2008) 1495–1505, https://doi.org/10.1007/s00216-007-1797-7

[149] M. Faisal, J.-Y. Suh, Y.-S. Lee, Understanding first cycle hydrogenation properties of Ti–Fe–Zr ternary alloys, Int. J. Hydrog. Energy 46 (2021) 4241–4251, https://doi.org/10.1016/j.ijhydene.2020.11.025

[150] T. Maeda, T. Fuura, I. Matsumoto, Y. Kawakami, M. Masuda, Cyclic stability test of AB2 type (Ti, Zr)(Ni, Mn, V, Fe)$_{2.18}$ for stationary hydrogen storage in water contaminated hydrogen, J. Alloy. Comp. 580 (2013) S255–S258, https://doi.org/10.1016/j.jallcom.2013.03.230

[151] S. Tan, Y. Shen, E.O. Şahin, D. Noréus, T. Öztürk, Activation behavior of an AB_2 type metal hydride alloy for NiMH batteries, Int. J. Hydrog. Energy 41 (2016) 9948–9953, https://doi.org/10.1016/j.ijhydene.2016.03.196

[152] E. Higuchi, K. Hidaka, Z.P. Li, S. Suda, S. Nohara, H. Inoue, C. Iwakura, Effects of modified fluorination treatment on structural and electrochemical characteristics of AB_2-type Laves phase alloy, J. Alloy. Comp. 335 (2002) 277–280, https://doi.org/10.1016/S0925-8388(01)01817-5

[153] T. Zhang, Y. Zhang, M. Zhang, R. Hu, H. Kou, J. Li, X. Xue, Hydrogen absorption behavior of Zr-based getter materials with Pd–Ag coating against gaseous impurities, Int. J. Hydrog. Energy 41 (2016) 14778–14787, https://doi.org/10.1016/j.ijhydene.2016.06.073

[154] T.R. Somo, M.W. Davids, M.V. Lototskyy, M.J. Hato, K.D. Modibane, Improved hydrogenation kinetics of $TiMn_{1.52}$ alloy coated with palladium through electroless deposition, Materials 14 (2021) 1833, https://doi.org/10.3390/ma14081833

[155] I.D. Wijayanti, L. Mølmen, R.V. Denys, J. Nei, S. Gorsse, K. Young, V. Yartys, Studies of Zr-based C15 type metal hydride battery anode alloys prepared by rapid solidification, J. Alloy. Comp. 804 (2019) 527–537, https://doi.org/10.1016/j.jallcom.2019.06.324

[156] I.D. Wijayanti, L. Mølmen, R.V. Denys, J. Nei, S. Gorsse, K. Young, M.N. Guzik, V. Yartys, The electrochemical performance of melt-spun C14-Laves type Ti-Zr-based alloy, Int. J. Hydrog. Energy 45 (2020) 1297–1303, https://doi.org/10.1016/j.ijhydene.2019.02.093

[157] I.D. Wijayanti, L. Mølmen, R. Denys, M.N. Guzik, S. Gorsse, J.-L. Bobet, V. Yartys, Studies of the effect of melt spinning on the electrochemical properties of the AB_2 Laves phase alloys, JMES – Int. J. Mech. Eng. Sci. 5 (1) (2021) 24–29, https://doi.org/10.12962/j25807471.v5i1.8466

[158] S.V. Mitrokhin, V.N. Verbetsky, Titanium-based Laves phase hydrides with high dissociation pressure, Int. J. Hydrog. Energy 22 (1997) 219–222, https://doi.org/10.1016/S0360-3199(96)00155-3

[159] S.V. Mitrokhin, Regularities of hydrogen interaction with multicomponent Ti (Zr)–Mn–V Laves phase alloys, J. Alloy. Comp. 404- 406 (2005) 384–387, https://doi.org/10.1016/j.jallcom.2005.02.078

[160] H.H. Van Mal, K.H.J. Buschow, A.R. Miedema, Hydrogen absorption in $LaNi_5$ and related compounds: experimental observations and their explanation, J. Less Common Met. 35 (1974) 65–76, https://doi.org/10.1016/0022-5088(74)90146-5

[161] A.R. Miedema, K.H.J. Buschow, H.H. Van Mal, Which intermetallic compounds of transition metals form stable hydrides? J, Less Common Met 49 (1976) 463–472, https://doi.org/10.1016/0022-5088(76)90057-6

[162] I. Jacob, On the "imaginary binary hydrides" model, J. Less Common Met 130 (1987) 329–337, https://doi.org/10.1016/0022-5088(87)90127-5

[163] J.F. Herbst, On extending Miedema's model to predict hydrogen content in binary and ternary hydrides, J. Alloy. Comp. 337 (2002) 99–107, https://doi.org/10.1016/S0925-8388(01)01939-9

[164] A. Andreasen. Predicting formation enthalpies of metal hydrides, Risø National Laboratory, Roskilde, Denmark, 2004. ⟨https://orbit.dtu.dk/files/7711359/ris_r_1484.pdf⟩.

[165] S. Fujitani, I. Yonezu, T. Saito, N. Furukawa, E. Akiba, H. Hayakawa, S. Ono, Relation between equilibrium hydrogen pressure and lattice parameters in pseudobinary Zr-Mn alloy systems, J. Less-Common Met. 172- 174 (1991) 220–230, https://doi.org/10.1016/0022-5088(91)90451-9

[166] S. Bera, S. Mazumdar, M. Ramgopal, S. Bhattacharyya, I. Manna, Prediction of enthalpy of formation and Gibbs energy change in pseudo-binary (Ti–Zr)(Fe–Cr)$_2$ and pseudo-ternary (Ti–Zr)(Fe–Cr)$_2$-H system using extended Miedema model, J. Mater. Sci. 42 (2007) 3645–3650, https://doi.org/10.1007/s10853-006-1377-9

[167] D.G. Westlake, Stoichiometries and interstitial site occupation in the hydrides of ZrNi and other isostructural intermetallic compounds, J. Less-Common Met. 75 (1980) 177–185, https://doi.org/10.1016/0022-5088(80)90115-0

[168] S.B. Gesari, M.E. Pronsato, A. Visintin, A. Juan, Hydrogen storage in AB_2 laves phase (A = Zr, Ti; B = Ni, Mn, Cr, V): binding energy and electronic structure, J. Phys. Chem. C. 114 (2010) 16832–16836, https://doi.org/10.1021/jp106036v

[169] R. Sarhaddi, H. Arabi, F. Pourarian, Structural, stability and electronic properties of C15-AB_2 (A = Ti, Zr;B = Cr) intermetallic compounds and their hydrides: an ab initio study, Int. J. Mod. Phys. B 28 (2014) 1450105, https://doi.org/10.1142/S0217979214501057

[170] L. Rabahi, M. Gallouze, T. Grosdidier, D. Bradai, A. Kellou, Energetics of atomic hydrogen absorption in C15-Fe_2Zr Laves phases with ternary additions: a DFT study, Int. J. Hydrog. Energy 42 (2017) 2157–2166, https://doi.org/10.1016/j.ijhydene.2016.11.131

[171] A. Robina, P. Bechthold, A. Juan, C. Pistonesi, M.E. Pronsato, Hydrogen storage in $Zr_{0.9}Ti_{0.1}(Ni_{0.5}Cr_{0.5-x}V_x)_2$ Laves phase, with x = 0, 0.125, 0.25, 0.375, 0.5. A theoretical approach, Int. J. Hydrog. Energy 43 (2018) 16085–16091, https://doi.org/10.1016/j.ijhydene.2018.06.131

[172] T.B. Flanagan, W.A. Oates, Thermodynamics of intermetallic compound-hydrogen systems, in: L. Schlapbach (Ed.), Hydrogen in Intermetallic Compounds I. Topics in Applied Physics, vol 63, Springer, Berlin, Heidelberg, 1988DOI: 10.1007/3540183337_10.

[173] Y. Kojima, M. Yamaguchi, Investigation on hydrogen dissociation pressure, heat of formation and strain energy of metal hydrides, J. Alloy. Compd. 840 (2020) 155686, https://doi.org/10.1016/j.jallcom.2020.155686

[174] L. Pasquini, The effects of nanostructure on the hydrogen sorption properties of magnesium-based metallic compounds: a review, Crystals 8 (2018) 106, https://doi.org/10.3390/cryst8020106

[175] H.B. Callen, Thermodynamics and an Introduction to Thermostatistics, second ed., John Wiley and Sons, New York, 1985.

[176] N. Zhou, M. Yamaguchi, H. Miyaoka, Y. Kojima, Temperature rise of $LaNi_5$-based alloys by hydrogen absorption, Chem. Comm. 74 (2021) 9374–9377, https://doi.org/10.1039/D1CC02358F

[177] K. Young, J. Nei, B. Huang, M.A. Fetcenko, Studies of off-stoichiometric AB_2 metal hydride alloy: Part 2. Hydrogen storage and electrochemical properties, Int. J. Hydrog. Energy 36 (2011) 11146–11154 DOI: 10.1016/j.ijhydene.2011.05.056.

[178] M. Bereznitsky, I. Jacob, J. Bloch, M.H. Mintz, Thermodynamic and structural aspects of hydrogen absorption in the $Zr(Al_xFe_{1-x})_2$ system, J. Alloy. Comp. 351 (2003) 180–183, https://doi.org/10.1016/S0925-8388(02)01074-5

[179] W.E. Wallace, H.E. Flotow, D. Ohlendorf, Configurational entropy and structure of β-$LaNi_5$ hydride, J. Less-Common Met. 79 (1981) 157–160, https://doi.org/10.1016/0022-5088(81)90061-8

[180] J.-M. Park, J.-Y. Lee, Hydrogenation characteristics of the $Zr_{1-x}Ti_xCr_{1-y}Fe_{1+y}$ laves phase alloys, J. Less Common Met 160 (1990) 259–271, https://doi.org/10.1016/0022-5088(90)90386-X

[181] G. Jansen, Z. Dehouche, H. Corrigan, R. Bonser, An autonomous Solar PV/Wind/regenerative hydrogen fuel cell energy storage system for cell towers, Hydrogen Storage: Preparation, Applications and Technology, Nova Science Publ., 2018, pp. 225–266.

[182] E.I. Gkanas, T. Statheros, M. Khzouz, Heat management on rectangular metal hydride tanks for green building applications, Int. J. Hydrog. Energy 44 (2019) 19267–19274, https://doi.org/10.1016/j.ijhydene.2018.06.030

[183] B.P. Tarasov, P.V. Fursikov, A.A. Volodin, M.S. Bocharnikov, Y.Y. Shimkus, A.M. Kashin, V.A. Yartys, S. Chidziva, S. Pasupathi, M.V. Lototskyy, Metal hydride hydrogen storage and compression systems for energy storage technologies, Int. J. Hydrog. Energy 46 (2021) 13647–13657, https://doi.org/10.1016/j.ijhydene.2020.07.085

[184] M.W. Davids, I. Tolj, T.-C. Jao, M. Lototskyy, S. Pasupathi, C. Sita, Development of a portable polymer electrolyte membrane fuel cell system using metal hydride as the hydrogen storage medium, ECS Trans. 75 (2016) 553–562, https://doi.org/10.1149/07514.0553ecst

[185] M.W. Davids, M. Lototskyy, M. Malinowski, D. van Schalkwyk, A. Parsons, S. Pasupathi, D. Swanepoel, T. van Niekerk, Metal hydride hydrogen storage tank for light fuel cell vehicle, Int. J. Hydrog. Energy 44 (2019) 29263–29272, https://doi.org/10.1016/j.ijhydene.2019.01.227

[186] M.V. Lototskyy, I. Tolj, A. Parsons, F. Smith, C. Sita, V. Linkov, Performance of electric forklift with low-temperature polymer exchange membrane fuel cell power module and metal hydride hydrogen storage extension tank, J. Power Sources 316 (2016) 239–250, https://doi.org/10.1016/j.jpowsour.2016.03.058

[187] M. Lototskyy, I. Tolj, Y. Klochko, M.W. Davids, D. Swanepoel, V. Linkov, Metal hydride hydrogen storage tank for fuel cell utility vehicles, Int. J. Hydrog. Energy 45 (2020) 7958–7967.

[188] D. Mori, K. Hirose, N. Haraikawa, T. Takiguchi, T. Shinozawa, T. Matsunaga, K. Toh, K. Fujita, A. Kumano H. Kubo. High-pressure Metal Hydride Tank for Fuel Cell Vehicles, SAE Technical Papers 2007–01-2011, pp.560–564. DOI: 10.4271/2007–01-2011.

[189] J. Li, X. Jiang, G. Li, X. Li, Development of $Ti_{1.02}Cr_{2-x-y}Fe_xMn_y$ (0.6≤x≤0.75, y=0.25, 0.3) alloys for high hydrogen pressure metal hydride system, Int. J. Hydrog. Energy 44 (2019) 15087–15099 DOI:10.1016/j.ijhydene.2019.03.241.

[190] C. Corgnale, M. Sulic, High pressure thermal hydrogen compression employing $Ti_{1.1}CrMn$ metal hydride material, J. Phys. Energy 2 (2020) 014003, https://doi.org/10.1088/2515-7655/ab47b0

[191] V. Charbonnier, H. Enoki, K. Asano, H. Kim, K. Sakaki, Tuning the hydrogenation properties of $Ti_{1+y}Cr_{2-x}Mn_x$ laves phase compounds for high pressure metal-hydride compressors, Int. J. Hydrog. Energy 46 (2021) 36369–36380, https://doi.org/10.1016/j.ijhydene.2021.08.143

[192] Z. Peng, Q. Li, J. Sun, K. Chen, W. Jiang, H. Wang, J. Liu, L. Ouyang, M. Zhu, Ti-Cr-Mn-Fe-based alloys optimized by orthogonal experiment for 85 MPa hydrogen compression materials, J. Alloy. Comp. 891 (2022) 161791, https://doi.org/10.1016/j.jallcom.2021.161791

[193] A.R. Galvis E, F. Leardini, J. Bodega, J.R. Ares, J.F. Fernandez, Realistic simulation in a single stage hydrogen compressor based on AB_2 alloys, Int. J. Hydrog. Energy 41 (2016) 9780–9788, https://doi.org/10.1016/j.ijhydene.2016.01.125

[194] A.R. Galvis E, F. Leardini, J.R. Ares, F. Cuevas, J.F. Fernandez, Simulation and design of a three-stage metal hydride hydrogen compressor based on experimental thermodynamic data, Int. J. Hydrog. Energy 43 (2018) 6666–6676, https://doi.org/10.1016/j.ijhydene.2018.02.052

[195] M.V. Lototskyy, V.A. Yartys, B.P. Tarasov, M.W. Davids, R.V. Denys, S. Tai, Modelling of metal hydride hydrogen compressors from thermodynamics of hydrogen – metal interactions viewpoint: Part I. Assessment of the performance of metal hydride materials, Int. J. Hydrog. Energy 46 (2021) 2330–2338, https://doi.org/10.1016/j.ijhydene.2020.10.090

[196] M.V. Lototskyy, V.A. Yartys, B.P. Tarasov, R.V. Denys, J. Eriksen, M.S. Bocharnikov, S. Tai, V. Linkov, Modelling of metal hydride hydrogen compressors from thermodynamics of hydrogen – Metal interactions viewpoint: Part II. Assessment of the performance of metal hydride compressors, Int. J. Hydrog. Energy 46 (2021) 2339–2350, https://doi.org/10.1016/j.ijhydene.2020.10.080

[197] X.H. Wang, Y.Y. Bei, X.C. Song, G.H. Fang, S.Q. Li, C.P. Chen, Q.D. Wang, Investigation on high-pressure metal hydride hydrogen compressors, Int. J. Hydrog. Energy 32 (2007) 4011–4015, https://doi.org/10.1016/j.ijhydene.2007.03.002

[198] H. Li, X. Wang, Z. Dong, L. Xu, C. Chen, A study on 70 MPa metal hydride hydrogen compressor, J. Alloy. Comp. 502 (2010) 503–507, https://doi.org/10.1016/j.jallcom.2010.04.206

[199] X. Wang, H. Liu, H. Li, A 70 MPa hydrogen-compression system using metal hydrides, Int. J. Hydrog. Energy 36 (2011) 9079–9085, https://doi.org/10.1016/j.ijhydene.2011.04.193

[200] P. Muthukumar, M. Groll, Metal hydride based heating and cooling systems: a review, Int. J. Hydrog. Energy 35 (2010) 3817–3831, https://doi.org/10.1016/j.ijhydene.2010.01.115

[201] M. Linder, R. Mertz, E. Laurien, Experimental results of a compact thermally driven cooling system based on metal hydrides, Int. J. Hydrog. Energy 35 (2010) 7623–7632, https://doi.org/10.1016/j.ijhydene.2010.04.184

[202] P. Muthukumar, A. Kumar, N.N. Raju, K. Malleswararao, M.M. Rahman, A critical review on design aspects and developmental status of metal hydride based thermal machines, Int. J. Hydrog. Energy 43 (2018) 17753–17779, https://doi.org/10.1016/j.ijhydene.2018.07.157

[203] F. Desai, S.P. Jenne, P. Muthukumar, M.M. Rahman, Thermochemical energy storage system for cooling and process heating applications: a review, Energy Convers. Manag. 229 (2021) 113617, https://doi.org/10.1016/j.enconman.2020.113617

[204] V.A. Yartys, M.V. Lototskyy, E. Akiba, R. Albert, V.E. Antonov, J.R. Ares, M. Baricco, N. Bourgeois, C.E. Buckley, J.M. Bellosta von Colbe, J.-C. Crivello, F. Cuevas, R.V. Denys, M. Dornheim, M. Felderhoff, D.M. Grant, B.C. Hauback, T.D. Humphries, I. Jacob, T.R. Jensen, P.E. de Jongh, J.-M. Joubert, M.A. Kuzovnikov, M. Latroche, M. Paskevicius, L. Pasquini, L. Popilevsky, V.M. Skripnyuk, E. Rabkin, M.V. Sofianos, A. Stuart, G. Walker, C.J.Webb Hui Wang, Min Zhu, Magnesium based materials for hydrogen based energy storage: past, present and future, Int. J. Hydrog. Energy 44 (2019) 7809–7859, https://doi.org/10.1016/j.ijhydene.2018.12.212

[205] P. Dantzer, F. Meunier, What materials to use in hydride chemical heat pumps? Mater. Sci. Forum 31 (1988) 1–18, https://doi.org/10.4028/www.scientific.net/MSF.31.1

[206] M.T. Hagström, J.P. Vanhanen, P.D. Lund, AB_2 metal hydrides for high-pressure and narrow temperature interval applications, J. Alloy. Comp. 269 (1998) 288–293, https://doi.org/10.1016/S0925-8388(98)00213-8

[207] T.G. Voskuilen, E.L. Waters, T.L. Pourpoint, A comprehensive approach for alloy selection in metal hydride thermal systems, Int. J. Hydrog. Energy 39 (2014) 13240–13254, https://doi.org/10.1016/j.ijhydene.2014.06.119

[208] H.-P. Klein, M. Groll, Development of a two-stage metal hydride system as topping cycle in cascading sorption systems for cold generation, Appl. Therm. Eng. 22 (2002) 631–639, https://doi.org/10.1016/S1359-4311(01)00115-6

[209] C. Weckerle, M. Nasri, R. Hegner, M. Linder, I. Bürger, A metal hydride air-conditioning system for fuel cell vehicles – performance investigations, Appl. Energy 256 (2019) 113957, https://doi.org/10.1016/j.apenergy.2019.113957

[210] F. Cuevas, M. Latroche, Intermetallic alloys as hydrogen getters, J. Alloy. Comp. 905 (2022) 164173, https://doi.org/10.1016/j.jallcom.2022.164173

[211] T. Zhang, Y. Zhang, M. Zhang, R. Hu, H. Kou, J. Li, X. Xue, Hydrogen absorption behavior of Zr-based getter materials with Pd–Ag coating against gaseous impurities, Int. J. Hydrog. Energy 41 (2016) 14778–14787, https://doi.org/10.1016/j.ijhydene.2016.06.073

[212] V.A. Yartys', I.Y. Zavaliy, M.V. Lototsky, A.B. Riabov, Y.F. Shmal'ko, Oxygen-, boron- and nitrogen-containing zirconium-vanadium alloys as hydrogen getters with enhanced properties, Z. Phys. Chem. 183 (1994) 485–489, https://doi.org/10.1524/zpch.1994.183.Part_1_2.485

[213] I.I. Okseniuk, V.O. Litvinov, D.I. Shevchenko, R.L. Vasilenko, S.I. Bogatyrenko, V.V. Bobkov, Hydrogen interaction with Zr-based getter alloys in high vacuum conditions: In situ SIMS-TPD studies, Vacuum 197 (2022) 110861, https://doi.org/10.1016/j.vacuum.2021.110861

[214] M.V. Lototsky, V.A. Yartys, Ye.V. Klochko, V.N. Borisko, R.I. Starovoitov, V.M. Azhazha, P.N. V'yugov, Applications of Zr–V hydrogen getters in vacuum-plasma devices: phase-structural and hydrogen sorption characteristics, J. Alloy. Comp. 404–406 (2005) 724–727, https://doi.org/10.1016/j.jallcom.2005.02.086

[215] Y.F. Shmal'ko, V.V. Solovei, M.V. Lotots'kyi, E.V. Klochko, I.Y. Zavalii, O.B. Ryabov, V.A. Yartys, Metal-hydride systems for processing hydrogen isotopes for power plants, Mater. Sci. 37 (2001) 689–706, https://doi.org/10.1023/A:1015041406755

[216] Kwo Young (Editor). Special Issue "Nickel Metal Hydride Batteries", MDPI-Basel, 2016. ⟨www.mdpi.com/journal/Batteries/special_issues/ni-mh-batteries⟩.

[217] F. Cuevas, M.B. Amdisen, M. Baricco, C. Buckley, Y.W. Cho, P. de Jongh, L.M. de Kort, J.B. Grinderslev, V. Gulino, B.C. Hauback, M. Heere, T. Humphries, T.R. Jensen, S. Kim, K. Kisu, Y.-S. Lee, H.-W. Li, R. Mohtadi, K.T. Møller, P. Ngene, D. Noréus, S.-I. Orimo, M. Paskevicius, M. Polanski, S. Sartori, L.N. Skov, M.H. Sørby, B.C. Wood, V.A. Yartys, M. Zhu, M. Latroche. Metallic and complex hydride-based electrochemical storage of energy, Progress in Energy, **4** (2022) 032001. https://doi.org/10.1088/2516-1083/ac665b.

[218] T.A. Zotov, R.B. Sivov, E.A. Movlaev, S.V. Mitrokhin, V.N. Verbetsky, IMC hydrides with high hydrogen dissociation pressure, J. Alloy. Comp. 509S (2011) S839–S843, https://doi.org/10.1016/j.jallcom.2011.01.198

[219] R.B. Sivov. Intermetallic hydrides of Ti and Zr with structures of Laves Phases with high dissociation pressures, PhD thesis, Moscow State Univ 2011.

[220] Y. Osumi, H. Suzuki, A. Kato, K. Oguro, T. Sugioka, T. Fujita, Hydrogen storage properties of $Ti_{1+x}Cr_{2-y}Mn_y$ alloys, J. Less-Common Met 89 (1983) 257–262, https://doi.org/10.1016/0022-5088(83)90277-1

[221] Z. Chen, X. Xiao, L. Chen, X. Fan, L. Liu, S. Li, H. Ge, Q. Wang, Influence of Ti super-stoichiometry on the hydrogen storage properties of $Ti_{1+x}Cr_{1.2}Mn_{0.2}Fe_{0.6}$ (x = 0–0.1) alloys for hybrid hydrogen storage application, J. Alloy. Comp. 585 (2014) 307–311, https://doi.org/10.1016/j.jallcom.2013.09.141

[222] S.N. Klyamkin, V.N. Verbetsky, V.A. Demidov, Thermodynamics of hydride formation and decomposition for $TiMn_2$-H_2 system at pressure up to 2000 atm, J. Alloy. Comp. 205 (1994) L1–L2, https://doi.org/10.1016/0925-8388(94)90753-6

[223] M.T. Hagstrom, J.P. Vanhanen, P.D. Lund, AB_2 metal hydrides for high-pressure and narrow temperature interval applications, J. Alloy. Comp. 269 (1998) 288–293, https://doi.org/10.1016/S0925-8388(98)00213-8

[224] L. Pickering, D. Reed, A.I. Bevan, D. Book, Ti–V–Mn based metal hydrides for hydrogen compression applications, J. Alloy. Comp. 645S (2015) S400–S403, https://doi.org/10.1016/j.jallcom.2014.12.098

[225] L. Pickering, J. Li, D. Reed, A.I. Bevan, D. Book, Ti–V–Mn based metal hydrides for hydrogen storage, J. Alloy. Comp. 580 (2013) S233–S237, https://doi.org/10.1016/j.jallcom.2013.03.208

[226] X. Guo, E. Wu, Thermodynamics of hydrogenation for $Ti_{1-x}Zr_xMnCr$ Laves phase alloys, J. Alloy. Comp. 455 (2008) 191–196, https://doi.org/10.1016/j.jallcom.2007.01.066

[227] Z. Cao, L. Ouyang, H. Wang, J. Liu, L. Sun, M. Felderhoff, M. Zhu, Development of Zr-Fe-V alloys for hybrid hydrogen storage system, Int. J. Hydrog. Energy 41 (2016) 11242–11253, https://doi.org/10.1016/j.ijhydene.2016.04.083

[228] M. Uchida, H. Bjurström, S. Suda, Y. Matsubara, On the equilibrium properties of some $ZrMn_2$-related hydride-forming alloys, J. Less Common Met. 119 (1986) 63–74, https://doi.org/10.1016/0022-5088(86)90196-7

[229] J.-M. Park, J.-Y. Lee, Thermodynamic properties of the Zr0.8Ti0.2(MnxCr1−x)Fe-H2 system, J. Less Common Met. 167 (1991) 245–253, https://doi.org/10.1016/0022-5088(91)90279-D

[230] L. Wang, K. Young, J. Nei, D. Pawlik, K.Y.S. Ng, Hydrogenation of AB_5 and AB_2 metal hydride alloys studied by in situ X-ray diffraction, J. Alloy. Compd. 616 (2014) 300–305, https://doi.org/10.1016/j.jallcom.2014.07.125
[231] K. Young, T. Ouchi, J. Yang, M.A. Fetcenko, Studies of off-stoichiometric AB_2 metal hydride alloy: part 1. Structural characteristics, Int. J. Hydrog. Energy 36 (2011) 11137–11145, https://doi.org/10.1016/j.ijhydene.2011.05.057
[232] C. Qin, C. Zhou, L. Ouyang, J. Liu, M. Zhu, T. Sun, H. Wang, High-pressure hydrogen storage performances of $ZrFe_2$ based alloys with Mn, Ti, and V addition, Int. J. Hydrog. Energy 45 (2020) 9836–9844, https://doi.org/10.1016/j.ijhydene.2019.11.242
[233] T.A. Zotov, V.N. Verbetsky, T.Y. Safonova, O.A. Petrii, Nonstoichiometric Ti-Zr-Ni-V-Mn alloys: the effect of composition on hydrogen sorption and electrochemical characteristics, J. Solid State Electrochem. 7 (2003) 645–650, https://doi.org/10.1007/s10008-003-0423-7
[234] G.Y. Yu, F. Pourarian, W.E. Wallace, The crystallographic, thermodynamic and kinetic properties of the $Zr_{1-x}Ti_xCrFe\text{-}H_2$ system, J. Less Common Met 106 (1985) 79–87, https://doi.org/10.1016/0022-5088(85)90368-6
[235] V. Zadorozhnyy, B. Sarac, E. Berdonosova, T. Karazehir, A. Lassnig, C. Gammer, M. Zadorozhnyy, S. Ketov, S. Klyamkin, J. Eckert, Evaluation of hydrogen storage performance of ZrTiVNiCrFe in electrochemical and gas-solid reactions, Int. J. Hyrogen Energy 45 (2020) 5347–5355, https://doi.org/10.1016/j.ijhydene.2019.06.157
[236] Z. Cao, L. Ouyang, H. Wang, J. Liu, L. Sun, M. Zhu, Composition design of Ti–Cr–Mn–Fe alloys for hybrid high-pressure metal hydride tanks, J. Alloy. Comp. 639 (2015) 452–457, https://doi.org/10.1016/j.jallcom.2015.03.196
[238] P. Zhou, Z. Cao, X. Xiao, L. Zhan, S. Li, Z. Li, L. Jiang, L. Chen, Development of Ti-Zr-Mn-Cr-V based alloys for high-density hydrogen storage, J. Alloy. Comp. 875 (2021) 160035, https://doi.org/10.1016/j.jallcom.2021.160035
[239] E.Yu Anikina, V.N. Verbetsky, Investigation of the hydrogen interaction with $Ti_{0.9}Zr_{0.1}Mn_{1.3}V_{0.7}$ by means of the calorimetric method, Int J. Hydrog. Energy 41 (2016) 11520–11525, https://doi.org/10.1016/j.ijhydene.2015.12.126
[240] S. Qian, D.O. Northwood, Thermodynamic characterization of $Zr(Fe_xCr_{1-x})_2$-H systems, J. Less Common Met 147 (1989) 149–159, https://doi.org/10.1016/0022-5088(89)90158-6
[241] D.G. Ivey, D.O. Northwood, Hydriding properties of $Zr(Fe_xCr_{1-x})_2$ intermetallic compounds, Int. J. Hydrog. Energy 11 (1986) 583–591, https://doi.org/10.1016/0360-3199(86)90125-4
[242] A. Drašner, Ž. Blažina, Thermodynamic properties of the $ZrCr_2T_{0.8}\text{-}H_2$ systems (T=Fe, Co, Ni), J. Less Common Met 168 (1991) 289–294, https://doi.org/10.1016/0022-5088(91)90310-Z
[243] M. Prakash, S. Ramaprabhu, Hydrogen absorption studies in $ZrMnFe_{0.7}Co_{0.3}$, Int. J. Hydrog. Energy 25 (2000) 871–878, https://doi.org/10.1016/S0360-3199(99)00109-3
[244] C. Qin, H. Wang, J. Liu, L. Ouyang, M. Zhu, Tuning hydrogen storage thermodynamic properties of $ZrFe_2$ by partial substitution with rare earth element Y, Int. J. Hydrog. Energy 46 (2021) 18445–18452, https://doi.org/10.1016/j.ijhydene.2021.03.012
[245] R.B. Sivov, T.A. Zotov, V.N. Verbetsky, Hydrogen sorption properties of $ZrFe_x$ ($1.9 \le x \le 2.5$) alloys, Int. J. Hydrog. Energy 36 (2011) 1355–1358, https://doi.org/10.1016/j.ijhydene.2010.06.118
[246] L. Jiang, Y. Tu, H. Tu, L. Chen, Microstructures and hydrogen storage properties of $ZrFe_{2.05-x}V_x$ ($x = 0.05–0.20$) alloys with high dissociation pressures for hybrid hydrogen storage vessel application, J. Alloy. Comp. 627 (2015) 161–165, https://doi.org/10.1016/j.jallcom.2014.12.045